Spring 2012

Liquefaction and ring shear device

Julian A. Sandoval
University of New Hampshire, Durham

LIQUEFACTION AND RING SHEAR DEVICE

BY

JULIAN A. SANDOVAL

B.S., University of Cauca, 1998

Ms.Sc. University of Florida, 2004

DISSERTATION

Submitted to the University of New Hampshire

in Partial Fulfillment of

the Requirements for the Degree of

Doctor of Philosophy

in

Civil Engineering

May, 2012

UMI Number: 3525063

UMI

Dissertation Publishing

ProQuest®

This dissertation has been examined and approved

_____
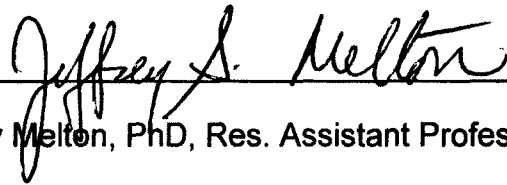
Dr. Pedro de Alba, PhD, Professor of Civil Engineer (Deceased)

_____
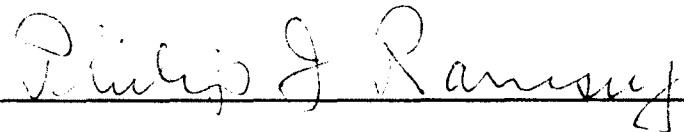
Dr. Jean Benoit, PhD, Professor of Civil Engineering

_____

Dr. Jennifer Jacobs, PhD, PE, Professor of Civil Engineering

_____

Dr. Jeffrey Melton, PhD, Res. Assistant Professor of Civil Engineering

_____

Dr. Philip Ramsey, PhD, Lecturer Mathematics and Statistics

DEDICATION

This dissertation is dedicated to the memory of Dr. Pedro de Alba, and Dr. Luciano Rivera Caicedo, for their support and pioneering work.

ACKNOWLEDGEMENTS

Scotland) for their friendship; thanks to the former members of the team of the Geotechnical Engineering Group at the University of Florida, Arvind, Minh, Badri, Ko, Tung, Thai, Evelio, Rutu and Alvaro for keeping this science an enjoyable one.

Overseas, I would like to thank to my friend Dr. Luciano Rivera (University of Cauca – Colombia), who encouraged me to pursue this degree in geotechnical engineering. To Dr. Christos Vrettos (Technical University of Kaiserslautern, Germany) for showing special interest in the machine

I am deeply grateful to my family, Idalia, Efrén, Paola and Leeloo for their encouragement, love and support.

TABLE OF CONTENTS

LIST OF TABLES

LIST OF FIGURES

ABSTRACT

LIQUEFACTION AND RING SHEAR DEVICE

By:

Julian A. Sandoval

University of New Hampshire, May, 2012

Liquefaction flow slides triggered by earthquakes or heavy rainfall in saturated granular soils have produced great damage in landslide-prone areas worldwide. A major aspect that needs more study is how the 'residual strength' remaining in the liquefied material evolves at the high strain levels imposed as the slide progresses. Strength of liquefied granular soils is usually studied in the lab by means of the triaxial test, since the strains required to trigger liquefaction are low, compared with those observed after it has been produced. More sophisticated devices are necessary in order to apply the high strains and shear strain rates that could replicate those of typical flowslides: In particular, these are required to investigate the behavior of the resistance of the flow, which is termed residual undrained strength (Sur). Preliminary tests by de Alba and Ballestero (2004) with a modified version of the triaxial cell suggested that the residual strength was not a constant number, but depended on the velocity at which the liquefied soil was being

sheared (i.e., the shear strain rate). However, in order to be able to control the strains and the shear strain rates, a more sophisticated machine is necessary: the ring shear device (RSD). The RSD is designed to apply a horizontal shearing stress (cyclic or monotonic) to a ring-shaped granular soil sample. This permits the application of very large total strains and controlled strain rates to the specimen. An RSD was designed and built at the University of New Hampshire with National Science Foundation support. A testing program using the current version of the RSD was carried out using a fine uniform sand, "Holliston sand". Results suggest that the residual strength is rate-dependent and that the data can be interpreted using the Herschel-Bulkley model. This model implies that shearing resistance increases with strain rate, but that the increase diminishes in an exponential fashion (i.e. flattens out) at high strain rates. Finally, data were compared with results from other RSD's and with data obtained from liquefaction case histories Seed and Harder (1990); the latter provided a reasonable match with residual strengths from this study.

CHAPTER I

INTRODUCTION AND BACKGROUND

Motivation

Landslides and flowslides are well known for causing huge material and human losses. Therefore a better understanding is necessary in order to prevent or reduce such catastrophes. There are several aspects of the flowslides that need to be investigated, and although a lot of research has been devoted to this topic, it is still matter of controversy especially because the deformations and velocities that have been observed in the field cannot be reproduced in the lab; also, it is very important to be able to predict both the run-out distance and the forces involved during the flowslide so defensive measures can be adopted. Even though cyclic loads (i.e, earthquakes, waves, etc) are the main events that trigger liquefaction, static loads have also been investigated, such as

1

rainfall events. The main purpose of this dissertation is to investigate the behavior of the undrained residual strength of liquefied soils when they are flowing (i.e., after liquefaction has been triggered).

This section is intended to introduce some important soil mechanics concepts that will help the reader understand the main goal of this project. For instance, consider an inclined granular soil mass, as shown in figure I-1; the water level is at the ground surface, which means that the soil pores are filled with water and that the soil is fully saurated.

Ground water level

Inclined surface

Saturated granular soil

H

Soil element
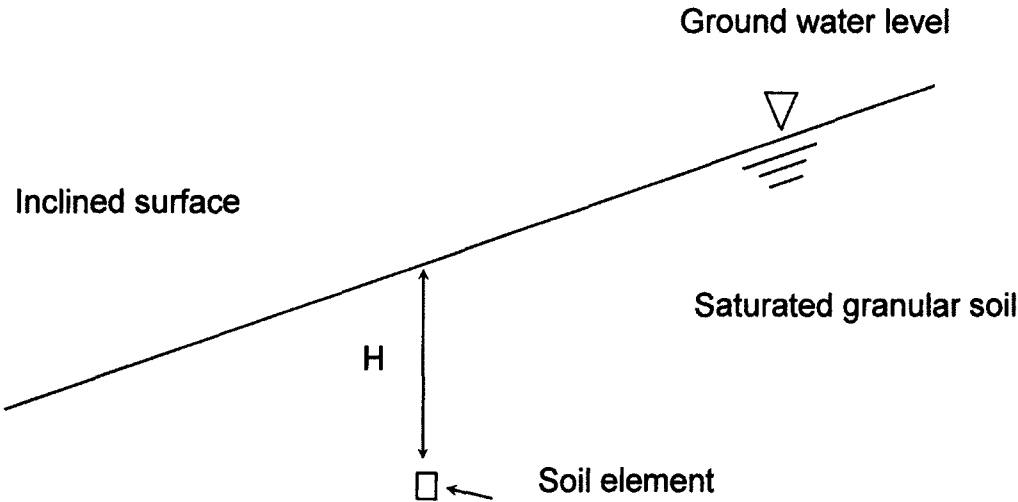
Figure I-1. Inclined saturated granular soil

The previous figure shows an inclined surface because this project is focused on flow slides produced by the loss of shear strength of the soil; this loss

of strength can be caused by either a monotonic load increase (constant load applied with time) or by a cyclic load event (earthquake).

The soil element under consideration is subjected to two different types of stresses: one of them is due to the contact between the particles (*effective stress*) and the other is the pressure due to the water (*pore water pressure*). According to the effective stress principle (Terzaghi, 1925, as cited in Holtz and Kovacs, 1981), the total stress is the sum of the pore water pressure and the effective stress, or:

$$\sigma'_v = \sigma_v - U_o \dots\dots\dots\dots\dots\dots\dots\dots\dots\dots\dots\dots\dots\dots\dots\dots(1)$$

Where

σ'_v is the vertical effective stress, σ_v is the total stress (or confining pressure) and U_o the pore water pressure.

An important concept from Terzaghi's effective stress principle is that the shear strength (τ) of the soil is given by the equation (Holtz and Kovacs, 1981):

$$\tau = \sigma'_f \tan \phi' \dots\dots\dots\dots\dots\dots\dots\dots\dots\dots\dots\dots\dots\dots(2)$$

Where

τ: shear strength of soil

σ'_f: effective stress on the failure plane

ϕ': effective internal friction angle

τ is dependent on the contact between the particles (effective stress), which means that whenever the pore pressure is increased, the shear strength of the soil is decreased and vice versa. Of course, there is a point when the effective stress can be zero (i.e. the pore water pressure equals the confining pressure); this condition of zero effective stress is known as *liquefaction* and does not mean that the shear strength is zero, but that it reduces to its minimum value (residual strength); in other words, equation (2) no longer applies once the effective stress goes to zero, but a non-zero shear value remains, with the liquefied sand behaving as a viscous fluid.

If one wanted to measure the shear strength of a soil element, the triaxial test is the most widely accepted way to model the behavior of the soil under undrained conditions (i.e., load is applied fast enough that water cannot escape from sample). Figure I-2 shows a simple configuration of a conventional undrained triaxial test: a hydrostatic pressure is applied to the sample to model isotropic conditions (i.e., same pressure in both vertical and horizontal directions); a loading piston is used to apply the external load which causes the sample to experience shear stresses.

Since no shear stresses are acting on the vertical and horizontal planes, they are considered principal planes, so in a triaxial compression test σ_1 is the major principal stress and σ_3 is called the minor principal stress and the difference between them is the deviatoric stress ($q = \sigma_1 - \sigma_3$).

Vertical stress: σ_1

Closed valve

Horizontal stress: σ_3
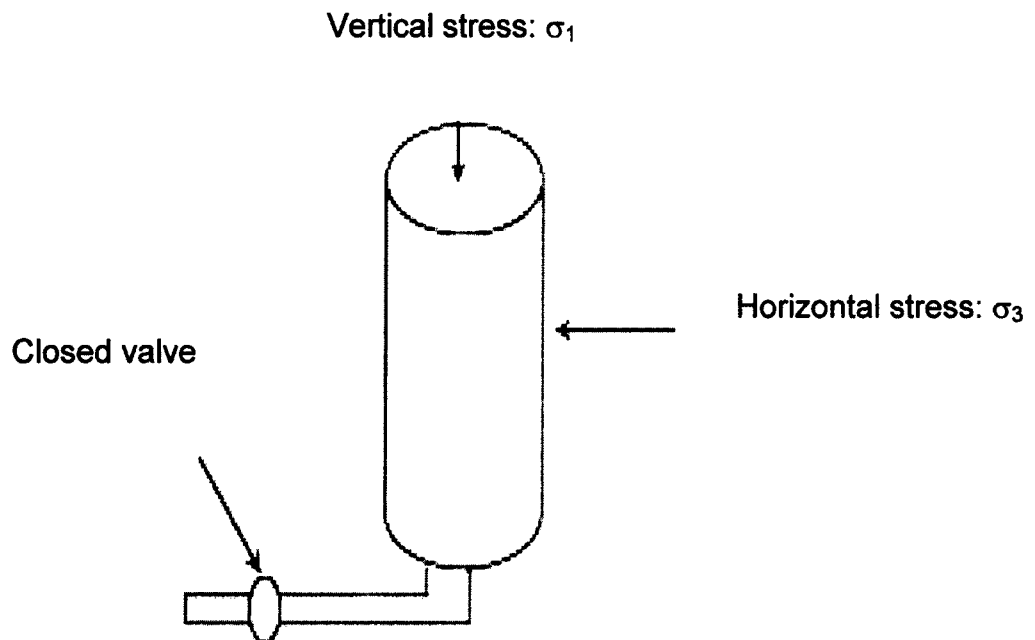
Figure I-2. Undrained triaxial test.

The response of the soil depends basically on its initial relative density (D_r): when the relative density is low (e.g., 20% to 30%) the sample is said to have a *contractive* behavior and it means that, since D_r is low, there are "empty" spaces in between the soil particles; when a shear stress is applied the particles try to occupy them, reducing the volume of the original sample in a drained test or producing a positive excess pore pressure in an undrained test, which brings a

decrease in the shear strength. On the other hand, when D_r is high (say, $D_r>60\%$) there are fewer empty spaces in the mass than there were in the previous case, so when a shear stress is applied, the particles start to roll over the others and have no space where to go; as a consequence, the volume of the sample increases or the sample *dilates*; in an undrained test, dilative tendency translates into decreased pore pressure, thus producing an increase in strength. Typical curves for a contractive and a dilatant sample in the triaxial cell are shown in figure I-3.
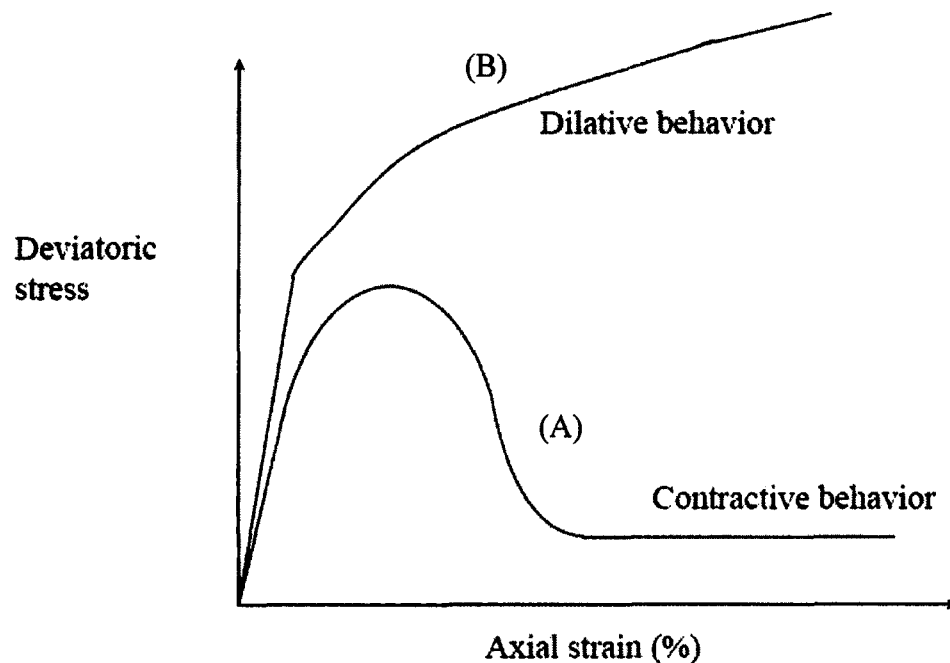
Figure I-3. Typical stress – strain curves for dilative and contractive soils from undrained triaxial test.

Since contractive soils are prone to dramatic loss of shear strength, this dissertation will be focused on flow slides produced in this type of soils and will

not consider what happens to dilatant soils.

Usually, the peak strength in curve (A) of figure 3 is achieved when the axial strain is about 5%; in the case of a flow slide this strain is achieved during early stages of the flow, i.e., peak strength is observed at the beginning of the failure of the sliding mass; after that, the soil mass reaches a minimum value of mobilized shear strength during the event, which is significantly lower than the peak. This lower strength (at large strains) is known as residual shearing strength or *residual strength (Sur)*, and is reached very quickly, eliminating all the initial conditions prior to failure, thus, it is the residual strength that should be used for stability analyses and liquefaction-induced landslide analyses, since it governs the behavior of the sliding mass. Being an important parameter for flow slide analysis, this dissertation is focused on the determination of the residual strength.

Also, it is important to mention that at large strains, in conventional triaxial tests, the effective stress is small, but not zero; this situation complicates any comparison with the undrained behavior of the soil during a flowslide, where the effective stress is indeed zero.

To illustrate that the strains during flow slides are considerable higher than those achieved in the triaxial test, consider figure I-4, where it is clear that the soil mass travels very long distances before reaching an equilibrium position.

7

Figure I-4. Flow slide after an earthquake (El Salvador earthquake, 2001)

This figure shows a flow slide produced by the 2001 earthquake in El Salvador (Mw=7.7). This phenomenon was observed in several places in the zone affected by the earthquake and was responsible for significant damage as well as human and material losses. In order to understand and to be able to model the flow slide, the residual strength needs to be measured properly in the laboratory.

Critical Void Ratio Concept

The shear strength of soils is probably the most important chapter in every soil mechanics textbook, since subsequent topics are based on it (i.e., bearing capacity of foundations, slope stability, etc). In the late 1930's, A. Casagrande

developed a testing program that represents a major contribution for the modern understanding of soil behavior (Casagrande, 1936); the program basically involved a series of drained, strain-controlled triaxial tests on low and high relative density cohesionless soils. At large strains, both dilative and contractive soils reached a constant void ratio, after which the shear strength did not change anymore; such state of large deformation was known as *steady state*, the constant void ratio was termed the *critical void ratio* (CVR) and it was found to be dependent on the effective confining pressure (σ'_{3c}), so it was possible to plot a curve in natural scale (figure I-5a), which in semi log scale plots as a straight line: the steady state line (SSL) (figure I-5b). Thus, in figure I-5b, drained test (1) dilates to SSL and test (2) contracts to SSL, after which the void ratio no longer changes.
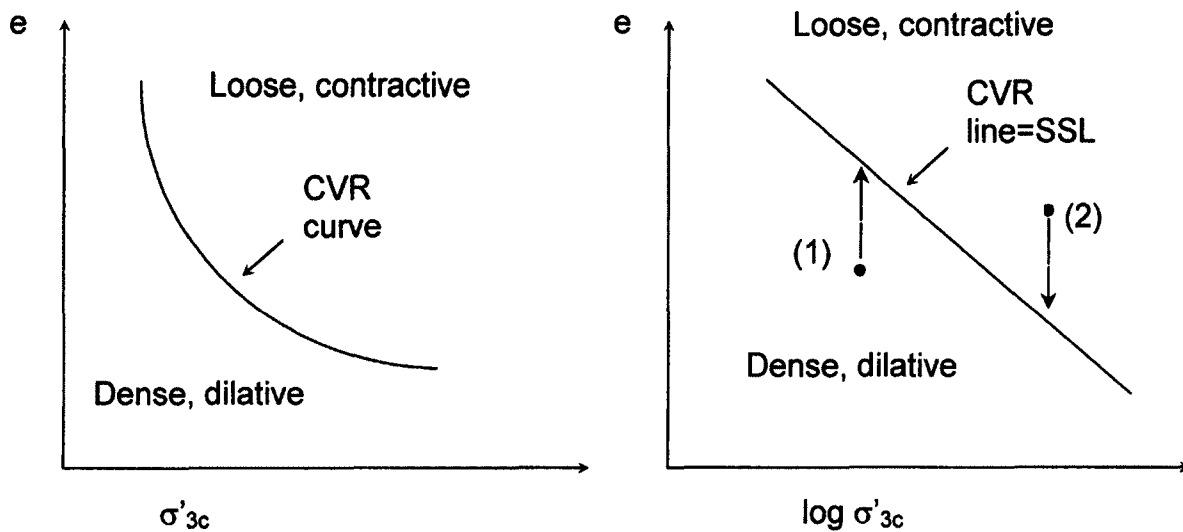
Figure I-5. a) Critical void ratio curve; b) Critical void ratio line.

Since the critical void ratio was used to define the boundary between dilative and contractive behavior, it was also considered a tool to define the boundary between states of flow liquefaction and no-liquefaction (see figure I-6).
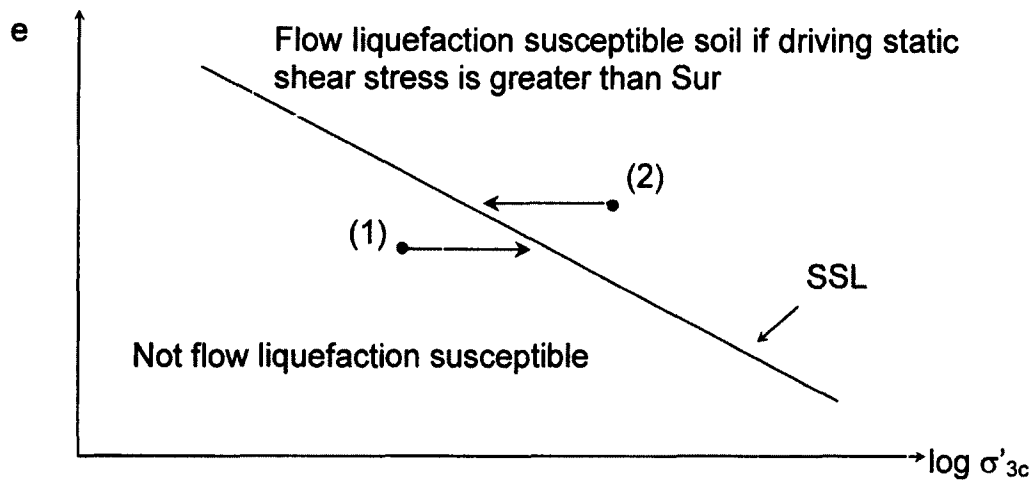
Figure I-6. Flow liquefaction susceptibility as a function of void ratio.

Unfortunately for Casagrande, appropriate pore water pressure measurement devices were not available at the time, so he hypothesized that, under undrained conditions, saturated contractive soils would develop positive excess pore water pressure increments and dilative soils, negative pore water pressure increments.

Another hypothesis proposed (but not tested) by Casagrande was that once the saturated soil reached large strains, in undrained conditions it could develop a fluid-like behavior, at very low σ'_{3c}, with a re-orientation of particles and a minimum friction resistance state (the steady state), i.e. test (2) in figure I-6. In

test (1), σ'_{3c} increases to SSL so the strength increases. As previously noted, Casagrande's tests were carried out on drained samples; undrained behavior was tested by Castro (1969), when he was able to run a series of undrained stress-controlled triaxial tests with pore pressure measurement on soils with different relative densities. Typical results are shown in figure I-7.

For instance, curve A represents the typical behavior of a conventional triaxial compression test on a sample with contractive behavior. Usually, for most sands the plot reaches a maximum value of the deviator stress [q] at an axial strain of ≈5% after which the shear strength decreases until it reaches a minimum value; at this point (≈20% axial strain) the shearing strength and the volume of the sample apparently don't change anymore. However, a small but measurable effective stress may remain, so strength may still be modeled as a Mohr-Coulomb material (using equation 2). Authors have given different names for this type of behavior: actual liquefaction (Casagrande, 1975), static liquefaction (Castro et al, 1977; Poulos et al, 1985; Vaid et al, 1990), flow failure (Vaid et al, 1983; Alarcon and Leonards, 1986) or collapse behavior (Sladen et al, 1985). Whichever term is being used, the most important characteristic for this study is that, at large axial strains (usually 20% to 25%), triaxial test results suggest that the shear strength and volume do not change any further with continuous deformation (implications of this observation will be discussed in following sections). Figure I-8 shows that regardless of what type of undrained

load is applied (monotonic or cyclic) to a saturated contractive sample, it reaches

minimum shear strength (residual shear strength).

Δu: excess pore water pressure
ε_a: axial strain
q: deviatoric stress (σ_1-σ_3)
p′: mean effective stress (σ'_1+2σ'_3)/3
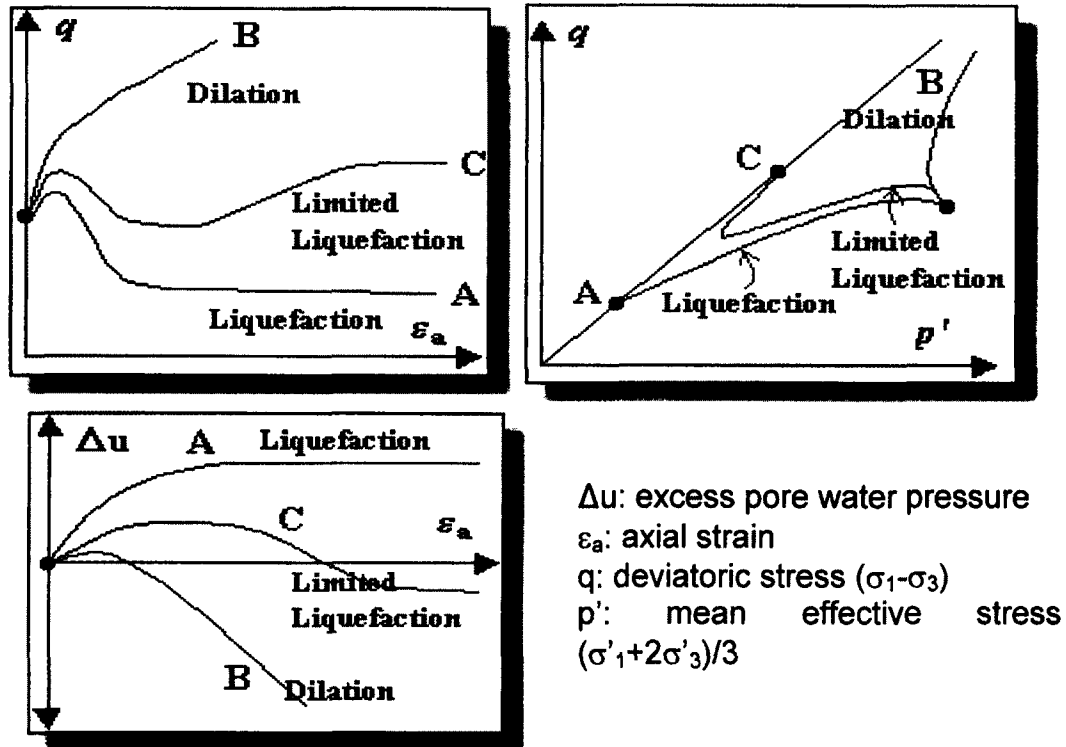
Figure I-7. Triaxial test results on saturated soils with different relative densities (after Castro, 1969).

Returning to figure I-7, curve C represents a phenomenon that is still matter of controversy and is called *limited liquefaction* (or *limited flow* or *quasi steady state*) (Vaid and Chern, 1985). Basically, after [q] reaches a maximum, the shear strength drops, but suddenly it reaches a minimum value (QSS) and it goes up again exhibiting a dilative behavior until the end of the test. Some authors do not agree with this kind of behavior arguing that it is rather a consequence of the device that is being used (a laboratory artifact, i.e., produced

by the end restraints of the specimen) (Zhang and Garga, 1997). This kind of behavior and the discussion about it is beyond the scope of this project.
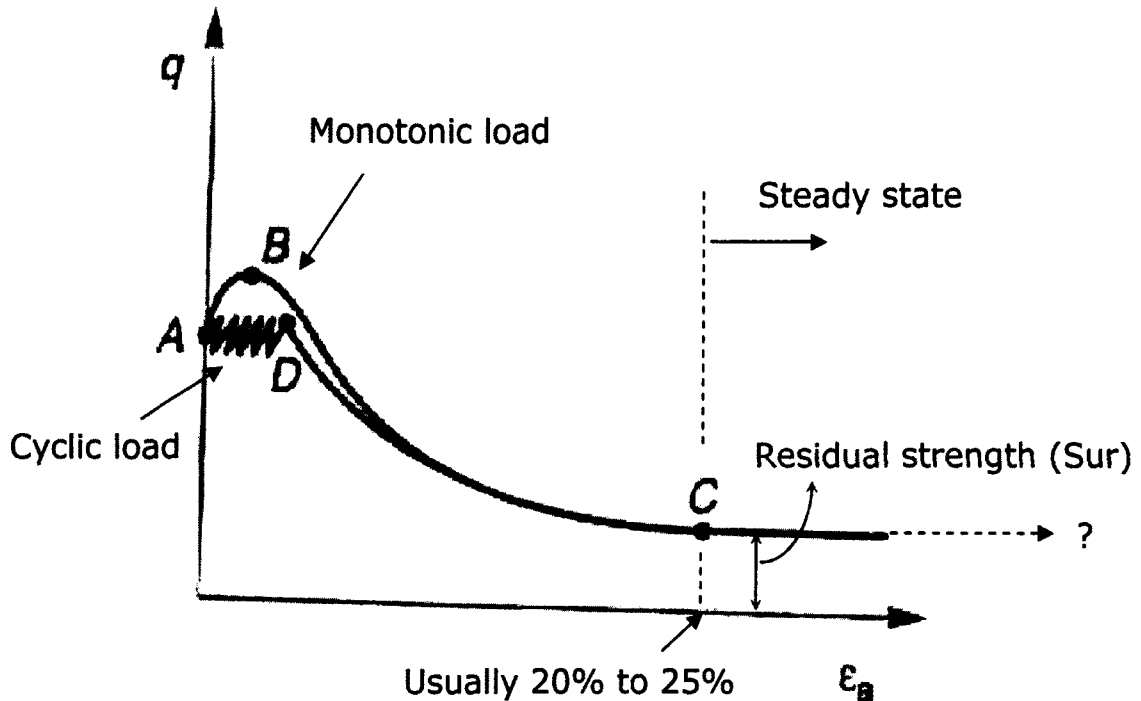
Figure I-8. Liquefaction induced by monotonic and cyclic loading.

Previous figures show results of induced liquefaction in the lab using the triaxial test on saturated granular materials, and an important observation to be made is the fact that the maximum axial strain achieved is not more than 20% to 25%; beyond this point, it is very difficult to calculate the stresses in the sample as the cross section becomes distorted, i.e. much greater at the midpoint. This behavior, as will be discussed in future paragraphs, is a key characteristic of this particular device (triaxial cell) and constitutes a disadvantage when dealing with

13

residual conditions (large strains). In figure I-8 it is clearly recognized where the peak strength is, as well as the point where the strength is apparently reduced to a minimum value, which seems to remain constant until the end of the test. However, the actual value of Sur depends on the stress calculated on the highly deformed sample and needs to be further corrected for the resistance of the membrane, which may be a significant fraction of the observed Sur. As mentioned previously the main objective of this dissertation is to develop a more reliable technique for measuring Sur.

Steady State Strength Measurement

In terms of the measurement of the strength at the steady state (residual strength, Sur), it can be evaluated in two ways (Byrne and Beaty, 1999):

A) Directly from testing undisturbed samples, combined with a lab testing framework.

This first option was initially evaluated by Poulos (Poulos, Castro and France, 1985) to evaluate both Sur and liquefaction potential, and the method can be summarized as follows (figure I-9):

A.1. Determine insitu void ratio. The authors mention three methods to find the void ratio of loose sand insitu: a) Fixed piston sampling; b) freezing of the ground and coring; and c) sampling in test pits. Details of these

14

procedures can be found in the cited reference (Poulos, Castro and France, 1985).

A.2. Determine steady – state strength line using triaxial test on compacted specimens. This is achieved by using different relative densities and confining pressures. Plot steady-state strength vs. void ratio.

A.3. Determine undrained steady state strengths for "undisturbed" specimens.

A.4. Correct measured undrained steady-state strengths to insitu void ratio as follows: plot Sur for "undisturbed" specimen versus its void ratio after sampling extrusion and consolidation (point A, figure I-9). Draw a parallel line to SSL from compacted specimens, through point A; use the in situ void ratio for the undisturbed specimen (step 1) to find the estimated Sur, using the parallel line mentioned previously.

A.5. Calculate insitu driving shear stress and the factor of safety before and after liquefaction.

A.6. Decide on required remediation measures.

Poulos note that *"The original structure is completely remolded at the steady state line. Therefore, the method of specimen preparation, which controls*

the original structure, has no influence on the position or slope of the steady state line for the particular soil used."
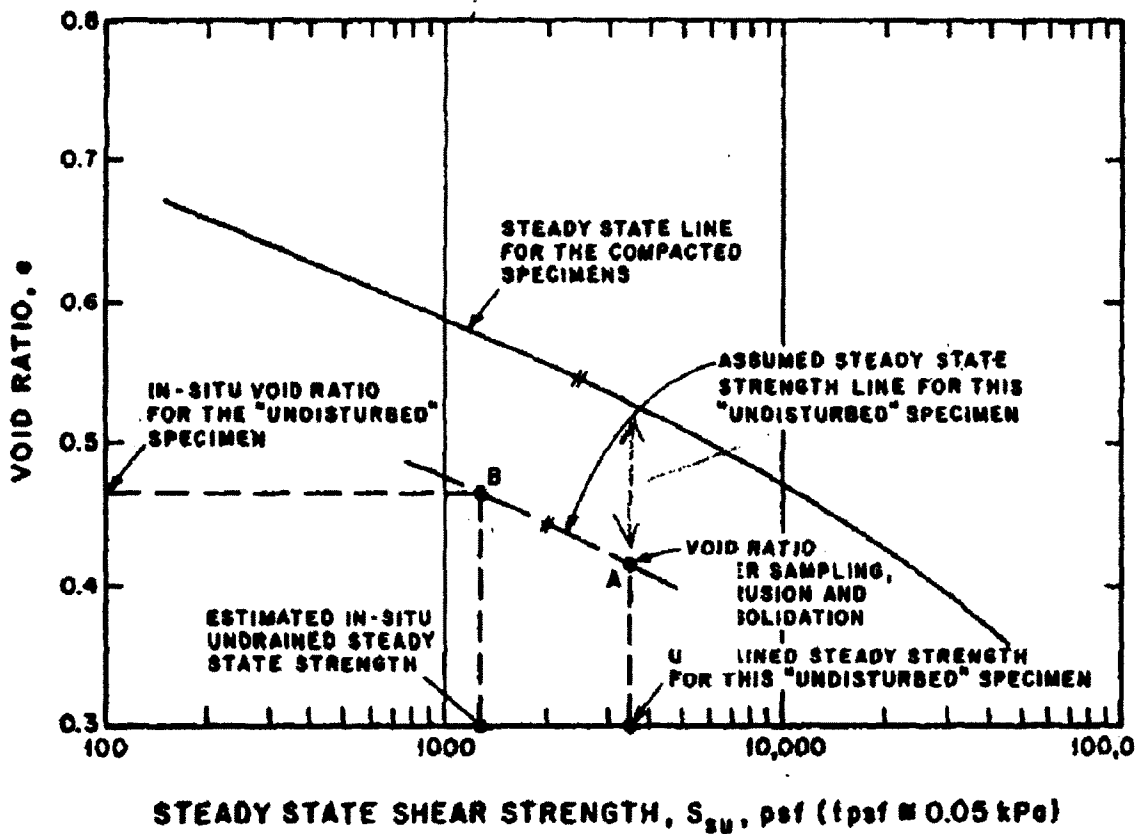
Figure I-9. Sur determination (Poulos, Castro and France, 1985).

However, it is noted by Byrne and Beaty (1999) that shear strains needed to erase initial conditions effects are considerable larger than those achieved in conventional triaxial tests.

B) Indirectly from penetration resistance linked to back calculation of field case histories:

R. B. Seed and L. Harder (1990) came up with a different approach, which involved determination of values for residual strength by back-analyzing embankments that experienced significant displacements after an earthquake. Residual strength values for sands with different fines content were related to a corrected "clean sand" Standard Penetration Test Resistance $(N_1)_{60\text{-}CS}$. Figure I-10 shows results by R. Seed and L. Harder (1990), expanding the original data set used by H. B. Seed.
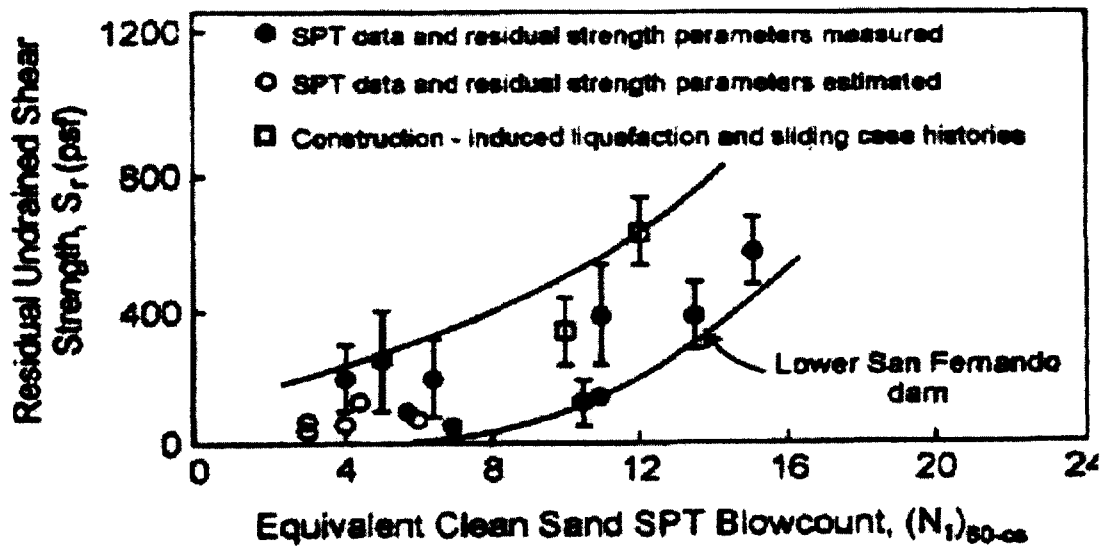
Figure I-10. Correlation between residual shear strength and $(N_1)_{60\text{-}CS}$ (R. Seed and Harder, 1990).

As can be seen, there are no data for $(N_1)_{60\text{-}CS}$ more than 15 blows per foot and the curve is sometimes extrapolated to obtain residual strengths for safety and hazard evaluation studies, and the major problem is the scatter in the data, so engineering judgment is required to select a value even if $(N_1)_{60\text{-}CS} <$ 15bpf.

17

In another study, the residual strength has been presented as a normalized function of the initial vertical effective pressure (σ'_{vo}), as shown in figure I-11 (Olson and Stark, 2003), where the authors show a correlation between the normalized SPT blowcount (N_1)$_{60}$ and the liquefied strength ratio (Sur/σ'vo).
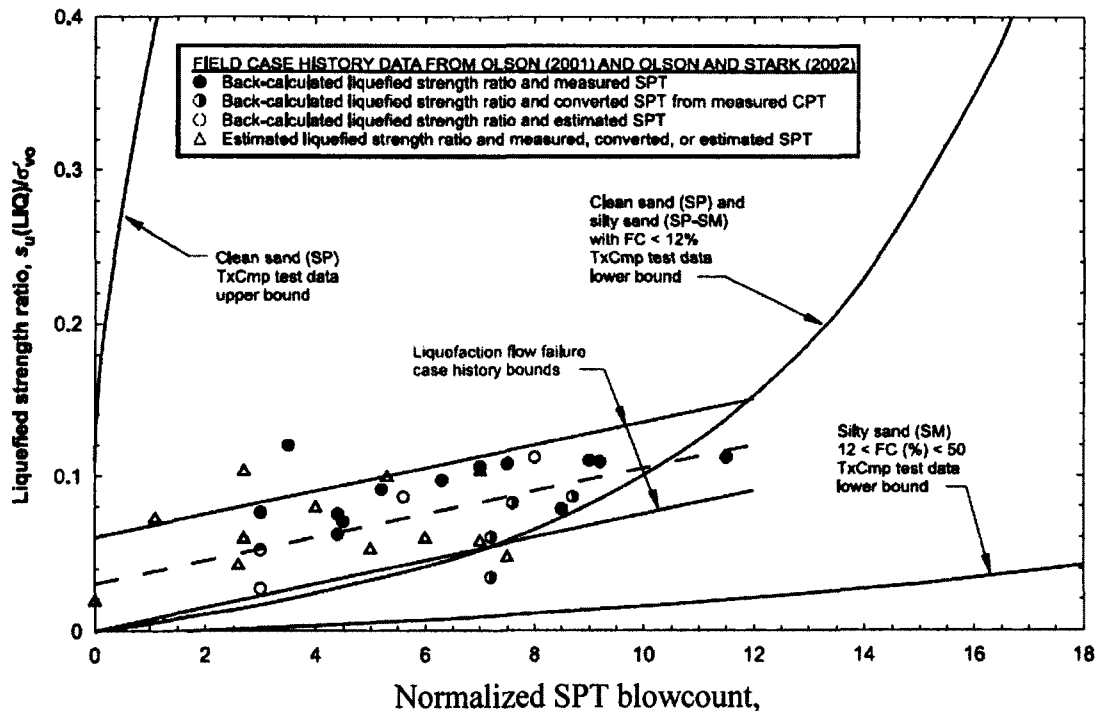
Figure I-11. Normalized SPT blowcount (N_1)$_{60}$ vs. liquefied strength ratio (Sur/σ'vo) (from Olson and Stark, 2003).

Liquefaction Flow Slides

As previously noted, liquefaction has been associated with rapid movement of soil masses (flow slides), since in such cases the soil shear

18

strength is reduced to its minimum value (S_{ur}), after the application of an external load (again, either cyclic or monotonic), and after initial conditions have been erased (i.e., fabric, initial relative density, etc). In fact, one of A. Casagrandes' first publications (1936) dealt with the stability of earth fills, where the massive slide of Fort Peck Dam was analyzed and much of our understanding of static liquefaction was drawn from this publication. Further review of case histories show that shear strains produced in flow slides can easily exceed 100% and the shear strain rate of the body can be in the order of 10 to 100 $\sec^{-1}$ (Bryant et al, 1983 as cited in de Alba and Ballestero, 2004). These numbers should be compared with those which can be obtained in the triaxial test; for example, in Castro's (1969) stress – controlled triaxial tests the shear strain rate was about 2 $\sec^{-1}$.

A different type of experiment with a triaxial cell, which should be mentioned, is the one carried out by de Alba and Ballestero (2004), which analyzes the post-liquefaction phenomena through a rheological approach, i.e., modeling the liquefied soil as a viscous fluid; the authors used a modified version of the triaxial cell: the height of the sample was increased to 24cm and the diameter was 7.1cm. The samples were prepared at low relative densities ($\approx$30%), and they had a plastic ball (1.27cm diameter) inside it, weighted by a load hanger (as shown in figure I-12). A cyclic load was applied and the excess pore pressure built up until sample liquefied; at that moment the ball started

moving through the liquefied sample and traveled to stop 2.5 cm above the base; this was done to lessen the effect of the boundary on the measured values.
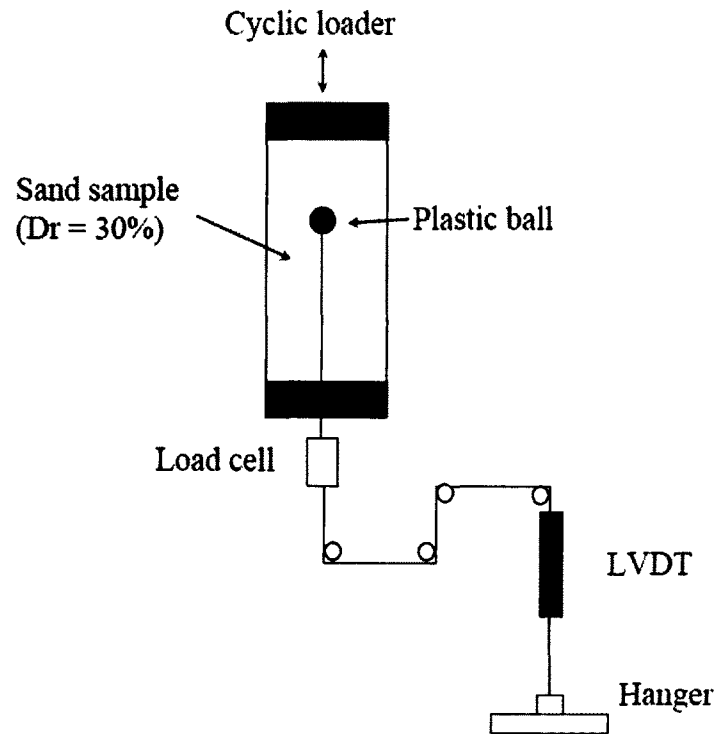
Figure I-12. Setup experiment of modified triaxial cell.

There are two important measurements during the test: displacement of the ball vs. time and resistance to flow (apparent drag) vs. time; these data are then used to calculate the velocity of the ball through the liquefied soil, and the variation in apparent drag with velocity.

The experiment was repeated several times at the same placement relative density at initial confining pressures of 70 and 140 kpa, using different

loads in the hanger; once the data was recorded, plots of velocity vs. time and velocity vs. apparent drag could be obtained; figure I-13 shows the results from tests at initial confining stress of 70 kpa (A) and 140 kpa (B).
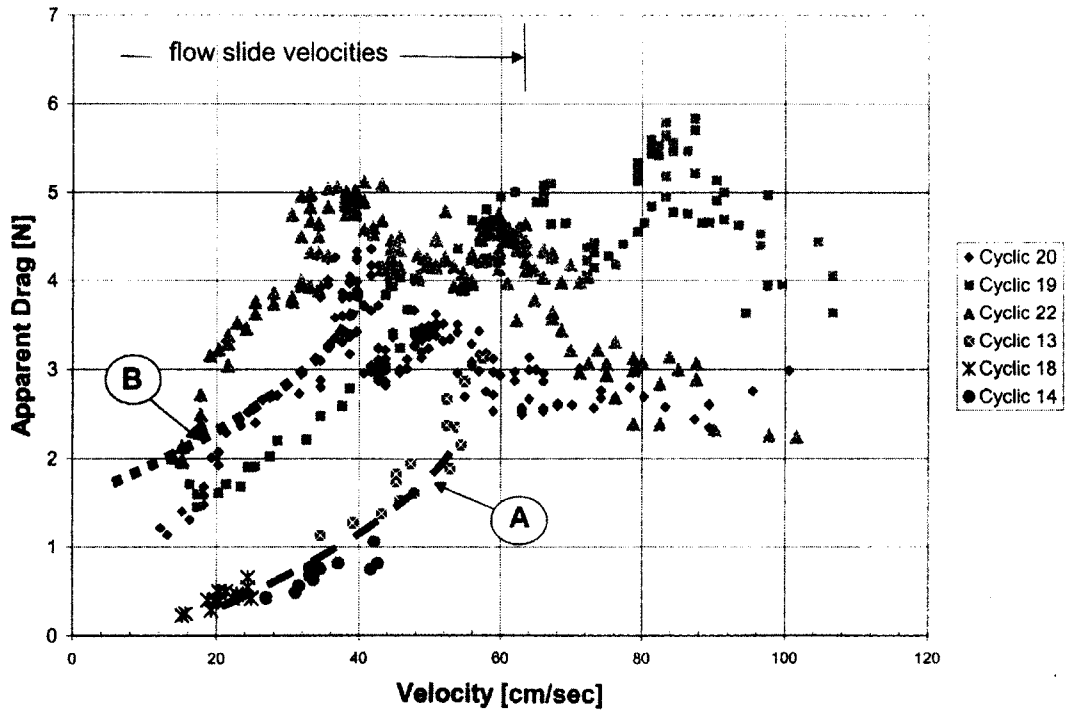
Figure I-13. Summary drag vs velocity, from modified triaxial cell at two different initial effective stresses, A: 70 Kpa; B: 140 Kpa (de Alba and Ballestero, 2004).

These tests showed that the large-strain behavior of liquefied sands needs to be studied by imposing large strains and strain rates on the specimen; however, in the de Alba and Ballestero tests shear strain rate could not be controlled, and total strains are limited to less than 300%.

Figure I-13 is an interesting one, and suggests that the drag (or resistance to flow) is not constant, but indeed depends on the velocity, i.e. the flow rate (rate

dependency) and it also depends on the confining pressure, which indicates that even at low velocities, there is a small resistance; this evidence led the authors to conclude that the behavior of liquefied sands could be modeled as non-Newtonian stress thinning fluid.

So far, the bulk of research carried out in order to understand the post liquefaction behavior has been conducted by inducing liquefaction failure in triaxial specimens. As stated in previous sections the conventional triaxial test does not model the large-strain and strain-rate behavior of liquefied sand. The de Alba and Ballestero modification can impose larger strain and higher strain rates, but cannot control the strain rate and is limited in the total strain that can be imposed. Therefore a different type of device has to be used, one that is able to impose "infinite" shear strains at high rates: the ring shear device (RSD).

The Ring Shear Device (RSD)

There exist several types of RSD: a famous version was developed in conjunction between Imperial College (UK) and the Norwegian Geotechnical Institute (Oslo) (Bishop et al. 1975), with a configuration similar to that of Hvorslev (1936). A modern version of the RSD can be used to measure residual strength of liquefied sands. The procedure basically consists in placing the saturated sample in a loose state (low relative density), applying a cyclic load

until excess pore pressure builds up and liquefaction occurs and finally measuring the shear strength of the liquefied sample.

K. Sassa RSD

Sassa (1996, 2002, 2005) and his co-workers developed the RSD depicted in figure I-14, which is intended to study the behavior of liquefaction in
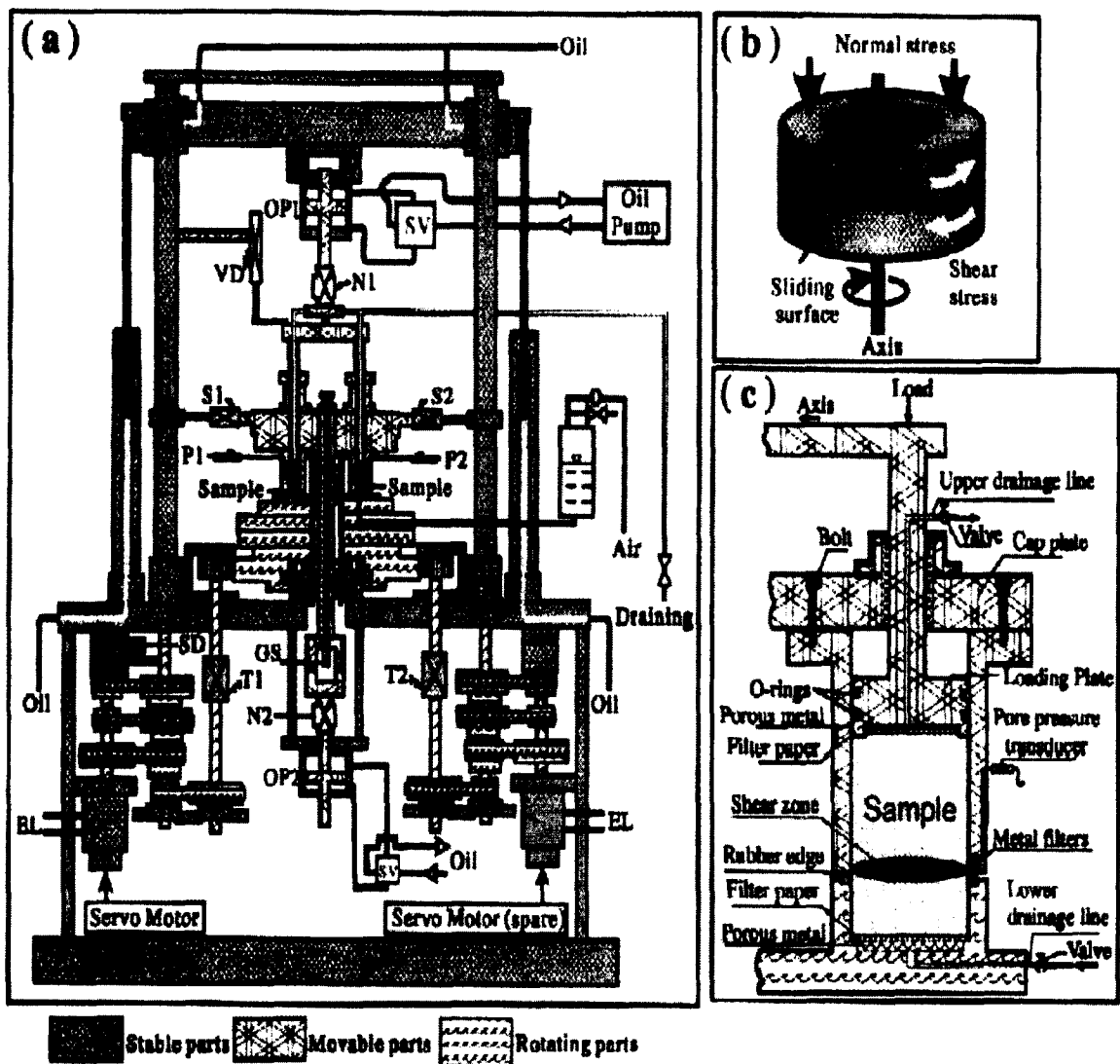
Figure I-14. Sassa's ring shear machine (Sassa, 2000)

narrow shear bands (Sassa, 2005). This device has the particular feature of having a pre-defined shear failure plane due to the ring being split at the centerline; a condition similar to the direct shear device, where the plane of failure is imposed. Also, it is important to note the complexity of the device, even though the economical aspect is unknown to the writer.

A typical result on a silica sand # 8 (fine sand; Dr=63.3%) sand from Sassa's machine is depicted in figure I-15 (Wang and Sassa, 2002); the figure shows the behavior of the pore water pressure development and the shear resistance with displacement and with time. Notice, even though very high pore pressures are generated, the liquefaction ratio (ru=generated pore water pressure / applied normal stress) does not reach a value of 100%, meaning that the sample may not be liquefied at all, or that the sample was actually dilating at large strain, instead of contracting; the initial confining pressure was 200 kpa (29 psi); a residual shear strength value of about 20 kpa (2.9 psi) is observed in figure I-15.a.

It is also important to mention that the velocity used by the authors to shear the sample is 10 mm/sec and did not apply any other value for subsequent tests. This means that a strain rate effect was not really investigated by the authors.

In a recent publication about this device Igwe, Sassa and Wang (2006) report the results of undrained tests, with an effective consolidation pressure of

250 kpa (36 psi) and a relative density of 29.5%. These results are depicted in figure I-16 and they indicate that in this case, the liquefaction ratio reached almost 100% (figure I-16a). An undrained residual strength of 2.2 psi is observed.
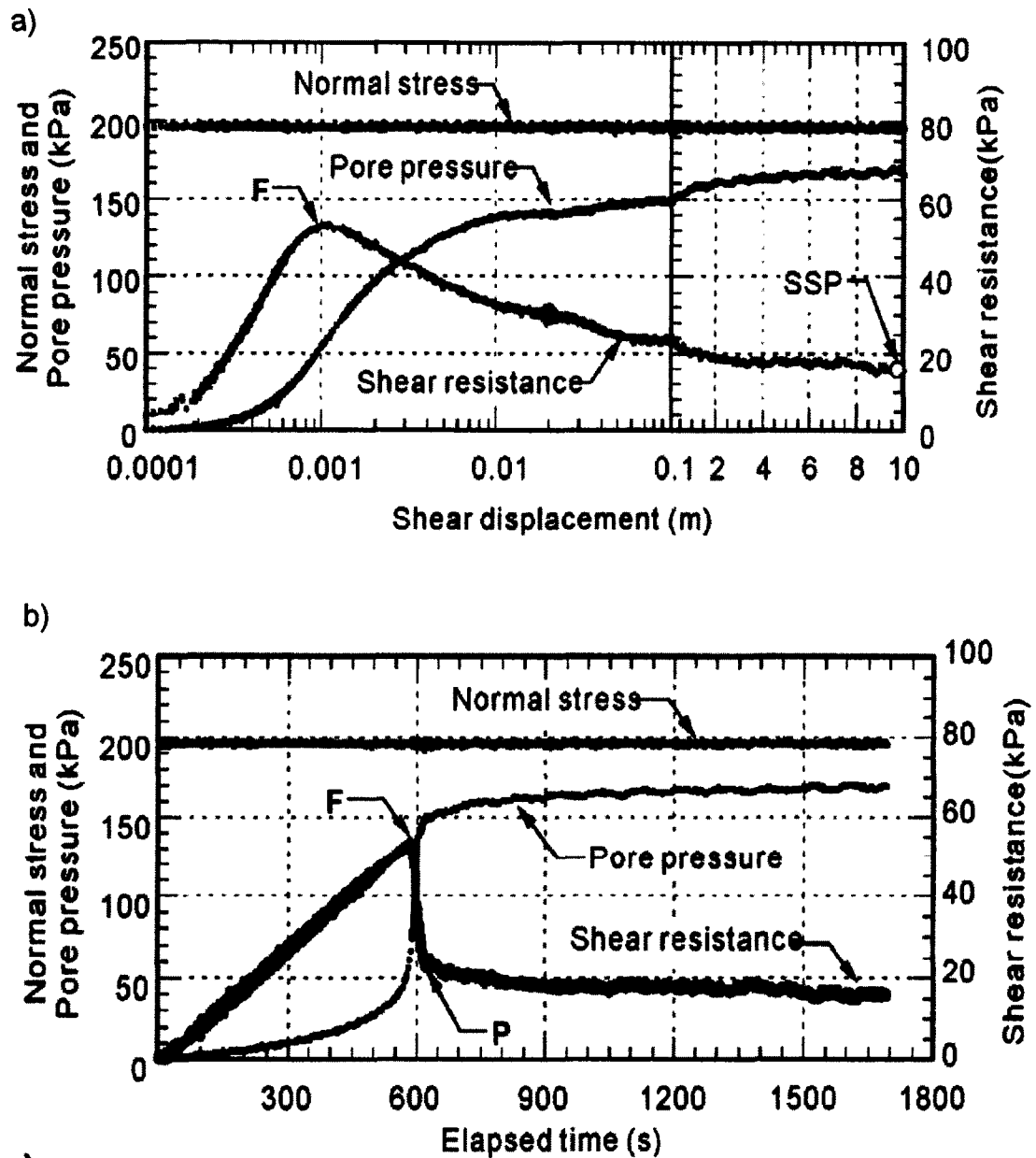
Figure I-15. Results from RSD on silica sand #8 (Dr=63.3%). a) pore pressure and shear resistance vs. shear displacement; b) vs. Time (Wang and Sassa, 2002) [F: point of peak strength; P: point where major strength decrease ends].
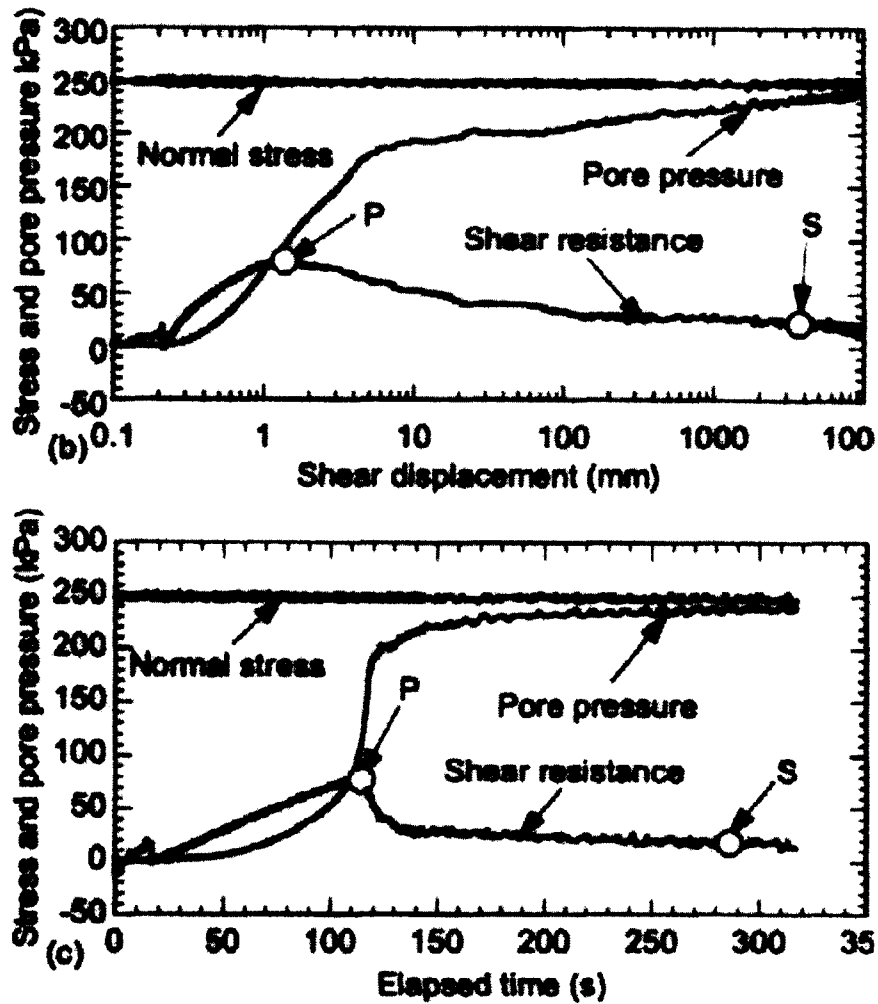
Figure I-16. Undrained response of well graded sand, Dr=29.5% (Igwe, Sassa and Wang, 2006)

University of Washington RSD

Another version of the RSD was developed at the University of Washington (Bennetts, 2003 and Kramer et al., 1999) and is depicted in figure I-17. It consists of a series of stacked metallic frictionless rings (outer diameter 18", inside diameter 13"); the uniform thickness of the sample is 2.5". A cross section of the sample is shown in figure I-18.

26

Figrue I-17. University of Washington ring shear machine (Bennetts, 2003)
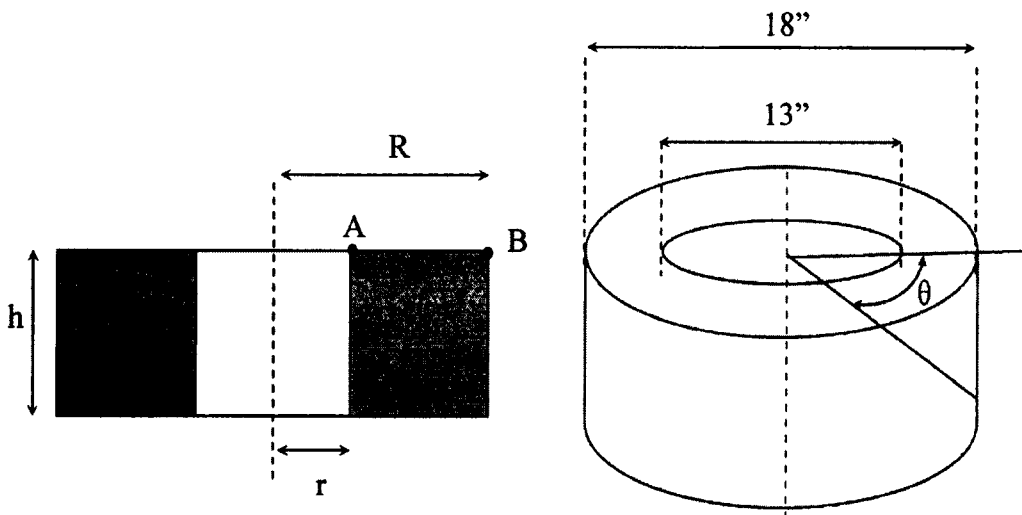
Figure I-18. Cross section of UWA ring shear machine (Bennetts, 2003) (not to scale).

If one wanted to calculate the shear strain (γ) at points A and B, it could be done so by using the following equations:

$\gamma_A = (r/h)\,\theta$, and

$\gamma_B = (R/h)\ \theta$,

θ in radians

Because the sample has a uniform thickness, a non-uniform shear strain is imposed along the sample. This is a feature that can be improved by the machine that is to be used for this project.

A typical result from UWASH ring shear machine is depicted in figure I-19. A residual strength of about 600 psf (4.2 psi) is observed; as in Sassa's study, the author argues that strain rate has no effect whatsoever on the residual strength and was not investigated, even though experimental evidence is not provided. As a consequence, a single strain rate is reported: 300 %/min.
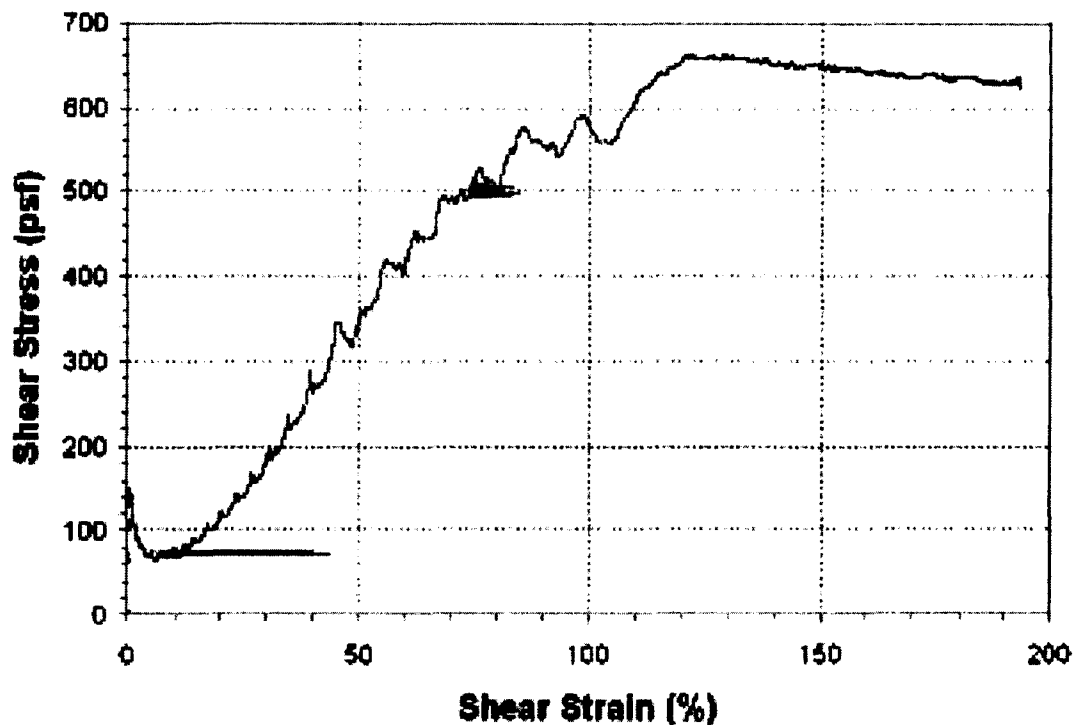
Figure I-19. UWASH RSD typical result on loose sand, Dr=38% (Bennetts, 2003)

28

Also, the author does not mention whether the sample was saturated or not and does not report pore water pressure information. The shear strain imposed during testing was reported as "...non-uniform. In the upper two-thirds of the specimen, large uniform shear strains were reached. In the lower third of the specimen, however, the shear strain was minimal..." (Bennetts, 2003).

Garga and Infante Sedano RSD

This version is a modified one of that designed by Bromhead (1979), and has a smaller section than that of the two devices described previously. A plan view and a cross section of this cell are shown in figure I-20.
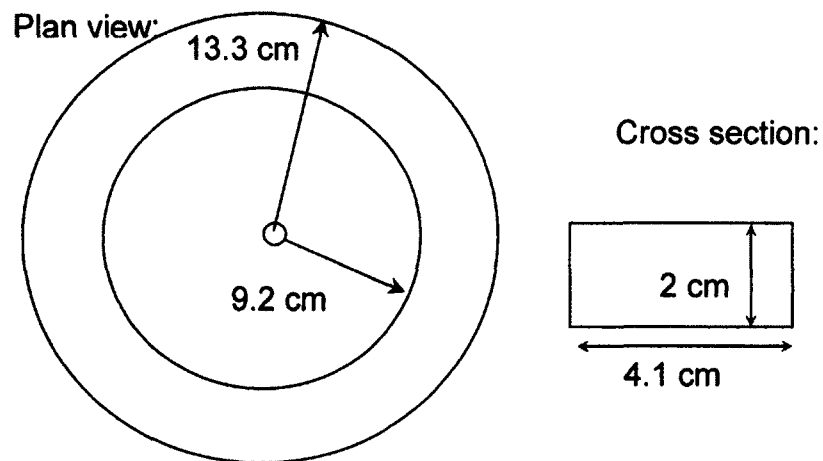
Figure I-20. Garga and Infante Sedano RSD version (Garga and Infante, 2002)

The load cell that reads thrust loads has a nominal capacity of 445 N, which gives room for about 250 kpa of external pressure (36 psi). Figure I-21 shows a typical result of this particular RSD machine. Since there is a vertical

displacement of the machine, a correction of the external pressure has to be applied during the test (that is why figure I-21 shows a change in normal stress), which means that it is a constant load type of test and that it would measure the undrained residual strength. The authors ran tests with both dry and saturated samples (no information about degree of saturation is provided).
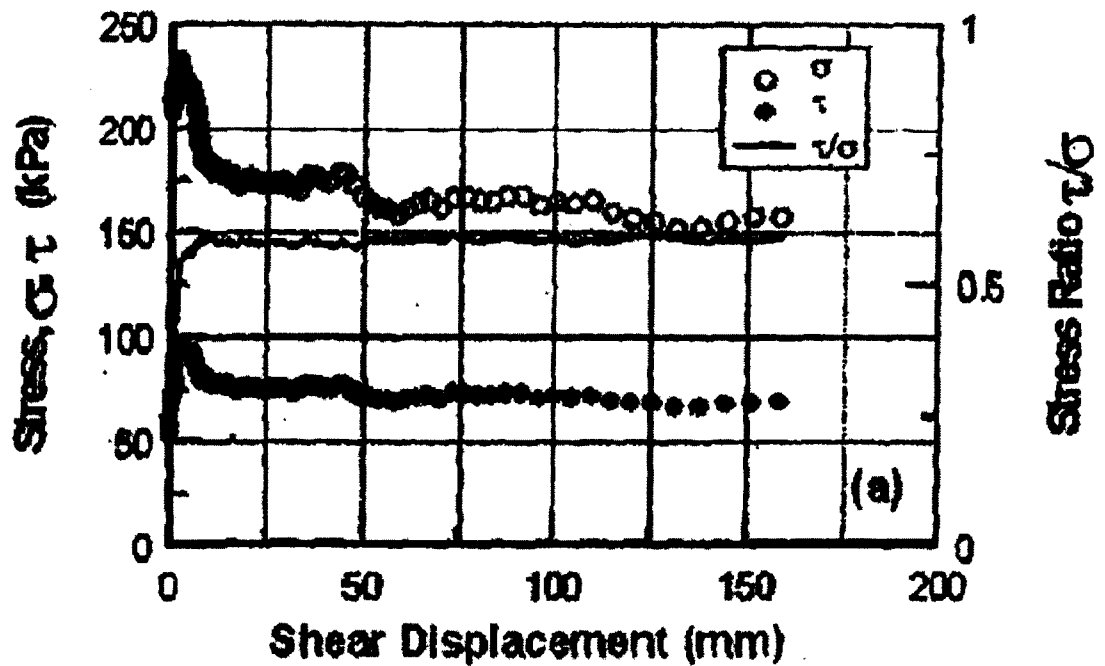
Figure I-21. RSD typical result for Unimin 2010 sand (fine sand), void ratio: 0.916. (Garga and Infante, 2002). Open circles: effective stress; closed circles: shear stress; continuous line: stress ratio.

According to the figure, a maximum displacement of 10cm was reached and a constant value of the stress ratio (τ/σ) of 0.6 was achieved, which would translate into 80 kpa of residual strength (11 psi). No relative density is reported. The placement void ratio was e=0.916.

Also, it is important to mention that Infante (1998) explored the effect of the strain

rate, using a maximum 1.75E-3 sec^{-1} (60°/min); the author reports no influence of strain rate on residual strength. However, velocities in flow slides can be at least 1000 times larger than the speed used by the author, which makes the test not suitable to model a real flow slide.

Even though the failure plane was not predetermined, it was observed that due to crushing of the particles, a failure plane might have been originated at the middle of the sample. This was found by excavating the sample in horizontal layers and performing sieve analyses with each layer.

Table I-1. Comparison of main aspects of three ring shear devices

	Sassa (1)	Sassa (2)	UWashington (3)	Garga and Infante (4)
Soil reported	Silica sand # 8	Industrial well graded sand	Unimin 4060 sand	Unimin 2010 sand
Test condition	Undrained	Undrained	Drained	Undrained (?)
Sur (psi)	2.9	2.2	4.2	11.0
Effect of strain rate on Sur?	NO	NO	NO	NO
Strain rate (1/sec)	7.1	7.1	0.31	1.75E-3
Relative density (%)	63.3	29.5	38	-
Void ratio	1.15	-	0.944	0.916

(1): Wang and Sassa (2002)
(2): Igwe, Sassa and Wang (2006)
(3): Bennetts (2003); Dr was calculated based on information found in reference
(4): Garga and Infante (2002) and Infante (1998)

The previous table summarizes the main characteristics of the three machines cited.

CHAPTER II

MATERIAL PROPERTIES AND SAMPLE PREPARATION TECHIQUE

This chapter is intended to describe the properties of the material used during testing and the sample preparation technique that was implemented for the ring shear chamber.

Material Properties

The material that was selected for this dissertation is washed and sieved fine sand "Holliston 00" (from Holliston Sand Co., Holliston MA), with the sieve curve (figure II-1).

The material is classified as SP according with the USCS nomenclature and has the following properties, based on Figure 1:$D_{50} = 0.3$mm

Cc = 0.89

Cu = 2.2
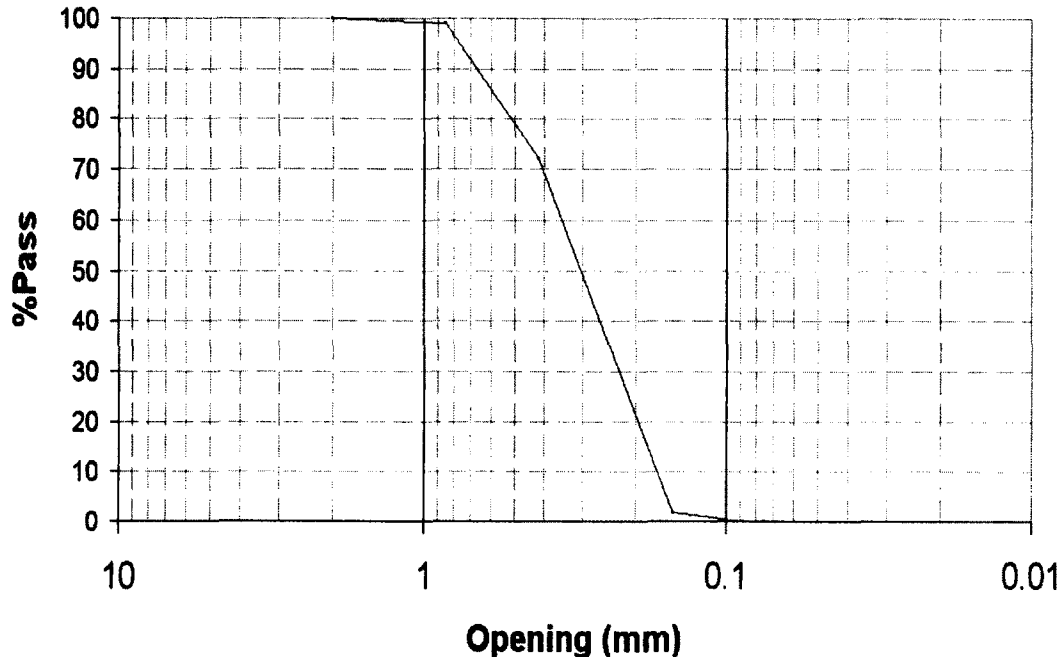
Figure II-1. Sieve analysis curve for Holliston 00 sand.

The maximum and minimum void ratios were measured in accordance with the Japanese standard test (JIS A 1224):

$e_{max} = 0.936$

$e_{min} = 0.601$

$\gamma_{max, dry} = 103$ pcf

$\gamma_{min, dry} = 87.4$ pcf

Sample Preparation Technique

There are two aspects that are to be explored with respect to the sample preparation technique: the uniformity of the sample in terms of the

33

relative density and its effect on the undrained behaviour of saturated sands. Both aspects will be analyzed separately.

There are three methods available to prepare samples for testing: moist tamping (MT), water pluviation (WP) and dry pluviation (DP).

The moist tamping (MT) technique consists in placing the moist sample in layers, usually 5, in triaxial specimens (Vaid et al., 1999), until the target relative density is obtained. This method has proven to produce non-uniform samples, especially if low relative densities are desired, because the compaction of a layer would induce more energy to the soil below it; as a consequence, a non-uniform relative density would be obtained. Some researchers have implemented undercompaction, which consists in placing layers at lower relative densities so when the upper part is formed, it would increase the packing of the lower layers. (Naeini and Baziar, 2001). Figure 2 shows a profile of void ratio with depth of Fraser river sand (Vaid et al., 1999) prepared using the MT technique.

Air and water pluviation have been used successfully to reproduce the sedimentation process of the soil; research by Mulilis (Mulilis et al., 1977), Emery (Emery el at., 1973) and the writer show that pluviation methods can provide uniform samples, and that water pluviation produces lower relative densities than air pluviation.
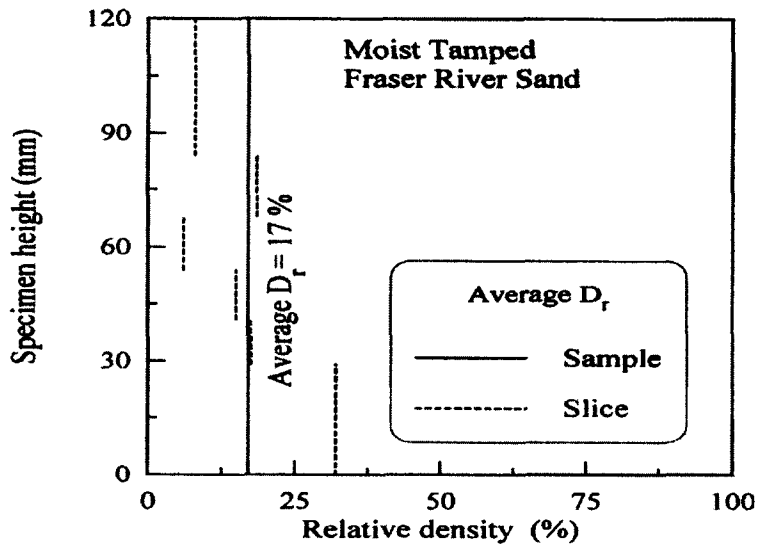
Figure II-2. Uniformity of reconstituted specimen with MT technique (after Vaid et al, 1999).

Vaid and Negussey (1988) suggest that the particles can be modelled as free falling spheres to investigate the effect of the height on the velocity (see figure II-3) by using the basic equation of motion of a body under free fall:

$$ma = mg - V\rho g - C_d \rho A \upsilon^2/2 \quad\text{...}(1$$
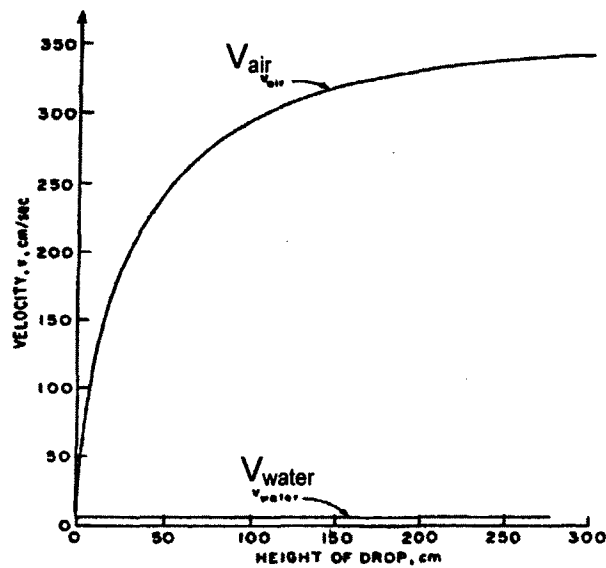
Figure II-3. Velocity of a free falling sphere in air and water (D_{50}=0.4mm) (Vaid and Negussey, 1988).

35

Where

a: particle acceleration

g: gravitational acceleration

V: volume of particle

A: projected area of particle

υ: particle velocity

C_d: drag coefficient, which depends on Reynolds number.

The authors also studied the effect of the size of the sphere on the velocity (figures II-4 and II-5).
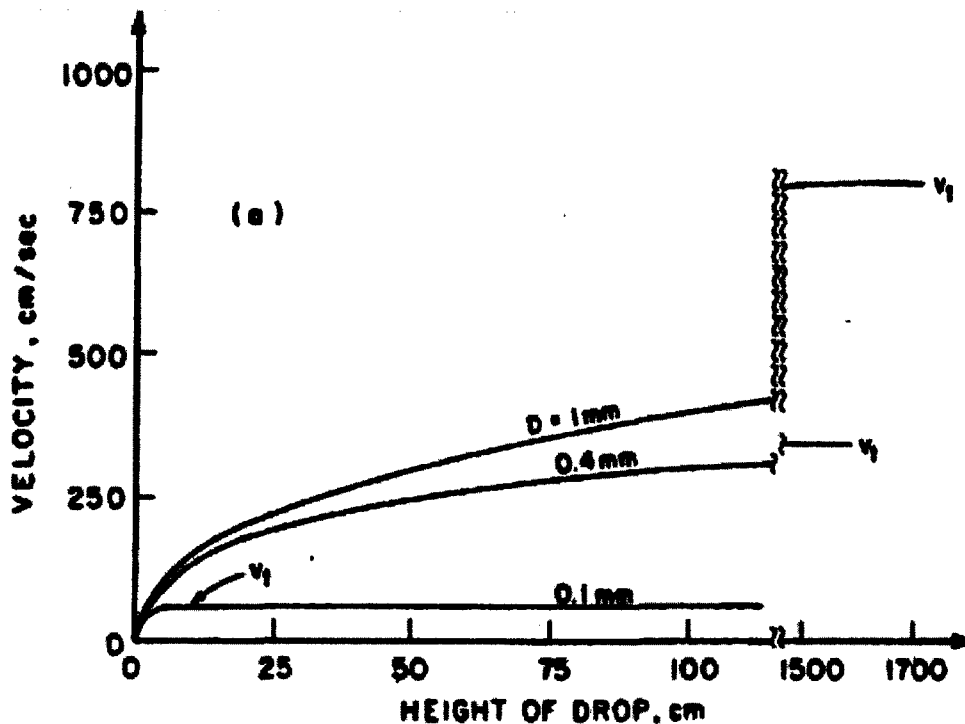
Figure II-4. Velocity of free falling spheres of different diameters, in air (Vaid and Negussey, 1988).
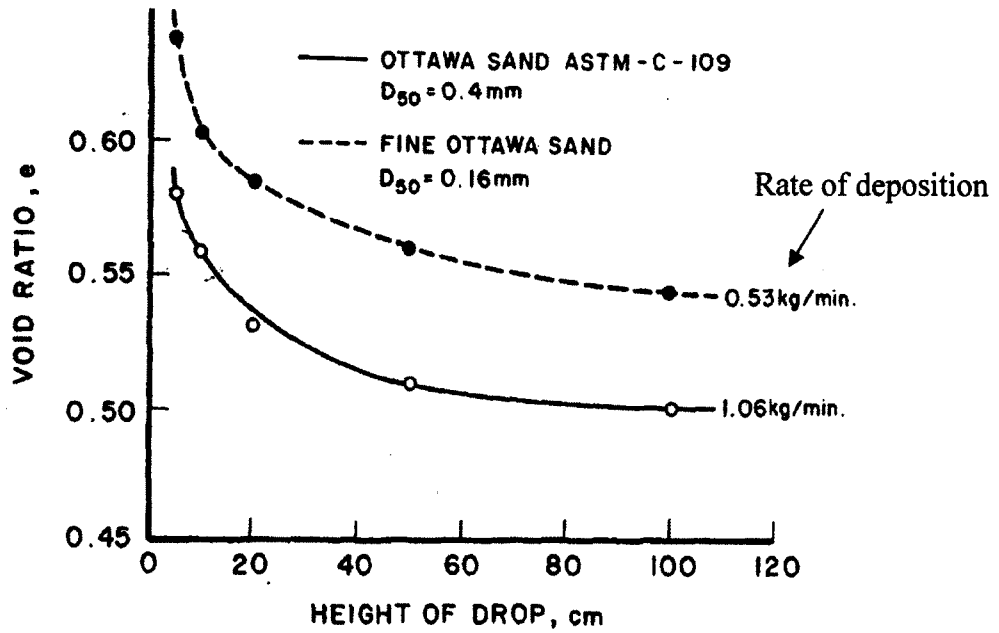
Figure II-5. Particle size and height of drop effect on void ratio, in air (Vaid and Negussey, 1988).

Previous figures suggest that in water pluviation, particles reach terminal velocity at lower heights than in air pluviation (0.2 cm, in water) and that relative density is directly proportional to the drop height: high relative densities are achieved when drop height is increased, and vice versa. However, it is also noted (as was also concluded by Mulilis, 1975) that the rate at which the relative density increases is diminished as the drop height increases (e.g. H> 50cm, figure II-5).

The effect of sample preparation technique on the undrained behaviour (and on the steady state strength –Sur-) of granular soils has also been evaluated and well documented by several researchers at shear strains less than 30% approximately, using different devices that try to model the sample when

subjected to cyclic or monotonic loads: triaxial test, direct shear test, etc. The

effect of sample preparation on the undrained behaviour of sand is illustrated in

figure 6 (Vaid et al., 1999), where a series of results from anisotropically

consolidated undrained compression triaxial tests on loose Fraser River sand are

compared using two different methods (water pluviation and moist tamping) and

the same state of stress.
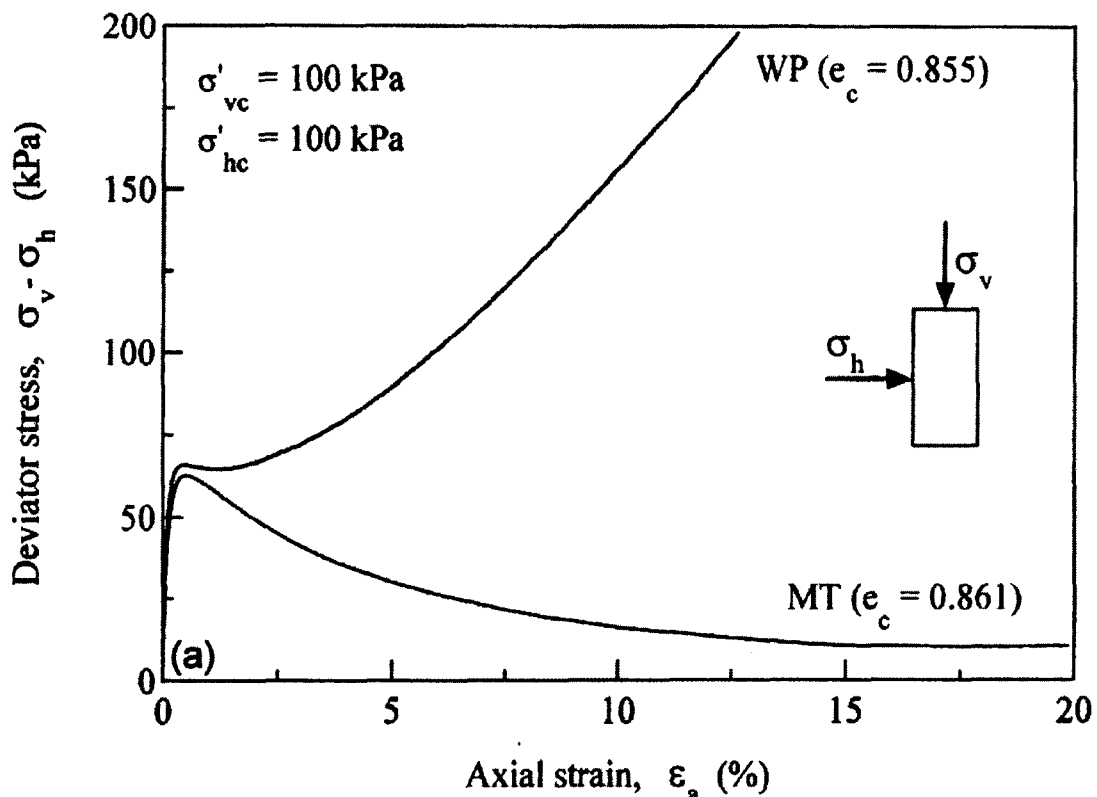
Figure II-6. Effect of sample preparation technique on undrained response of loose Fraser River sand – conventional compression triaxial test (Vaid et al., 1999).

Note, the moist tamped sample shows a contractive behavior (strength

reduces to about 7 kpa) and the water pluviated sample shows a dilative

behavior (strength increases as load is applied).

A similar trend is observed when two saturated sands (Syncrude sand and Fraser River sand) are subjected to undrained simple shear: water pluviated samples show higher shear strength than air pluviated or moist tamped samples (figures II-7 and II-8).
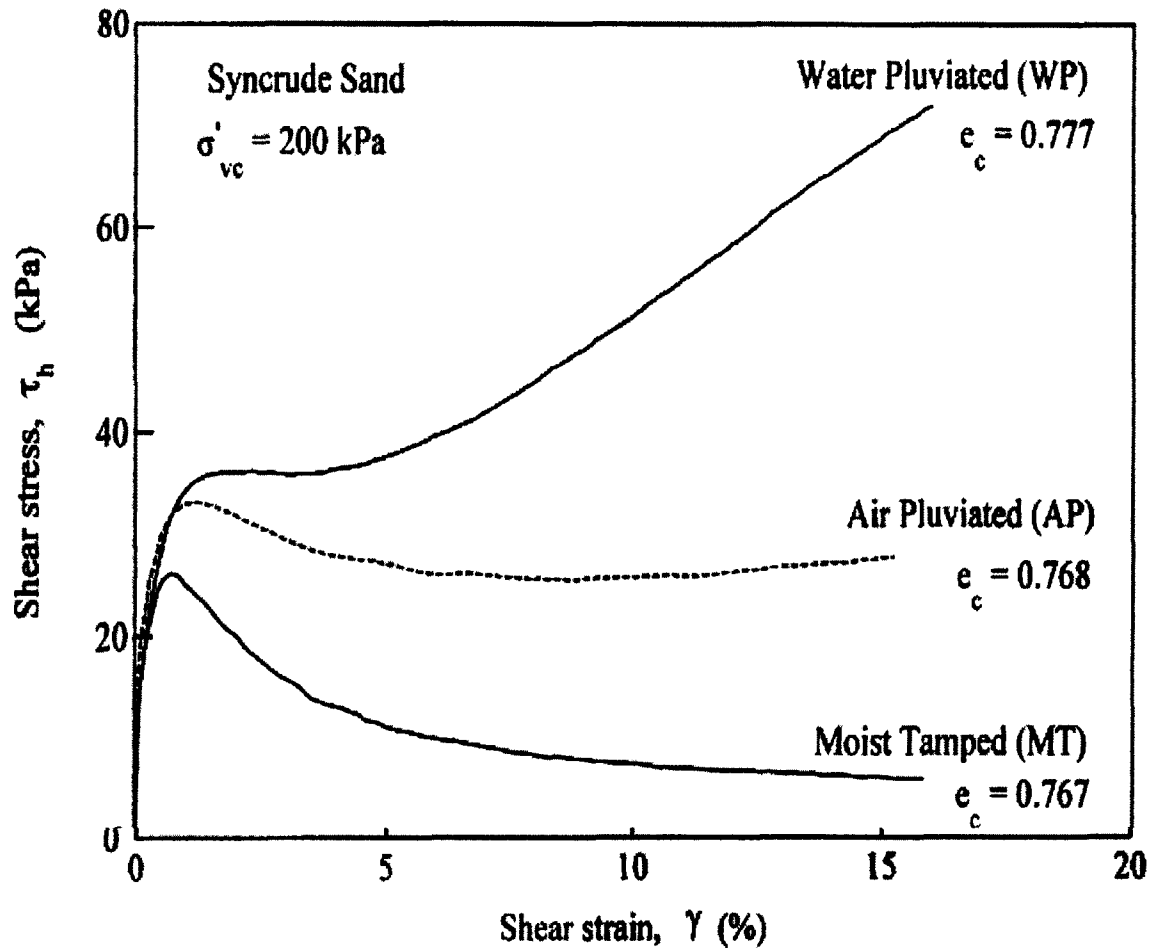
Figure II-7. Response of Syncrude sand under undrained simple shear (Vaid et al., 1999).

Previous paragraphs describe methods that have been used with triaxial cell and with simple shear; tests in the case of the ring shear device (RSD), these methods can also be implemented.
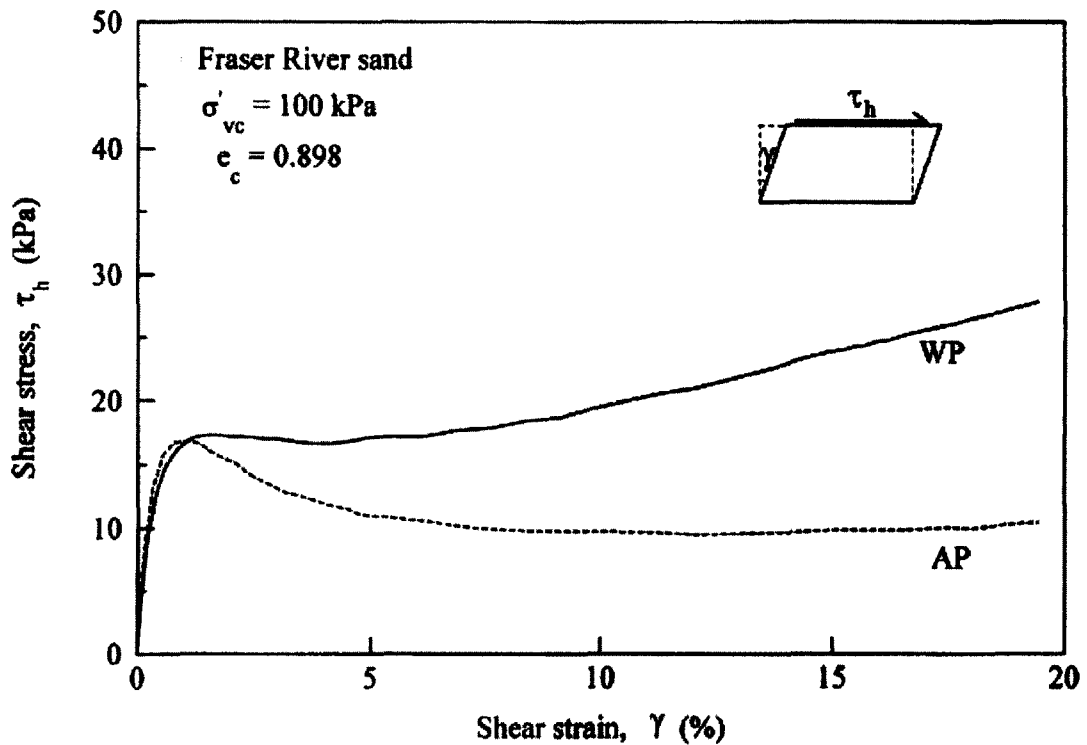
Figure II-8. Response of Fraser river sand under undrained simple shear (Vaid et al., 1999); AP: air pluviated; WP: water pluviated.

Sassa and his co-workers report using moist tamping (MT) and dry pluviation (DP) (Wang and Sassa, 2002). Relative densities in the range of 61% to 95% were reported in his 2002 study. However, the issue of the uniformity of the sample along its area or/and its volume does not seem to be addressed by the authors.

Sample Uniformity

The University of Washington version of RSD has included a procedure to check the uniformity of the sample, which consists in impregnating the sample

with a gelatine solution for relative density measurement upon drying. Figure II-9

shows the results from the gelatine impregnation technique with respect to void

ratio.
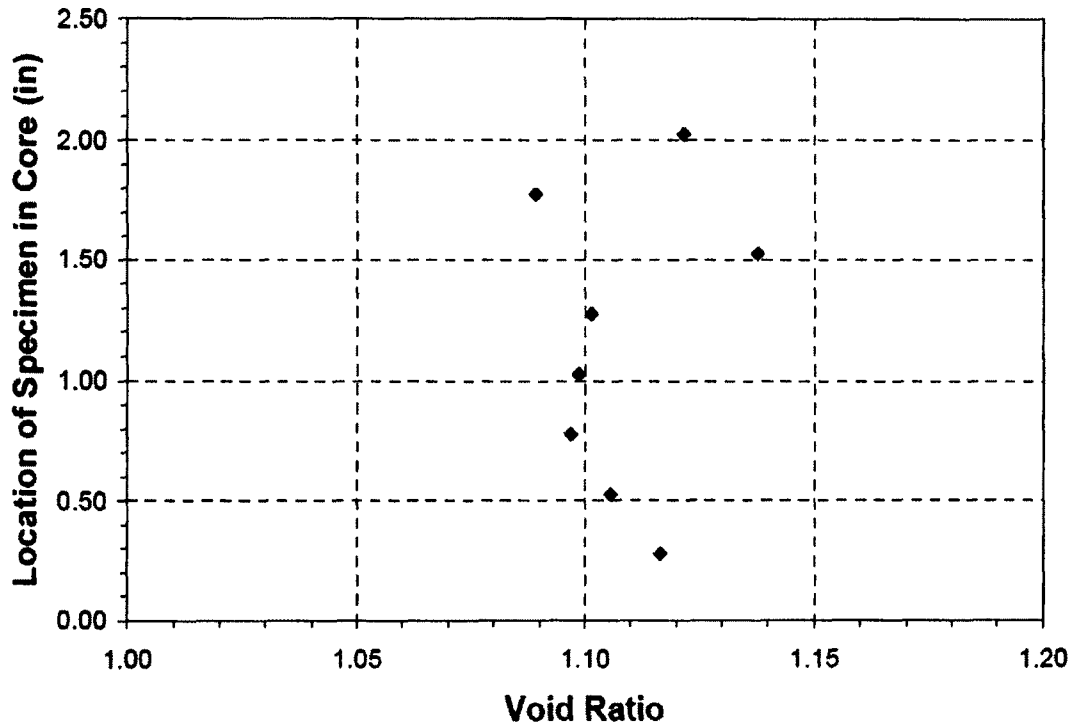
Figure II-9. Void ratio determined by gelatine impregnation (Bennetts, 2003).

The author (Bennetts, 2003) reports some discrepancy between the

average void ratio and the one obtained with the gelatine impregnation and some

scatter, as shown in figure II-9. Such scatter is attributed to the handling process

that the sample is subjected to during impregnation.

Garga and Infante (2002) used a version of the gelatine impregnation

technique to check the uniformity of the sample in the ring shear chamber. The

authors impregnated the entire sample, in an acrylic dummy cell of the same dimensions as the test cell and found a relative density variation within 2% of the average, for dry pluviation, and 3% for water pluviation (sample was extruded in slices, 2.5mm thick).

For this project, a couple of details were implemented from other versions: a plastic dummy ring cell and the gelatine impregnation technique. Initially, the water pluviation method was implemented and an acrylic hopper was used to pluviate the soil (Holliston sand) into the dummy cell, filled with water (figure II-10).

Figure II-10. Dummy cell and hopper for water pluviation

The hopper has two ¼" wide square-opening screens, mounted one over the other, which reduces the velocity at which the sand is deposited (figures II-10, II-11 and II-12); the screens are aligned so there is an offset to reduce the size of the openings. Additionally, three small metallic containers, for which the volume was determined previously, were placed in the bottom of the cell and levelled with modelling clay.

To pour the sample into the cell, the hopper was filled with sand and a small acrylic plate prevented it from pouring; when ready to start the deposition, the plate was removed and the hopper was rotated at a given speed (0.33 rev/min) over the water – filled dummy cell.
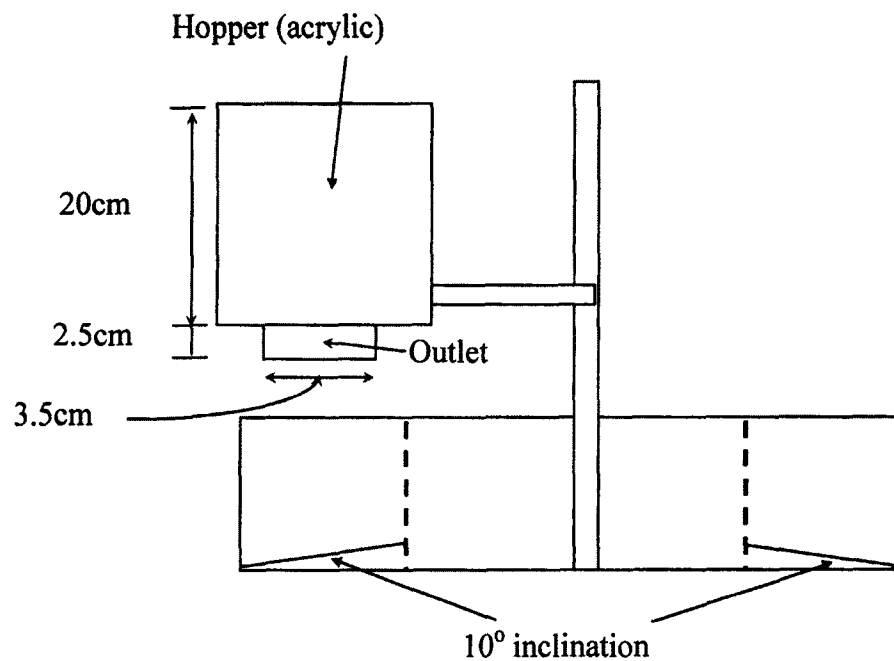
Figure II-11. Sketch of dummy cell and acrylic hopper.

Once the procedure was complete, the containers were removed from the cell, oven dried and weighed for relative density calculations.

This procedure was repeated several times and relative densities in the range of 6% to 10% were achieved. Also, it is noted a difference within 5% between containers, which suggest that the sample is not uniform along the cross section of the cell.
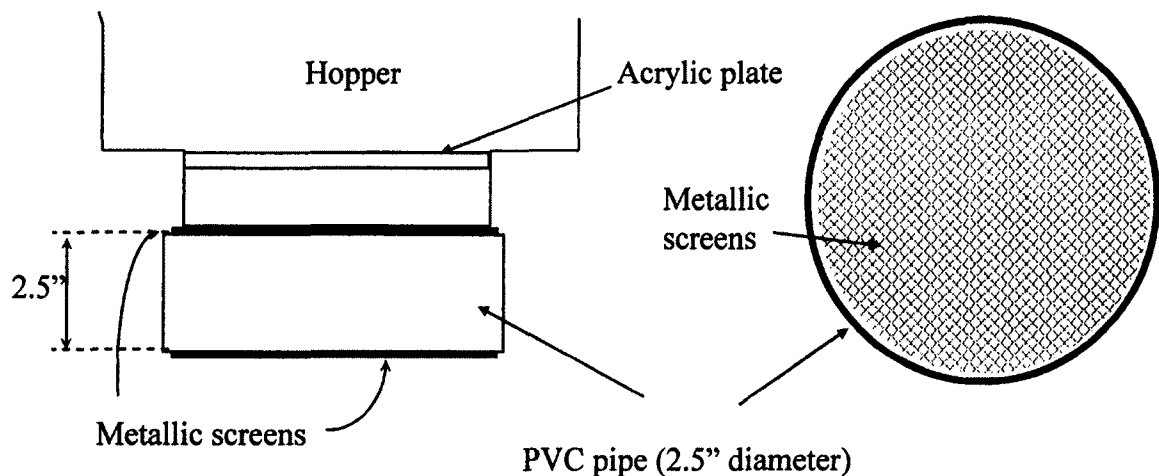
Figure II-12. Detail of metallic screens and plate.

Consequently, a dry pluviation technique was implemented because previous method would result in segregation in case soils with fines are tested, because the samples are not uniform and because of the difficulty in attaching the hopper to the device. The dry pluviation procedure is similar to that used for triaxial samples, except that the rainer is circular (figure II-14).

Figure II-13. Hopper outlet (bottom view) and dummy cell

The rainer has two metallic screens (opening size: 0.5mm) and they are placed so there is an offset of about 2.5mm. It has the same dimensions of the base of the cell so it can be placed into it, and then the soil is deposited with a scoop; the rainer is pulled up slowly to keep the drop height as small as possible and constant all the time.

Once the sample was deposited, a nozzle and a vacuum cleaner were used to level the surface of the sample.
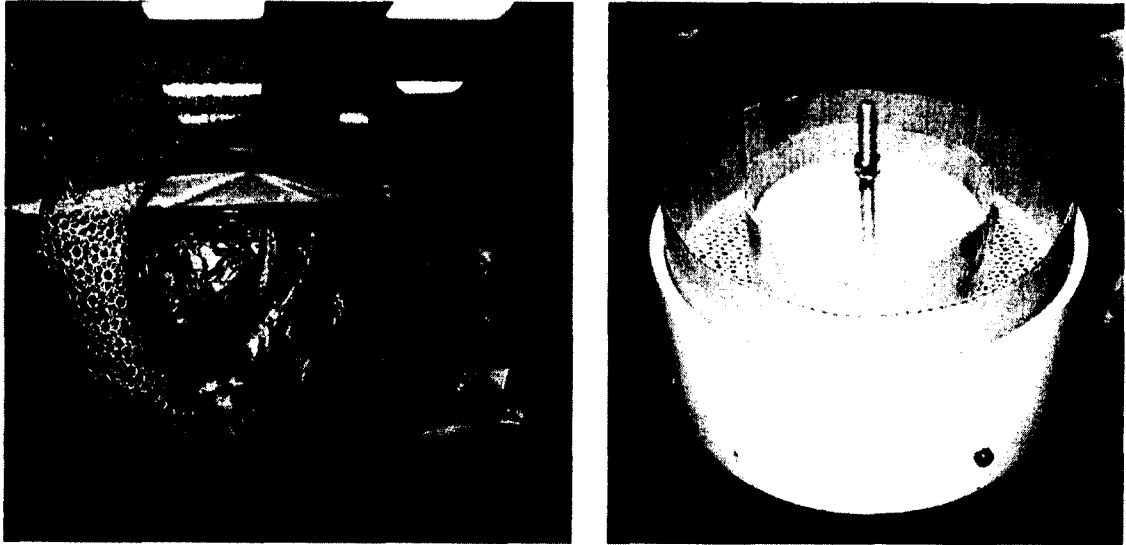
Figure II-14. Rainer and dummy cell for dry pluviation.

An acrylic plate with three fitting holes was placed on top of the sample, to attach the hoses that are to be used to inject the gelatine solution (3% to 4%), as shown in figures II-15 and II-16.

Top plate (Acrylic)
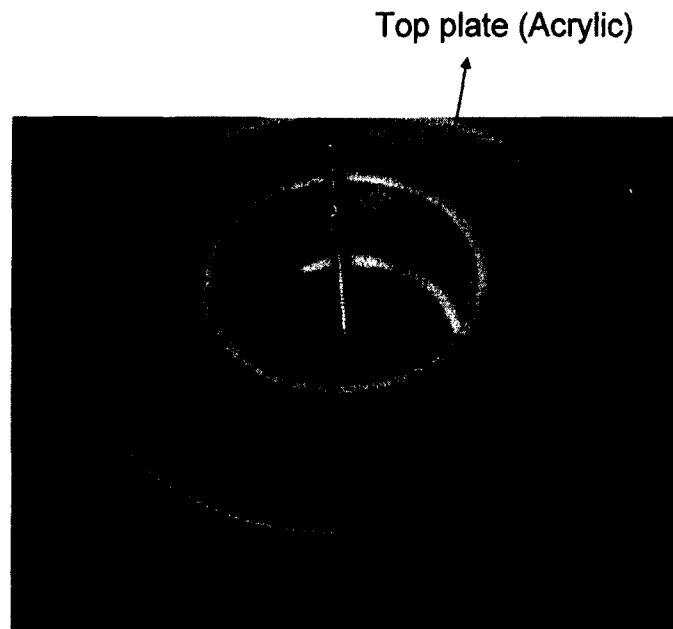
Figure II-15. Top plate with fittings.
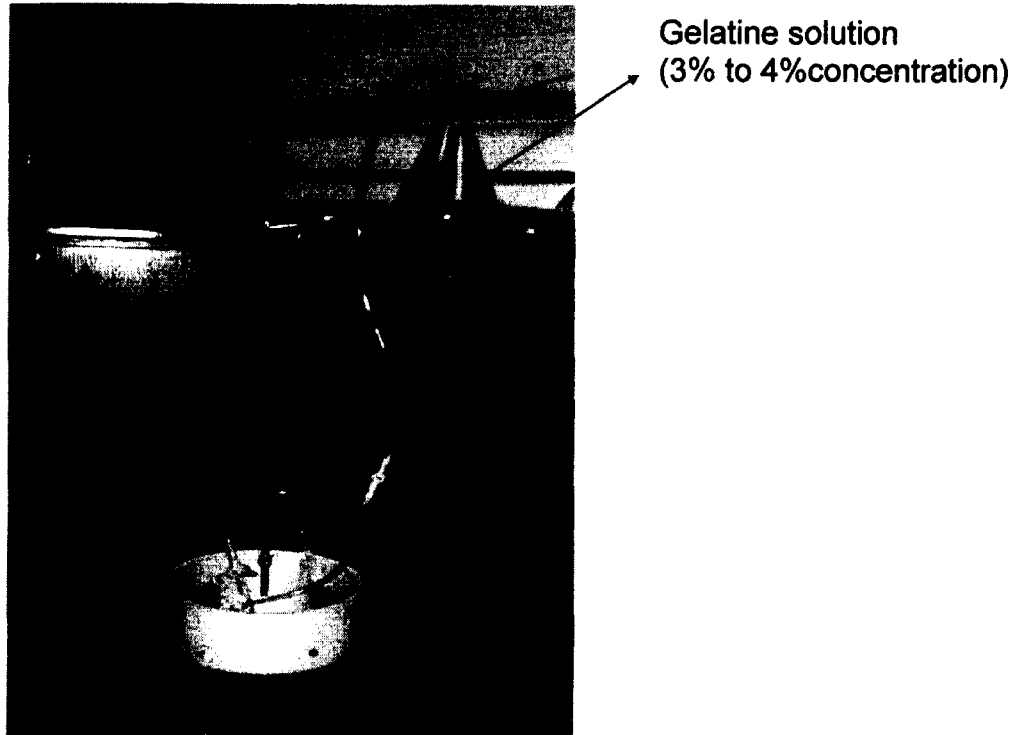
Figure II-16. Gelatine impregnation.

Once the impregnation was finished, it was recommended to put the cell in a refrigerator for about 20 hours to help the solidification of the gelatine, after which the sample could be extruded for relative density measurement (figure II-17).

Since the sample was solidified, the relative density can be calculated similarly as the bulk density:

- Weigh sample

- Calculate volume of sample by water displacement

- Rinse the sample, remove the gelatine and dry it to obtain the dry unit weight

- Use dry unit weight to calculate relative density:

$$Dr = [(1/\gamma_{min} - 1/\gamma_{dry})] / [(1/\gamma_{min} - 1/\gamma_{max})] * 100$$

Figure II-17. Solidified sample after impregnation.

Since the uniformity of the sample was to be explored in both horizontal and vertical directions, several chunks could be extruded to calculate the relative density. Several tests were run and densities in the range of 26% to 29% are achieved. Figure II-18 shows the spreadsheet used for calculations.

#	(gr) Wwire	(gr) Wsample	(gr) Wwire.sub	(gr) WsoilSubm	(gr) Wsieve	Wsieve+ dry soil	(cc) Vwire	(cc) Vsample	(gr) Wdry.soil	(gr/cc) UW	e	% Dr
1	14,1	920	11,9	426,1	347	1055,8	2,2	493,9	708,8	89,55076	0,846551	27,24635
2A (top)	14,1	335,3	11,9	159,4	341,2	590	2,2	173,7	248,8	89,37893	0,8501	26,16865
2B (bot)	14,1	630,5	11,9	267,1	340,3	860,5	2,2	363,4	520,2	89,32438	0,85123	25,82565
3	14,1	662,4	11,9	340,9	347	808,9	2,2	321,5	461,9	89,65026	0,844501	27,86856
4A (top)	14,1	268,24	11,9	135,49	341,2	528,3	2,2	130,55	187,1	89,42964	0,849051	26,48716
4B (bot)	14,1	504,4	11,9	240,39	340,3	720,3	2,2	264,01	380	89,81478	0,841122	28,89424
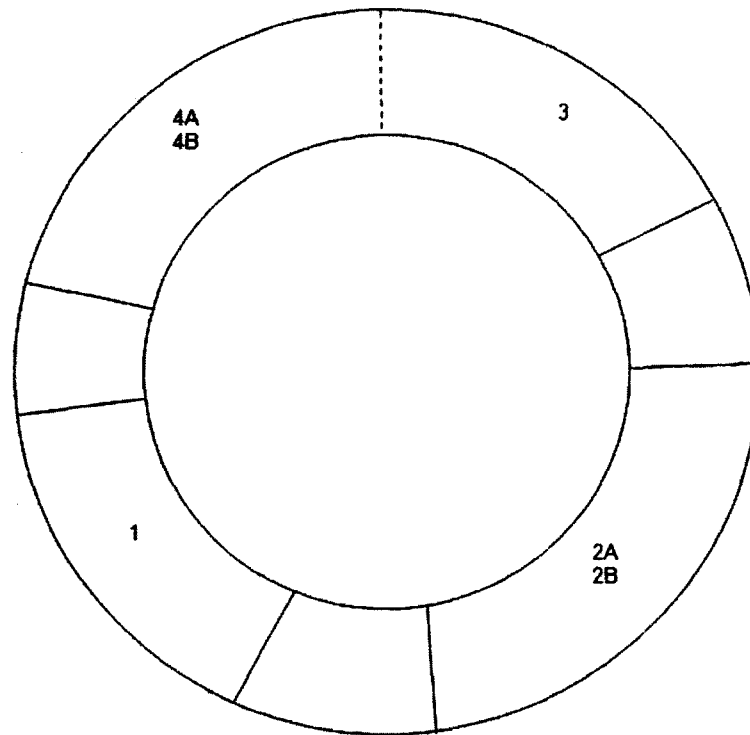
Figure II-18. Spreadsheet used for calculations.

Also, measurements show that similar results are observed in the two directions; this is due to the fact that the thickness of the sample is not more than 1".

Sample Preparation in the Real Ring Shear Cell

Previous methods were implemented with a dummy cell. For the test dry-pluviated samples, more precise total volume measurements were required since impregnation to measure density was not possible; two acrylic dummies (of known height) were used to obtain the average height of the specimen (see figure II-19).

a)

b)
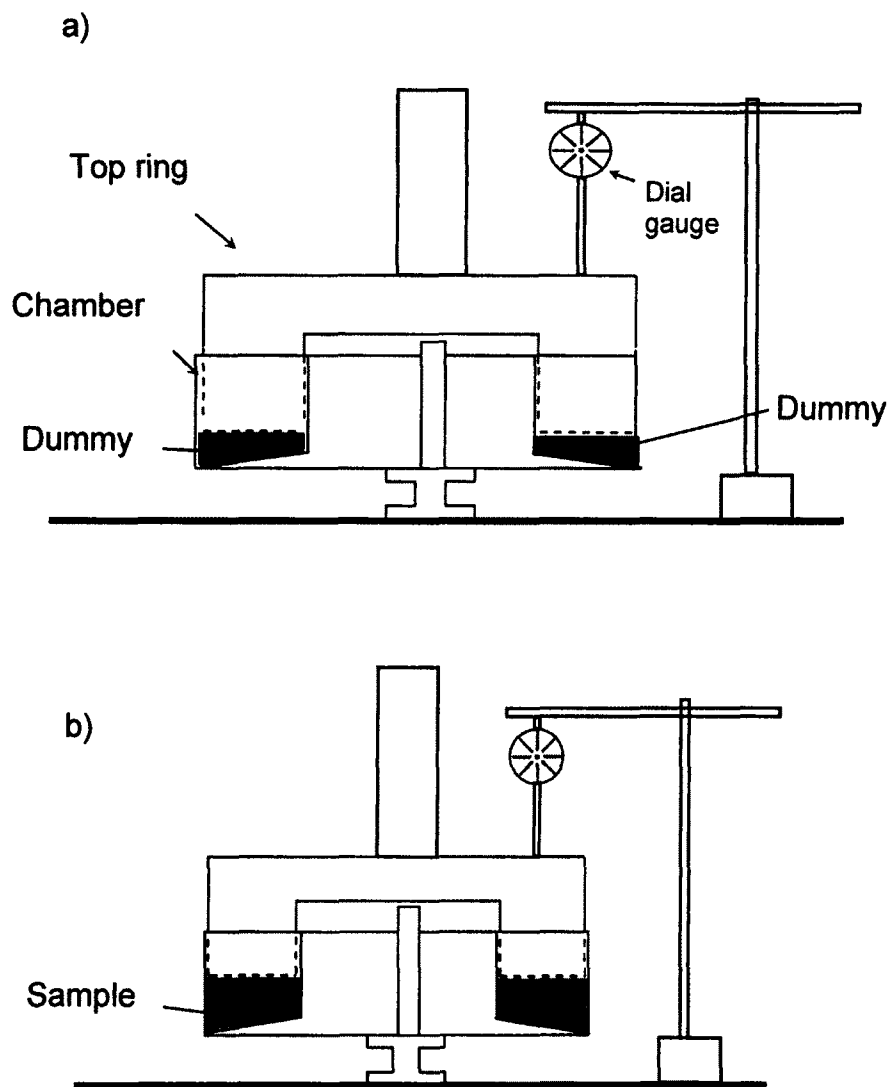
Figure II-19. Readings on dummies (a) and on sample (b) to find the height of the sample.

The following procedure is recommended to prepare the sample and to measure the relative density (see figures II-19 and description of the machine, chapter III):

1. Clean the chamber so no excess sand is involved in calculations.

2. Remove o-rings from top ring and place them to one side.

3. Place the two dummies in chamber and bring top ring down.

4. Apply a vertical pressure similar to that to be used during testing (i.e. 2000 lbs on Labview display – or 2.5 psi on the bladder pressure regulator) and take readings with a dial gauge to 0.001" of an inch (2 readings in opposite sides of the top ring).

5. Lift top ring and remove dummies.

6. Insert rainer in cell.

7. Deposit sand with scoop.

8. Pull the rainer up slowly and keeping a constant speed.

9. Level the surface using the nozzle and a vacuum cleaner (see figure II-20).

10. Clean any excess sand around the walls of the chamber.

11. Wash, lubricate and place the o-rings back in the top ring.

12. Bring top ring down and apply external pressure.

13. Take readings on sample using the same dial gauge and placing it at the same locations as before.

14. Use difference with known dummy height to obtain average height of sample.

Figure II-20. Nozzle to level the surface of the sample.

After testing, the sample has to be totally removed from the cell, dried and weighed; this value is used with the volume calculated from step 14 to obtain the relative density of the sample.

CHAPTER III

DESCRIPTION OF THE MACHINE

The basic machine was designed and built at the University of New Hampshire by a team of senior mechanical engineering students as a capstone design project (team members are listed in Appendix A) under the supervision of Professors Barry Fussel and Pedro de Alba, and the writer. Progressive improvements to the original design were made by the writer as discussed in the following sections.

The UNH ring shear device (RSD) shares several characteristics of other versions of the machine: an annular chamber containing the sample, a top ring that can be moved either cyclically or monotonically to provide shear stresses at the top of the sample, a motor that drives the top ring, etc. Some of the characteristics of this particular design are intended to improve small details of other versions, such as using non-uniform cross-section height of the sample, to ensure a uniform distribution of shear strain in the vertical direction. The structural components were designed so a total stress of 50 psi can be imposed: 30 psi of confining stress and 20 psi of backpressure; such pressures are

considered to be representative of samples at 25 ft (7.6m) depth, which corresponds to depths that have been observed to be prone to liquefaction and in flow slides.
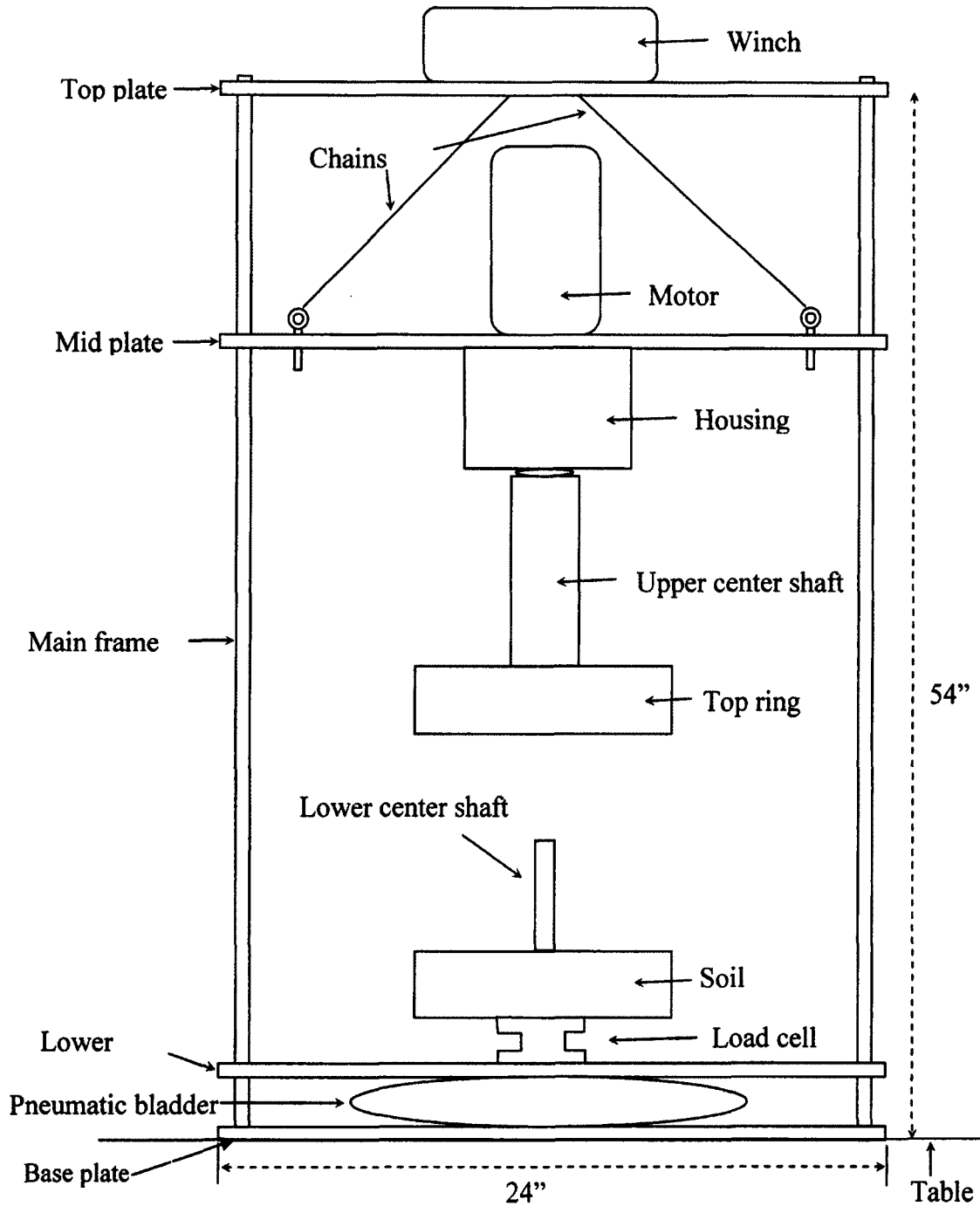
Figure III-1. Sketch of the RSD machine (not to scale).

The ring shear machine is made up of several components: main frame, ring shear chamber, and loading, saturation and measurement systems; a sketch and a general view are shown in figures III-1 and III-2. The following paragraphs describe the components; detailed technical specifications of major components are given in Appendix B.
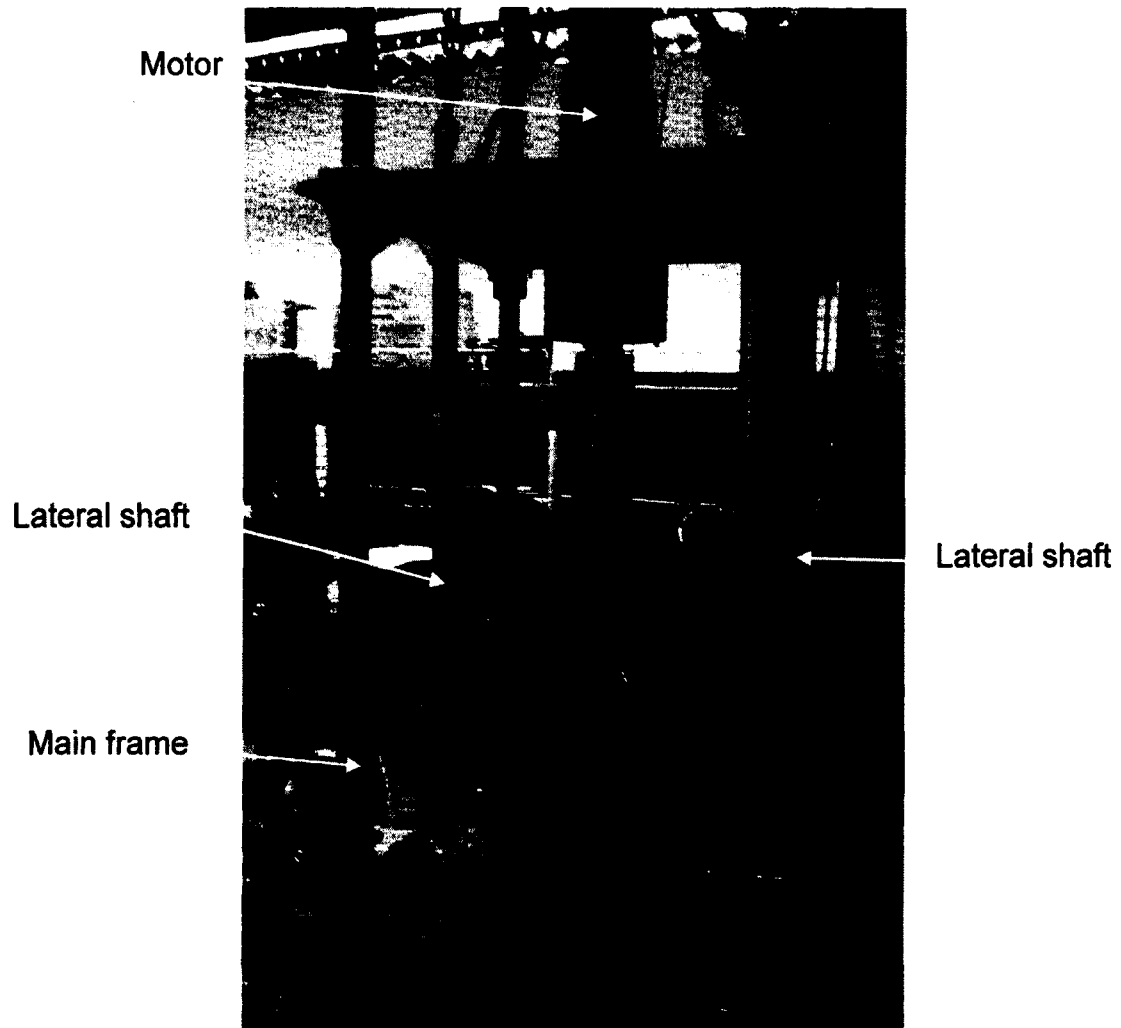
Figure III-2. Ring shear device (RSD), general view.

- Main frame. It is composed of four 1.5" diameter steel shafts and by four 0.5" thick steel plates. The table supporting the frame was designed to hold up to

10000 lbs of load, which is more than the loads that are expected during testing. Main frame shafts are fixed to base plate and top plate; the lower plate can move upward to apply vertical stress to test specimen. The mid plate is fixed in testing position by two additional lateral shafts which are clamped to the lower plate.

- Winch. This is used to bring the top ring up and down. It is attached to the mid plate by a set of two chains.

- Driving motor. This unit is a Parker SM Series Brushless Servo Motor and provides the rotary movement of the top ring (see figure III-2). Since the strain rate effect is being investigated, several velocities are to be used during the unidirectional rotation of the top ring.

- Top ring. See figure III-3. This is a metallic unit, and has 4 grooves for the o-ring seals (not shown); initially, the unit was designed to have two o-rings to seal the outer and internal contact surfaces; since the seal was of great concern, it was envisaged that a counter pressure might have to be applied between the o-rings to prevent leakage and ensure undrained conditions during testing. Experience has shown that one o-ring works well for backpressures to 15 psi. Since the top ring is responsible for providing the shear stress to the sample, it has a ring of sandpaper attached to its bottom (see figure III-4), and it covers the entire section of it, except where the drainage port is located.
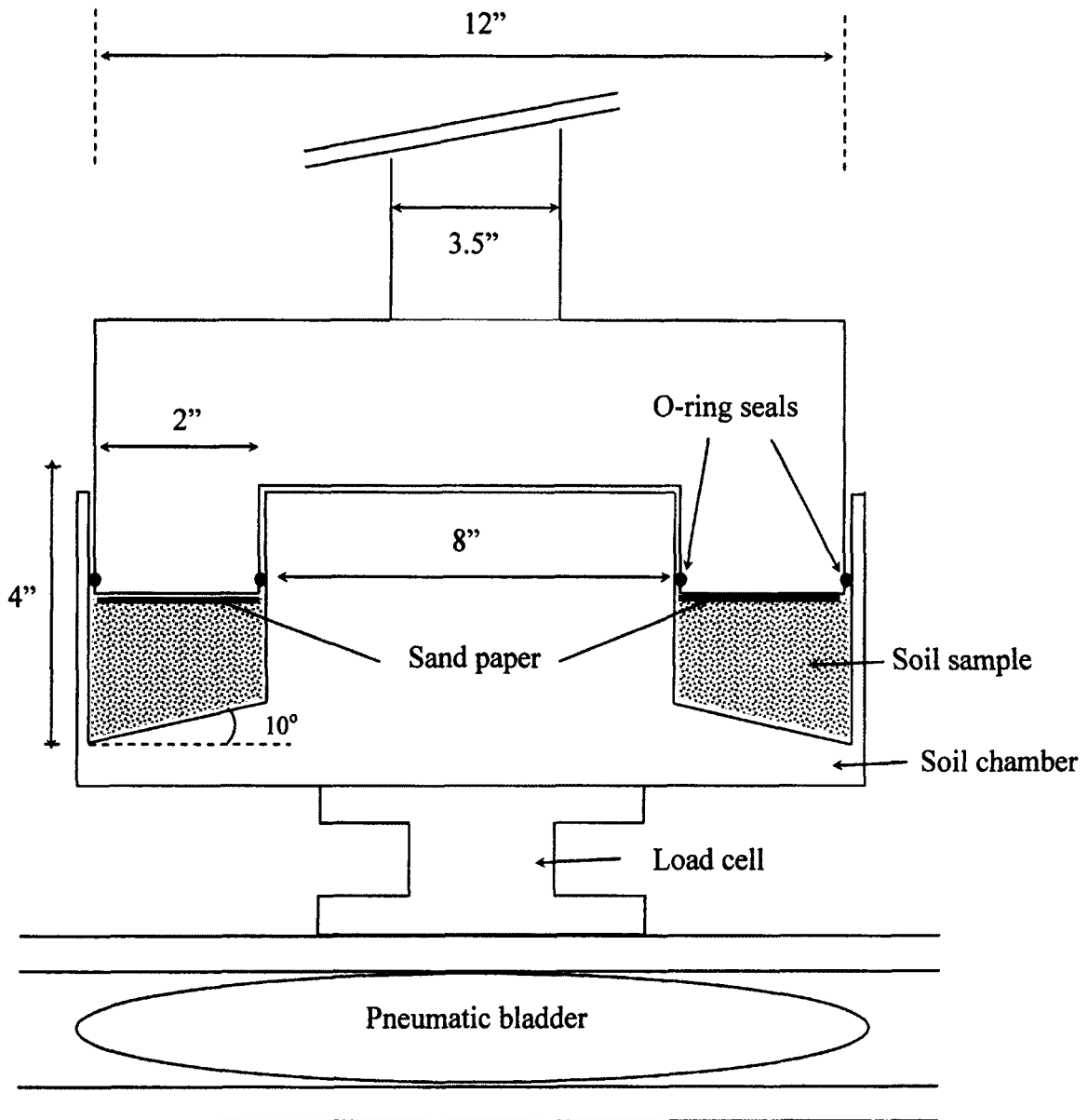
Figure III-3. Detail of top ring and chamber (not to scale).

The top ring is attached to the motor using an upper center shaft (see figure III-5), which engages to another shaft that comes from the motor, through a coupling that has as a primary function to transmit the cyclic/monotonic rotational movement to the top ring. The upper center shaft pushes on a ball bearing (see figure III-5) transmitting the vertical load to the

housing, which in turn send the vertical load to the main frame. It is important to mention that the coupling is not designed to receive vertical loads at all, and to avoid this from happening, a bolt was placed below the coupling (it is a safety measure and does not act all the time, i.e, if a vertical load is to be transmitted, it would receive it and send it to the housing, instead of send it to the coupling).
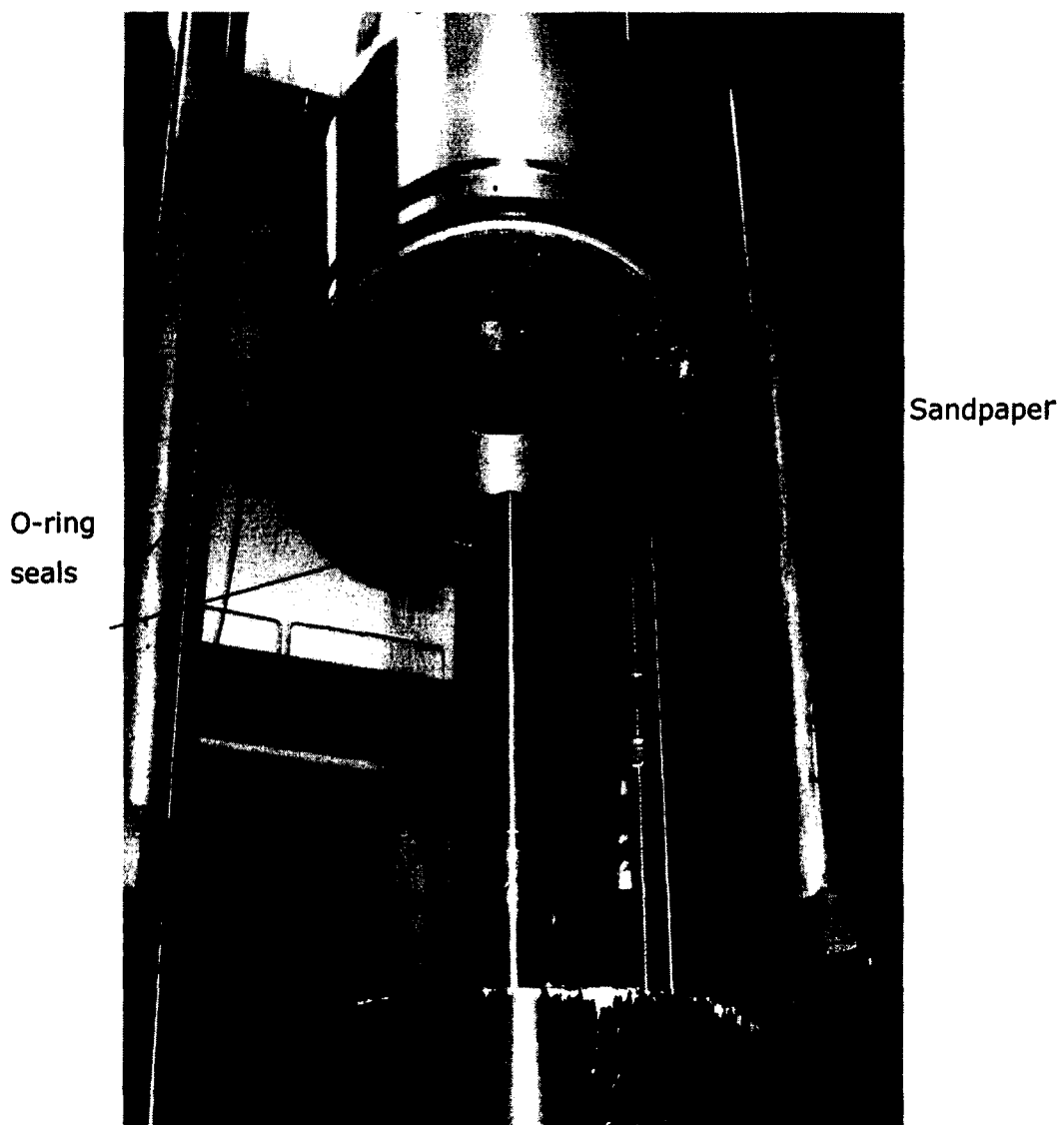
Figure III-4. Detail of sandpaper attached to the top ring.
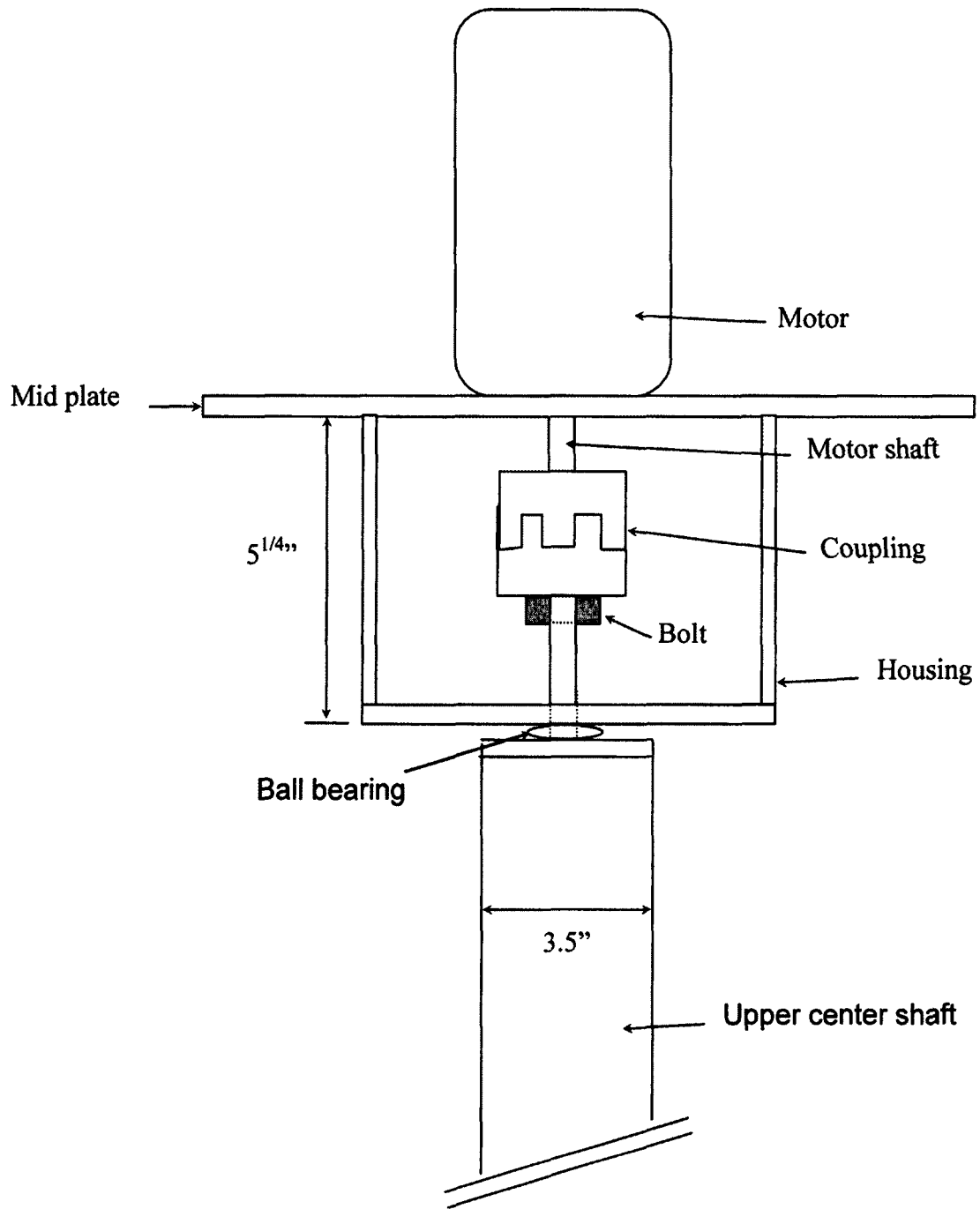
Figure III-5. Detail of housing and coupling (not to scale)

- Soil sample chamber (figure III-6). The chamber that holds the sample is an anodized aluminum unit and has diametrically-opposed ports in the base for

saturation and drainage, where porous stones are placed. Also, since there will be shear stresses transmitted by the top ring, a rough surface is needed at the bottom of the chamber. This is accomplished by using a thin sand layer glued with epoxy to its bottom. The geometry of the chamber is such that a uniform shear strain is imposed during testing: it has a $10°$ slope in the bottom so the outer section of the sample is thicker than the inner part; a cross section of the chamber is shown in Figure III-7.
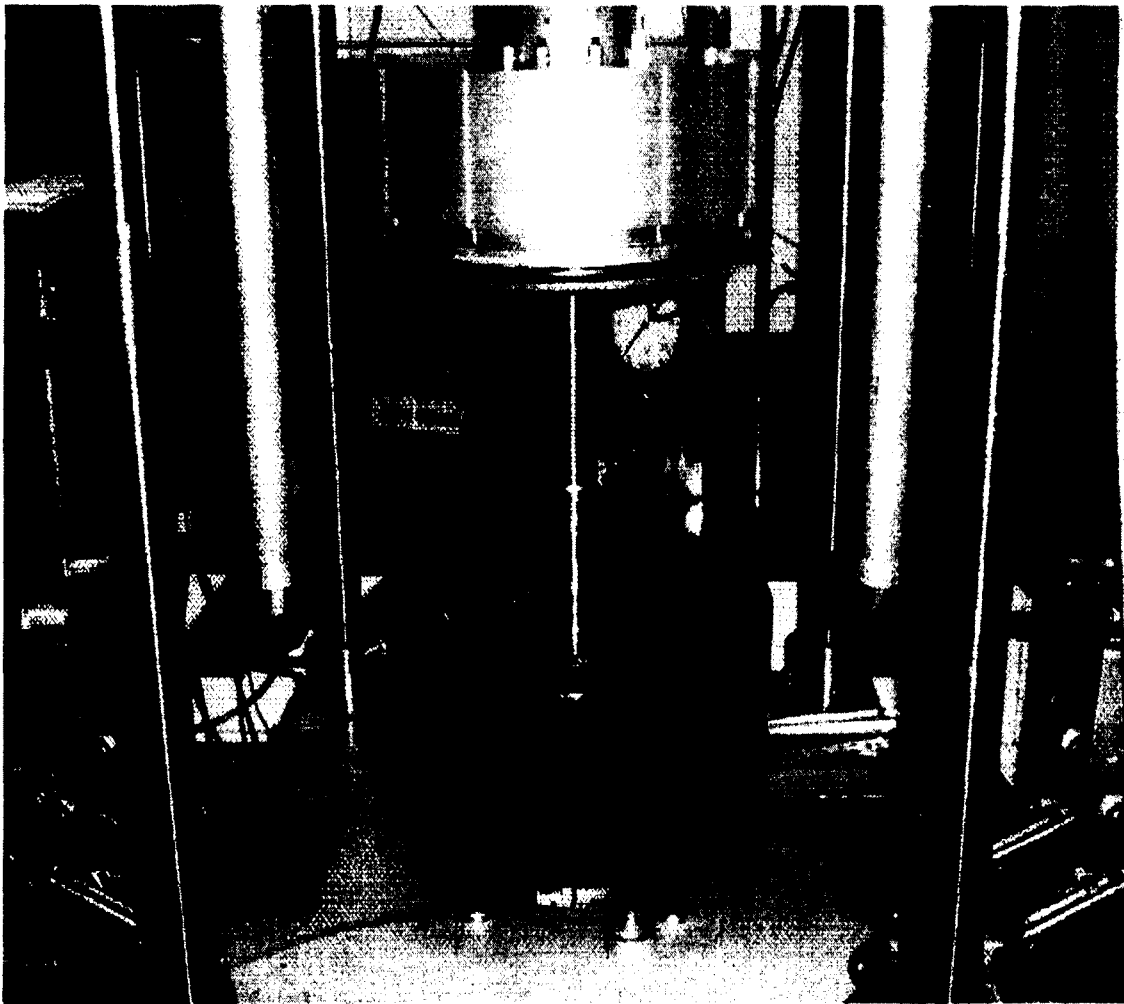
Figure III-6. Soil chamber.
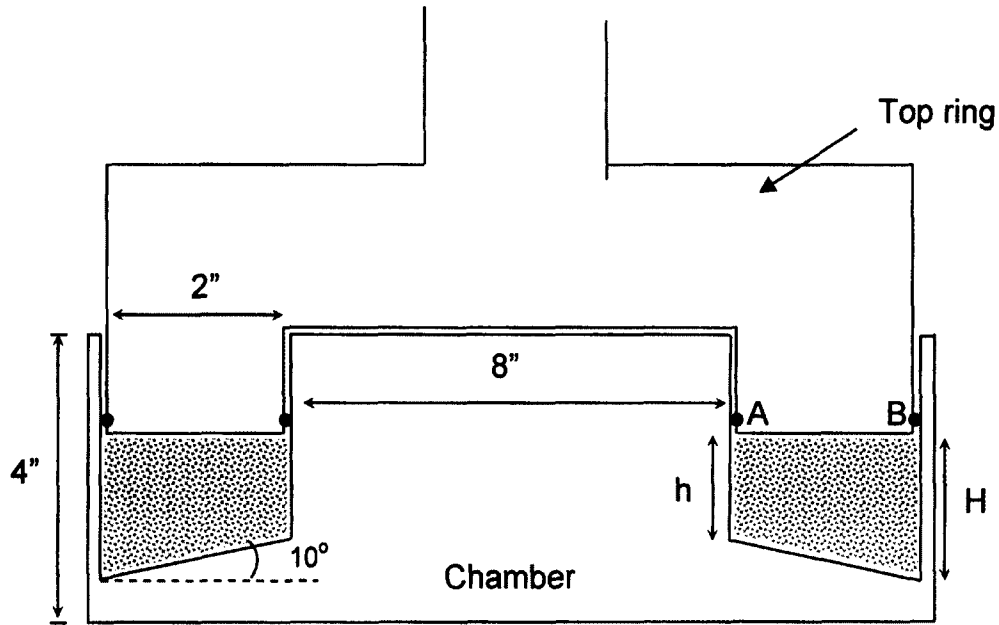
Figure III-7. Chamber cross section (not to scale).

Recalling the equations used to calculate the shear strain in the outer and inner points of the section (chapter I) these quantities are equal and calculated as follows:

$$\gamma_A = (r/h)\ \theta$$

$$\gamma_B = (R/H)\ \theta,$$

θ in radians

In this case: R = 6" and r=4"

Typically the value of H is about 1.3", which would make h=0.647"; in this case, the strains at the two points (A and B) are the same.

- Torque-thrust load cell (figure III-8). This sensor is located immediately below the chamber and it measures the vertical load that is applied to the sample and the torque produced by the top ring, from which the shear stress can be calculated. The signals of the sensor are sent to a computer, which uses LabView to display the readings (thrust and torque). Load cell specifications can be found in Appendix B.
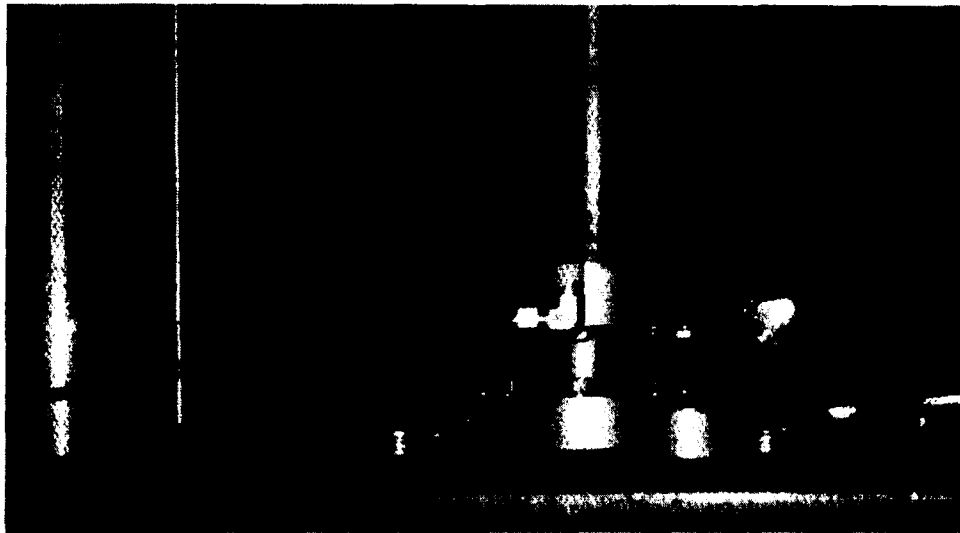
Figure III-8. Torque/Thrust sensor.

- Pneumatic bladder (figures III-1, III-3 and III-9). Located below the bottom table and is used to apply the vertical force needed to simulate the initial vertical confining pressure on the sample. To inflate it, a compressed air source is used and a regulator maintains a constant pressure level at any point of the test. A pressure transducer receives the bladder pressure signal from the air source and sends it to LabView so it can be monitored in the computer as well.
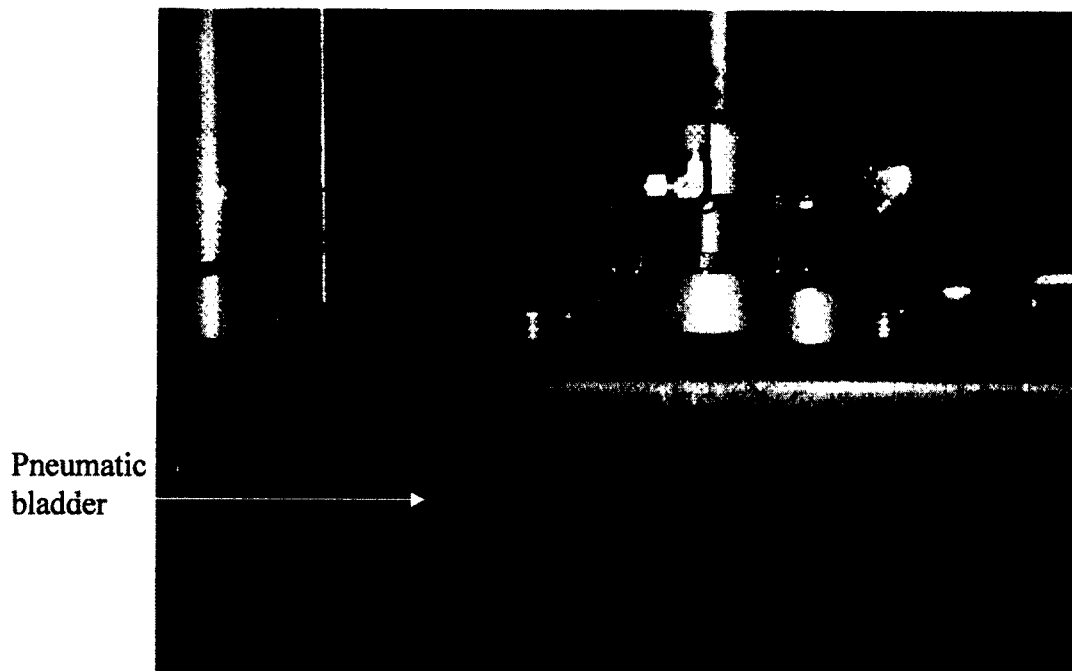
Pneumatic
bladder

Figure III-9. Pneumatic bladder.

- Pressure transducers and saturation lines (figures III-10 and III-11). The pressure transducers are responsible for reading any type of pressure that is to be experienced by the sample; there are two of them: one is a pore water pressure transducer which reads the backpressure and the excess pore water pressure produced during testing. The other transducer reads the pressure that is applied to the bladder (initial vertical confining pressure). They are also communicated to the LabView program so the changes in pressure can be recorded and plotted on Excel once the test is finished. The saturation lines are 1/8" diameter and are distributed so water and CO_2 can be circulated through the sample by opening and closing a series of valves (procedure for saturation will be described in a different section).
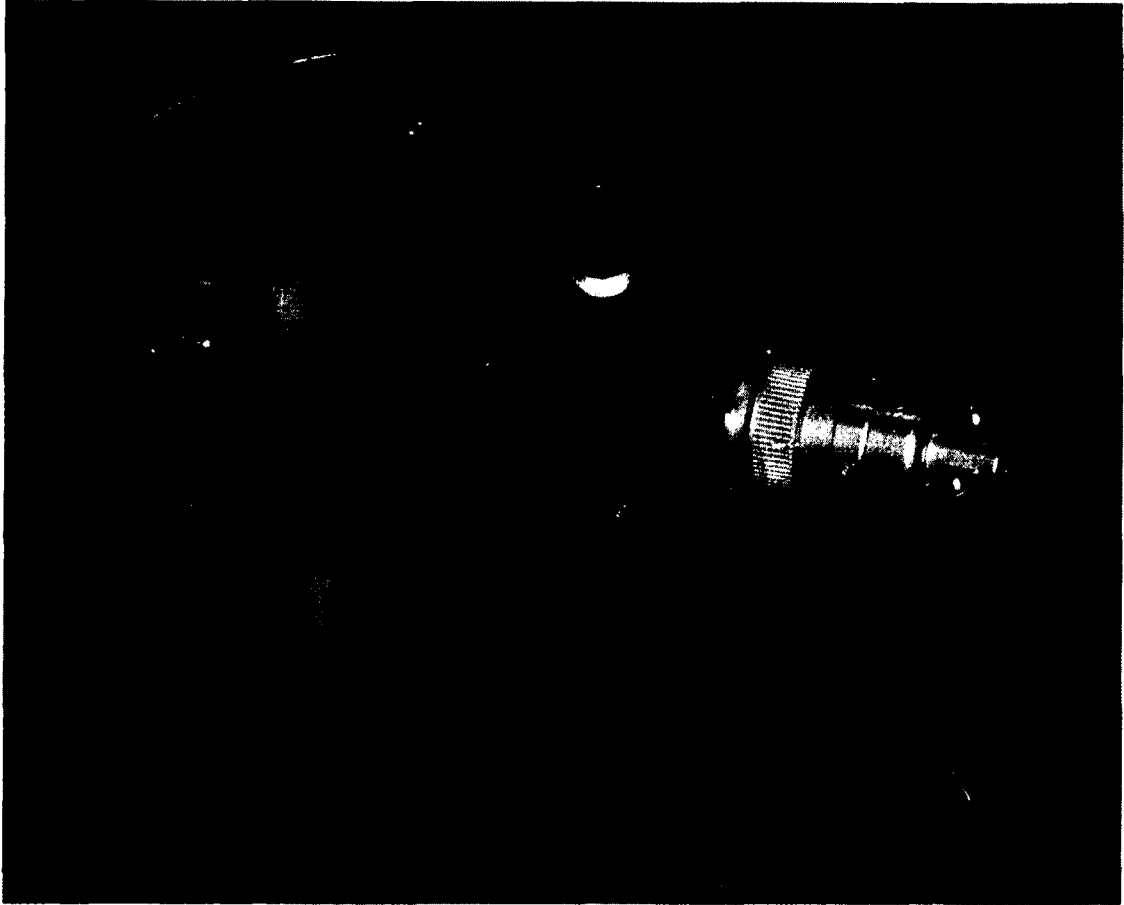
Figure III-10. Pore water pressure transducer.

- Clamping system (figure III-12). It is very important to keep the machine as rigid as possible during testing so constant volume (undrained) conditions can be achieved. Initially, a set of four clamps was used to keep the feet of the lateral shafts attached to the table and from moving up as the top ring moves. During early stages of testing, it was observed that this clamping system permitted unacceptable vertical deformations and needed to be changed; instead, two feet were installed at the bottom of the lateral shafts and have two holes each so they can be bolted to the table.
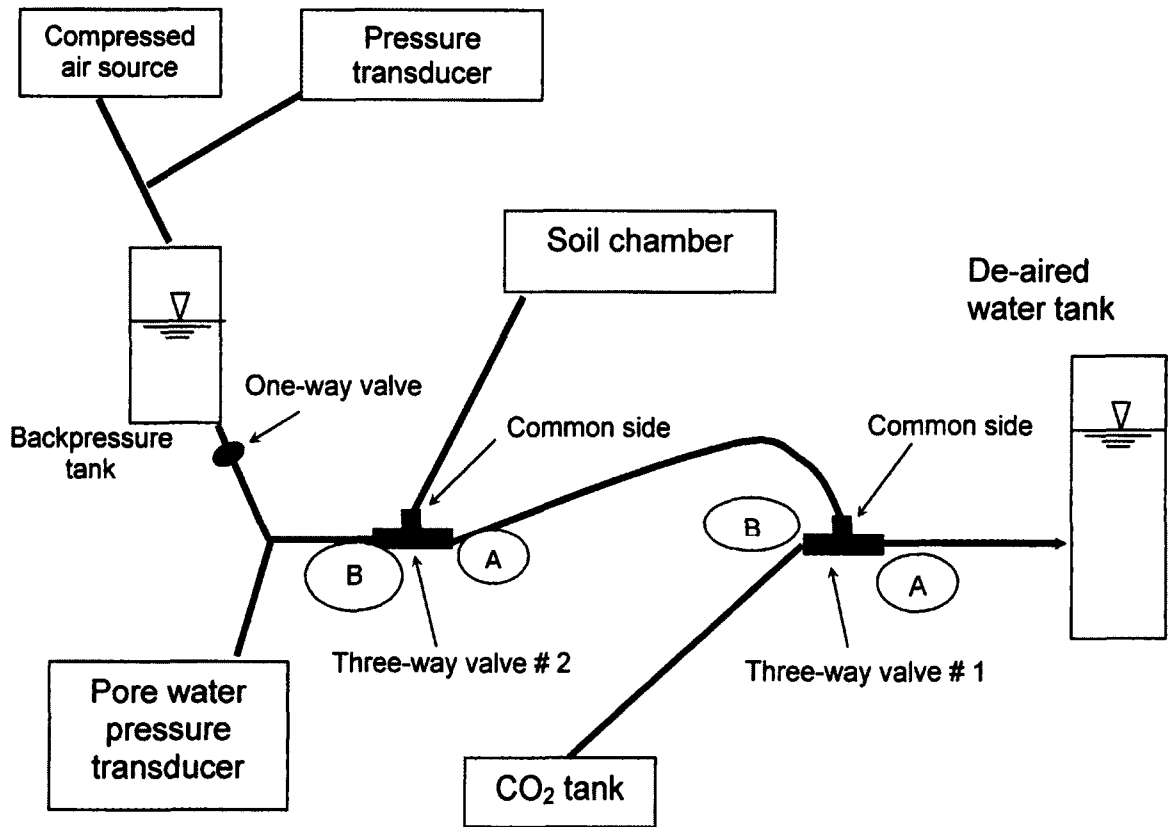
Figure III-11. Distribution of pressure transducers and saturation lines.
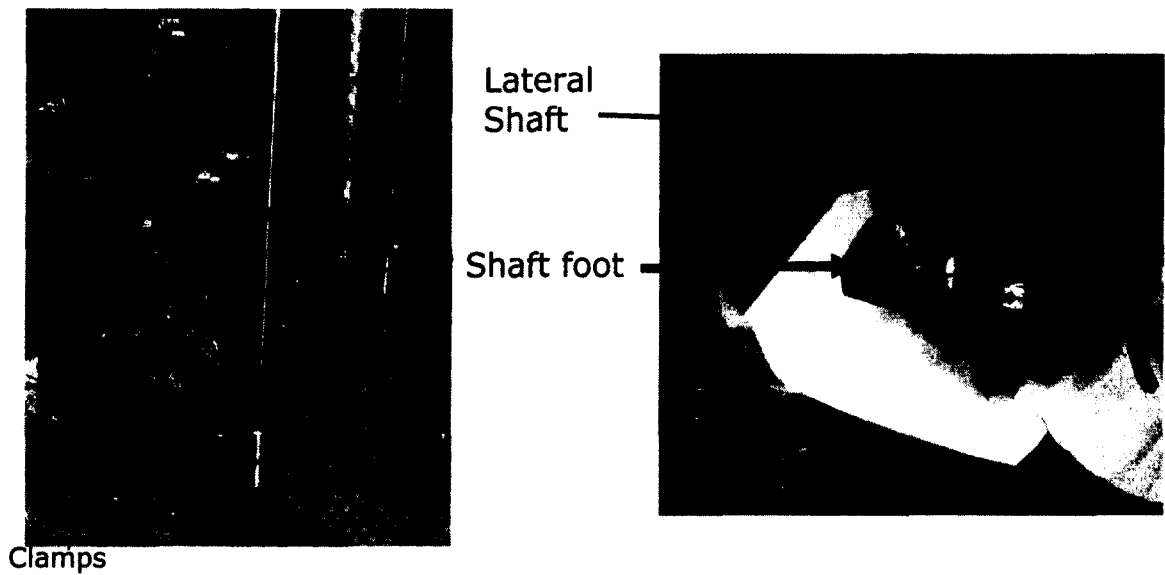
Figure III-12. Original and modified clamping system.

De-aired water tank. This tank stores water that is used to saturate the sample. It has a vacuum source in the top, and a valve that controls it. This valve should be kept open when the machine is not being used.

Backpressure chamber. This is used to apply the backpressure needed for saturation. It is connected to the bottom of the soil chamber through a series of 1/8" lines.

Compressed air source. This is used to apply both the backpressure for saturation and the initial confining pressure to the bladder.

Vacuum source. This is used to help the saturation process; it is connected to the top ring so a small vacuum can be applied to the sample before starting with the circulation of de-aired water.

- Jacks to help saturation process. Since the test is undrained, a fully saturated sample is desired and in order to achieve a suitable B value during saturation, two jacks are used to lift the machine so there is a highest (water outlet) and a lowest (inlet) point. Figure III-13 illustrates how the machine can be tilted using the jacks.

Jacks to lift the table
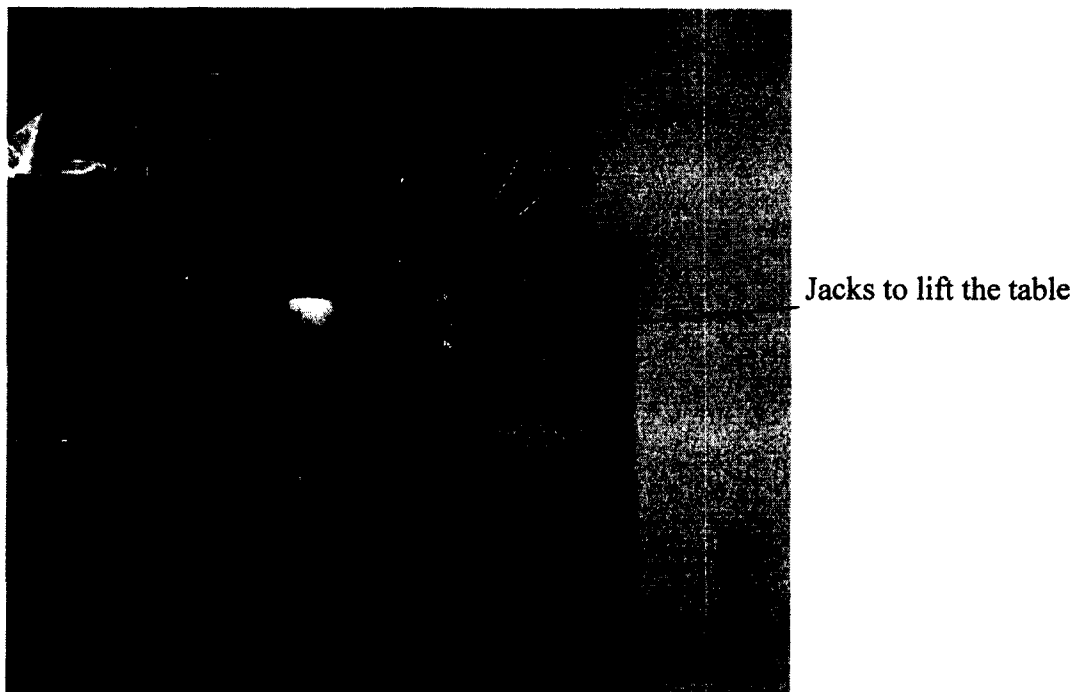
Figure III-13. Jacks to lift the table.

- Test measurement sensors. Several sensors are installed so measurements such as torque induced by the top ring to the sample, thrust, and vertical displacement of the top ring can be monitored during the test. All the signals are sent to LabView so they can be processed and analyzed after each test. The following sketch illustrates how the electronic components are installed in the machine (figure III-14).
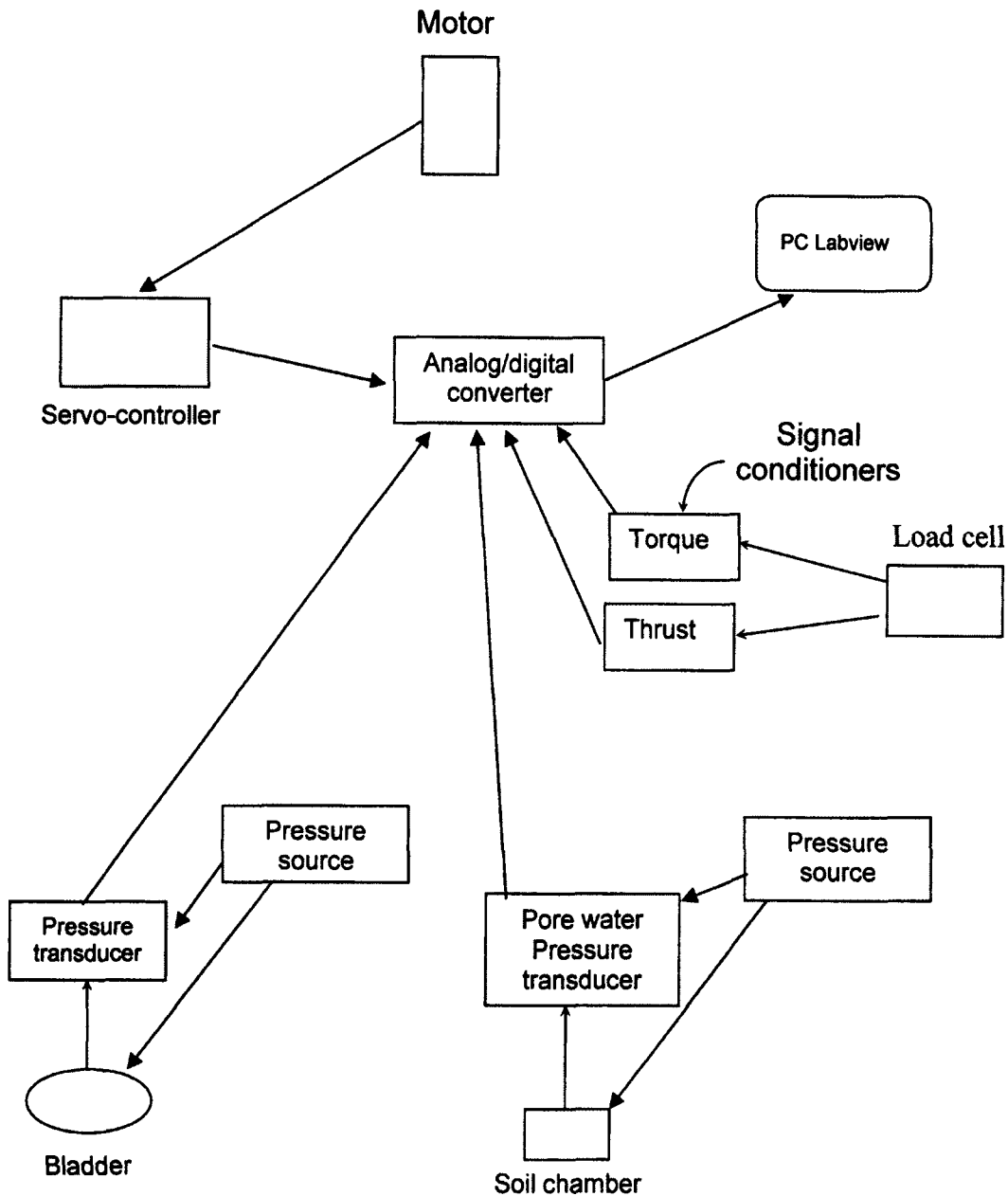
Figure III-14. Schematic flow chart for electronics.

- Miscellaneous. The machine is equipped with other devices and instruments that have different functions, depending on the stage of the test. The following list summarizes and briefly describes them.

67

CHAPTER IV

TESTING WITH THE RING SHEAR DEVICE.

The ring shear device has been implemented as a tool to help the understanding of the behavior of flow slides and liquefied soils. However, because there is no a standard device nor recommendations that lead to a single design, every single RSD is different from other versions, depending on the needs of the researcher and/or the way to approach the flow slide problem. This chapter describes in detail the way the UNH version has been used so far and includes some examples of the results that are obtained.

General Procedure

The first step is to clean the machine and remove any excess of soil that was left after previous tests. This is done so the weight of the sample is not affected by extraneous material. The following list describes the procedure

in detail. Note that some steps from the chapter "Material properties and sample preparation technique" are repeated here, just as a reminder:

1. Before starting, flush water from the saturation lines with compressed air.

2. Measure the friction due to the o-rings: start the LabView and Motion Planner software and bring the torque signal to zero; fill the chamber with water, clean and lubricate the o-rings, bring the top ring down and apply a small pressure; run the monotonic part of the test, using the speeds that are to be used during testing (i.e., 5, 10, 15 and 20 rev/min).

3. Remove pressure and bring top ring up.

4. Place dummies diametrically opposed.

5. Bring top ring down and make two height readings on dummies to 0.001". Since the sample has a trapezoidal shape, an average height is used to calculate the thickness of the sample. Figure IV-1 shows the dimensions of the dummies.

6. Clean the grooves for the o-rings and make sure that no sand is trapped in them; clean the o-rings with orange soap and apply lubricant evenly (acrylic lubricant). Set them aside (they will be installed at the very last moment before apply the external pressure).
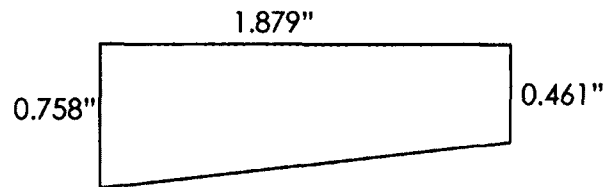
Figure IV-1. Dummies to measure the height of the sample.

7. Prepare sample as described in chapter "Sample preparation technique."

8. Bring top ring down, bolt the feet of the lateral shafts to the table and apply initial confining pressure (σ_0) using the bladder.

9. Place the bottom plate supports (green jacks) below bottom table and tighten them until they don't move anymore, applying a torque of 20 in-# (see figure IV-2).
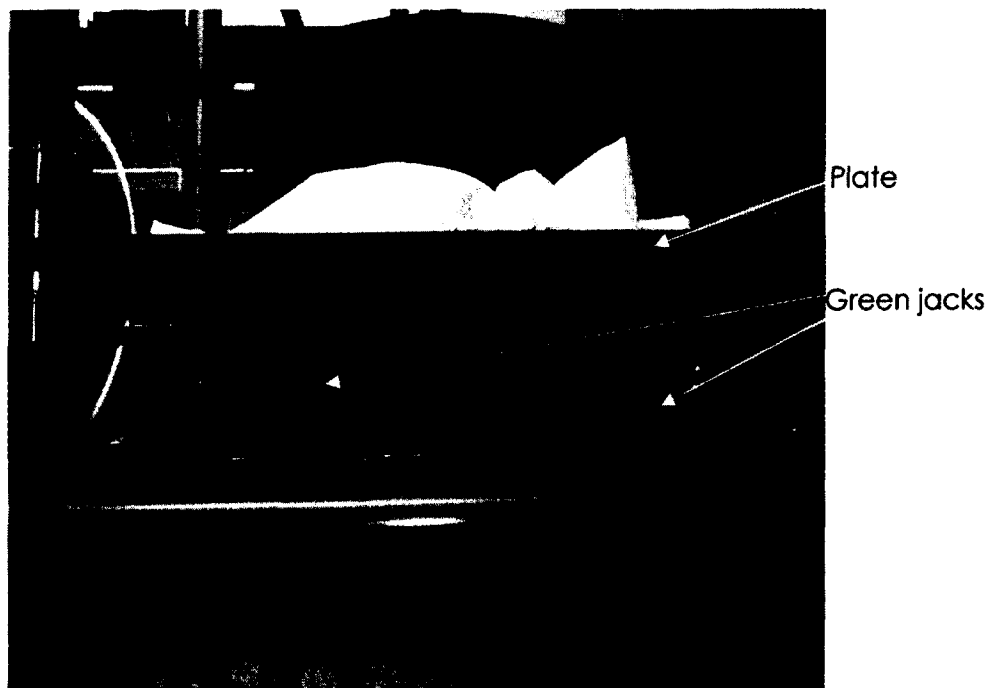
Figure IV-2. Green jacks below table

10. Take height readings on sample, taking care to place the dial gauges in the same places where they were placed in step 4.

11. Apply a small vacuum (5 mm. HG) for 10 minutes to top drain.

12. Use the two table-tilting red jacks (figure III-13, chapter 3) to lift the table so the outlet on the top ring ends up being the highest point; DON'T LIFT IT TO AN UNSAFE POINT; tentatively, 2 inches is recommended.

13. Circulate CO_2 for 20 min. and stop for 5min. Circulate CO_2 again for another 5min.

14. Circulate de-aired water until no more bubbles come out (figure IV-3). Let it flow for 25min. Stop another 5 min. and re-circulate again for 10min.
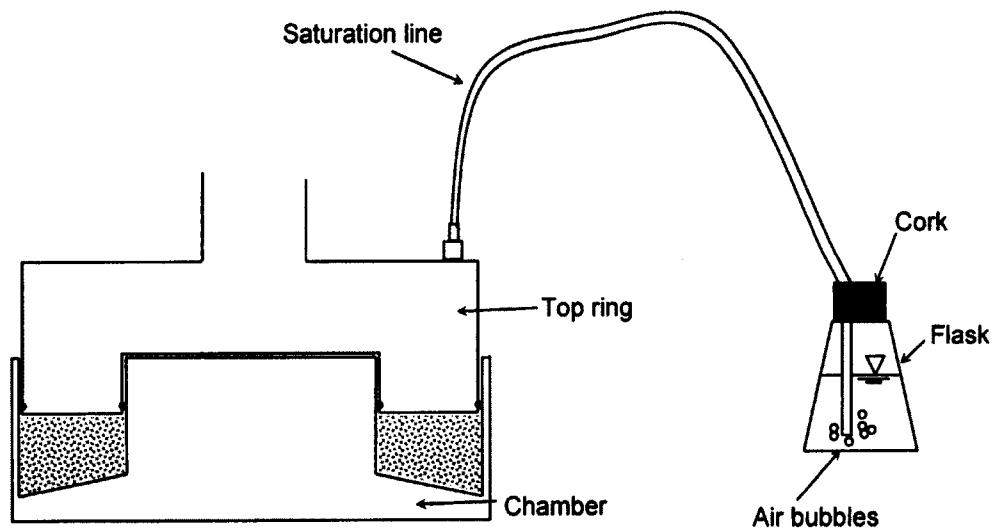
Figure IV-3. Flask arrangement in top ring.

15. Bring table down CAREFULLY and remove red jacks.

16. Install the LVDT designated to monitor the vertical displacement of the top ring. Readings are sent to LabView and taken into account when calculating the volume of the sample. There is no need to set LVDT initial reading to zero, since the software captures the entire displacement history and relative quantities can be calculated.

17. Run LabView and apply backpressure (Uo); this will allow monitoring the movement of the top ring during application of backpressure. Let it act for 15min.

18. Open top valve gently so water circulates until no more bubbles are observed, with backpressure still applied.

19. Close top valve again, stop for 5min and open again for another 5min.

20. Close backpressure chamber valve and see if reading on water pressure is constant.

21. Check B value: start a new file in LabView, close backpressure chamber valve and apply 600 lbs. (thrust); monitor and record the change in pore water pressure. Calculate B value using the equation derived by Miller (1995):

$$B = \frac{\Delta U}{\frac{1}{3}\Delta\sigma_1 + \frac{2}{3}\left(K_0\Delta\sigma_1 - K_0\Delta U + \Delta U\right)}$$

Where:

ΔU: change in pore water pressure

$\Delta\sigma_1$: change in external pressure

Ko: coefficient of earth pressure at-rest pressure, which can be calculated based on the internal friction angle (ϕ'):

Ko = 1-sinϕ'

The internal friction angle depends on the relative density of the material and can be found from the following experimental curve (source: Miller, 1994):
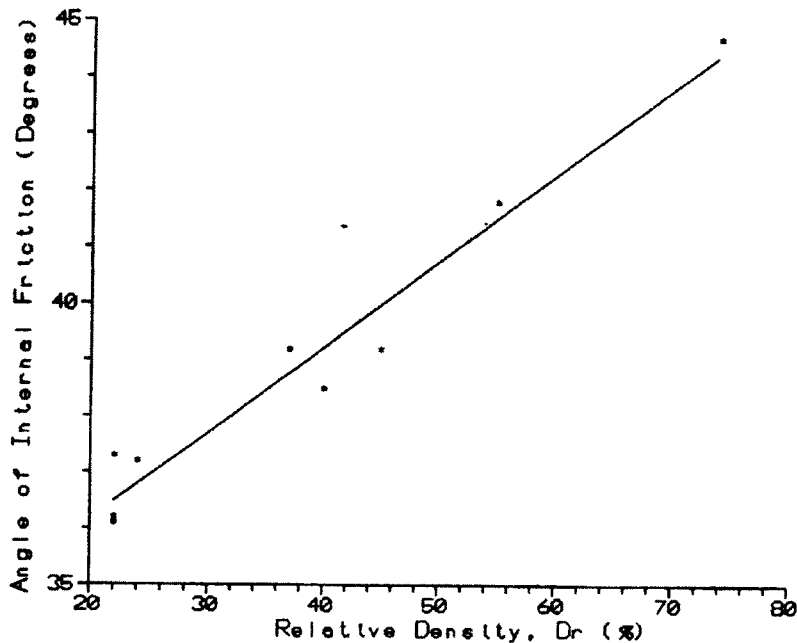
Figure IV-4. Dr% vs. internal friction angle for Holliston sand (Miller, 1994).

74

22. Remove additional thrust and open backpressure chamber valve again and wait until ready to run the test.

23. Start Lab-View again and Motion Planer (MP) software.

24. Set desired parameters for loading (in Motion Planner):

    vari1 = vari2: Angle of rotation during cyclic loading (i.e. 5000 counts – 5 degrees)

    vari3: number of cycles (i.e. 10).

25. vari4: speed of rotation during monotonic movement (i.e., 50,000 means 5 rev/min).

26. Close the backpressure chamber valve.

27. Run the cyclic part of the test until the pore water pressure reaches a constant value.

28. Run the monotonic part of the test. When torque reading reaches a constant value, stop the machine (from Motion Planner) and change the command of "vari4" using a different speed (for 5, 10, 15 and 20 rev/min, type "vari4=50000", "vari4=100000", "vari4=150000" and "vari4=200000", respectively), and run the program again, until the desired set of velocities are completed.

29. Disassemble the chamber:

o Open backpressure tank again.

o Remove backpressure.

o Remove green jacks.

o Open valve on top ring to atmosphere and let water to flow.

o Remove pressure from bladder.

o Remove bolts from the feet of the lateral shafts.

o Lift top ring carefully.

30. Recover sample for weighing and dry it for 24 hours.

Once the process is complete, the data saved on the PC can be transferred to Excel file and reduced. The following figure shows the results from a typical test:

a)
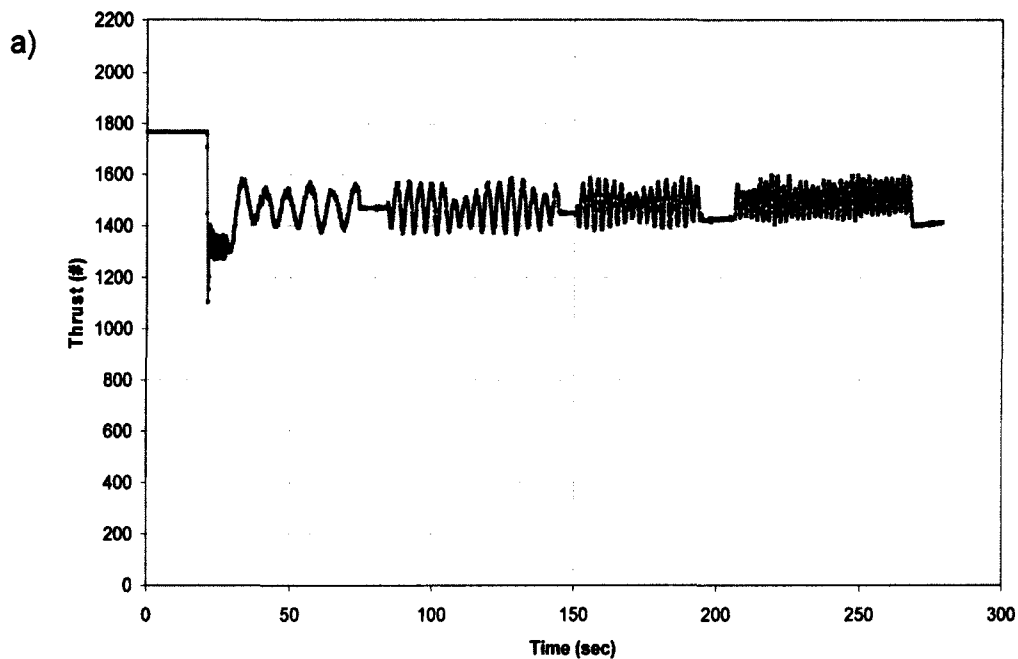
Figure IV-5a. Typical test from ring shear device (thrust).
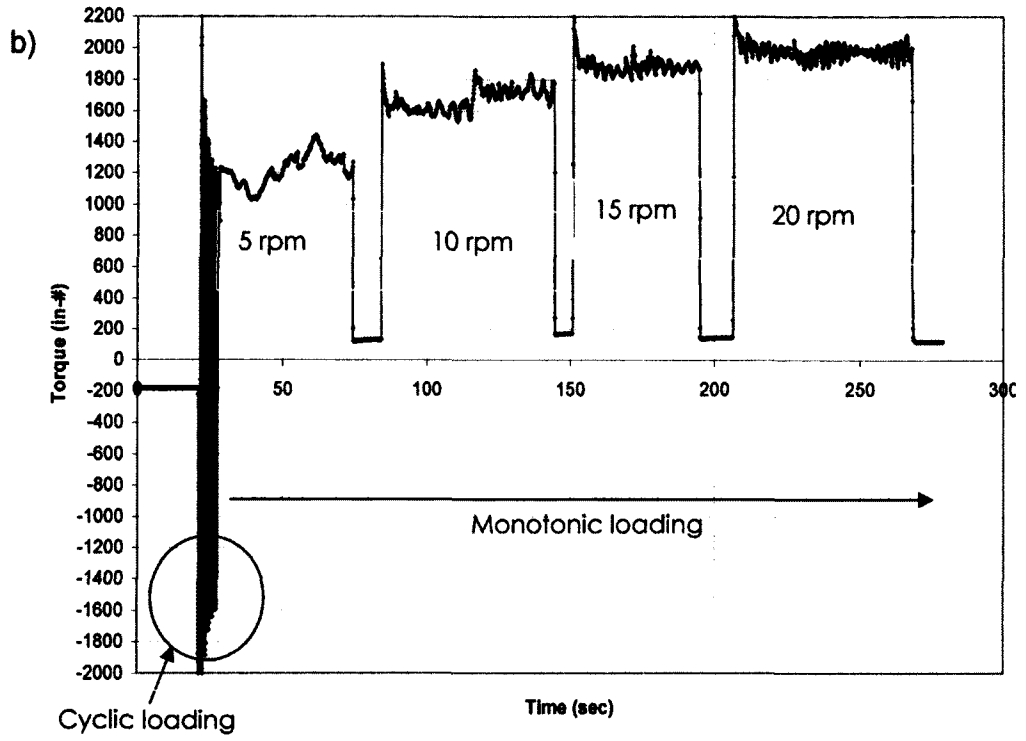
Figure IV-5b. Typical test from ring shear device (Torque)
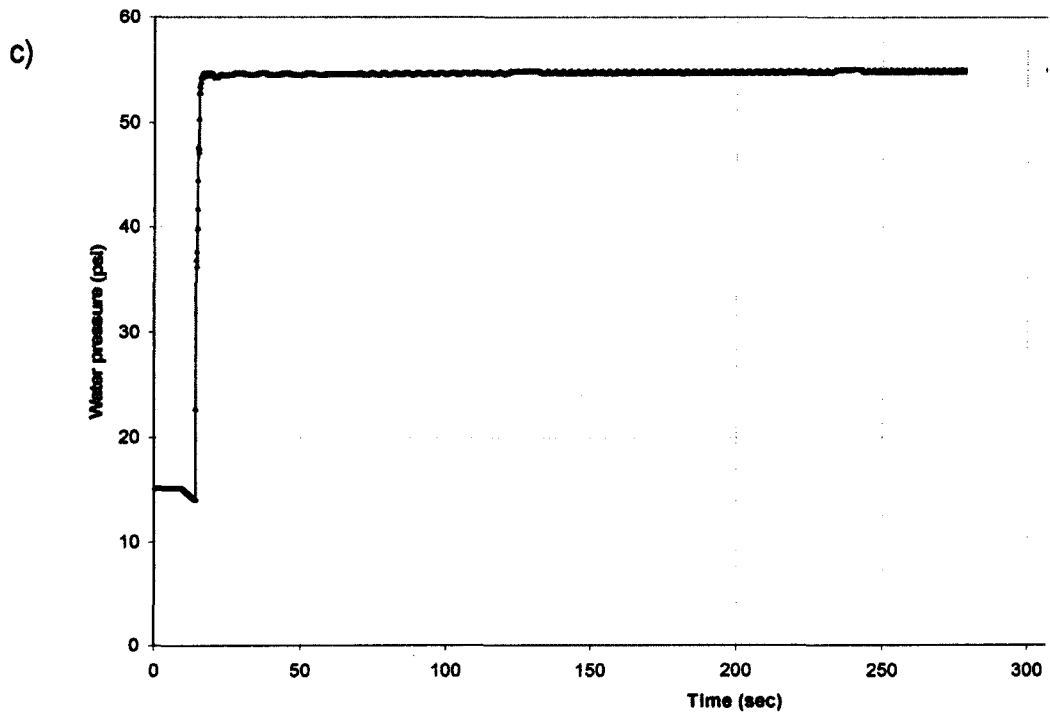
Figure IV-5c. Typical test from ring shear device (Water pressure).

77

All tests were run using a total stress of 30 psi and an initial pore water pressure of 15 psi, which gives an initial vertical effective stress (σ'_{vo}) of 15 psi. The target value for the (τ/σ'_{vo}) ratio in cyclic loading is 0.15.

It is observed that the pore water pressure jumps to a value of about 55 psi almost immediately after the movement starts, which is more than it is expected to be (about 30 psi); this is typical in every test: no more than 2 complete cycles are needed to build up the pore water pressure to a value similar to that of figure IV-5(c). In order to investigate the reason of this behavior, an LVDT was installed to monitor the displacement of the top ring with respect to the chamber. The following graph shows a typical displacement monitoring result obtained from the LVDT and recorder by LabView.
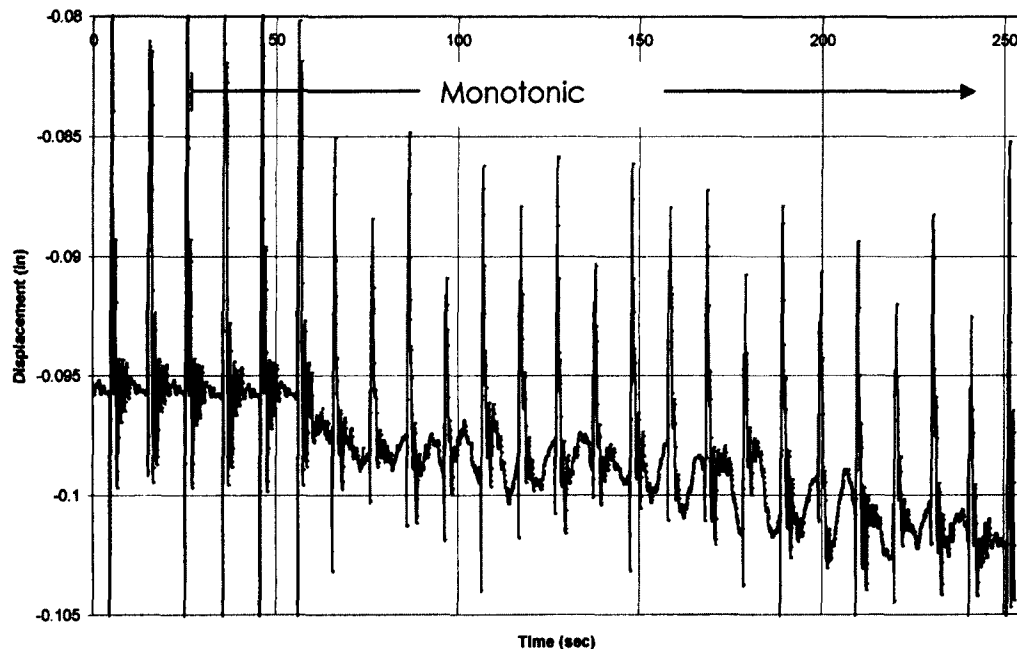
Figure IV-6. Displacement of top ring with respect to the chamber.

78

Usually most of the vertical displacement is produced during the monotonic part of the test. Also, a change in the thrust reading is observed, which is supposed to be stable; according to the manufacturer of the load cell, once the torque is applied, the thrust reading is no longer correct, since it is affected by the torque.

It was found that the top ring was moving down during testing, which means that the sample does not loses contact with the sand paper on the top ring; usually, the displacement was observed to be in the range of 0.004" to 0.009".

This is an interesting observation and it can explain the behavior of the pore water pressure change by means of the relationship between change in water pressure and the compressibility of the sample (water and soil), as follows (Akers, 2001):

$$Cl = \frac{n}{n-\varepsilon}\left\{\frac{Uo}{Uf^2}(1-So+SoH)+SoCw\right\}$$

Where:

Cl: sample compressibility.

n: porosity.

ε: vertical strain.

Uo: initial pore water pressure.

Uf: final pore water pressure.

So: initial degree of saturation (based on B value).

Cw: compressibility of water, 4.5E-5 $(kg/cm^2)^{-1}$, or 3.1638E-6 $(psi)^{-1}$

H: Henry's constant (0.02055).

The following values can be used to evaluate the compressibility (or modulus) of the sample:

For Dr = 27% : e = 0.781 and n = 0.438

Vertical strain: 0.007"/1.011" = 0.00692

$$Cl = \frac{0.438}{0.438 - 0.00692}\left\{\frac{15}{55^2}(1 - 0.97 + 0.97*0.02055) + 0.97*3.1638E - 6\right\}$$

Cl = 2.4E-4 $(psi)^{-1}$

So, the modulus would be:

E = 1/Cl = 1 / 2.14516E-4 = 4200 psi.

The increase in water pressure due to this modulus and the measured strain would be:

$$\Delta U = E^* \, \varepsilon = 4200 * 0.00692 \approx 29 \text{ psi}$$

This value is similar to those observed and recorded by LabView.

For the test shown in figure IV-5, to reduce the data, the following table can be used:

Table IV-1. Raw and reduced data.

Speed (rpm)	Raw Torque * (in-#)	Torque in o-rings * (in-#)	Torque in soil (in-#)	Shear stress (psi)
5	1280	603	677	2.2
10	1730	914	816	2.6
15	1910	1010	900	2.9
20	2050	1080	970	3.1

* Take an average of the readings from LabView.

Speed (1/sec): Speed (RPM).

Torque in soil: Raw Torque – Torque in o-rings.

Shear stress = T * r / A.

T: torque in soil.

r: average radius of ring, 5in.

A: cross sectional area, 62.8 in^2

81

These results are plotted in the following chart (shear strain rate vs. shear stress):
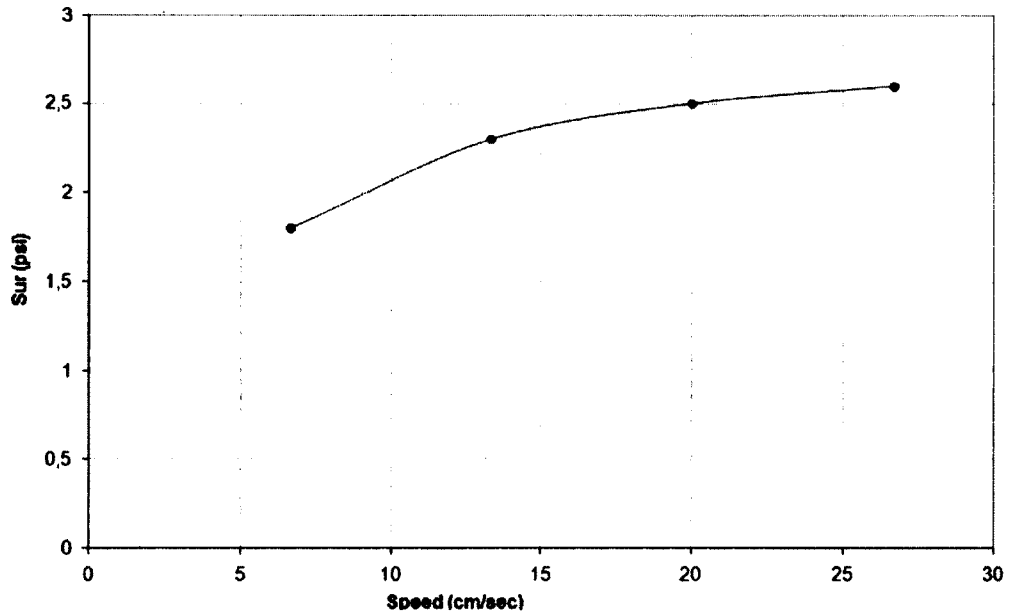
Figure IV-7. Shear stress vs. shear strain rate plot (Dr=27%)

The following table summarizes the successful tests, including their corresponding B value:

Table IV-2. List of successful tests.

Dr [%]	5	10	15	20		Date	B value
24	1.1	1.4	1.5	1.7		july 3	0.92
24	1.2	1.5	1.6	1.8		aug 7	0.93
25	1.3	1.6	1.9	2		Mar-15	0.86
25	1.4	1.7	1.8	1.9		21-Mar	0.85
26	1.5	2.2	2.4	2.5		Jun-04	0.91
27	1.8	2.3	2.5	2.6		May-30	0.91
28	1.9	2.3	2.6	2.8		aug 3	0.95
30	2.3	2.7	3.12	3.3		aug 9	0.95
33	3	3.5	3.9	4.2		Mar-06	0.86
34	3.1	3.4	3.6	3.7		aug 13	0.97
19	0.7	0.95	1	1.1		Sep-10	0.97
36	4.1	4.3	4.4	4.5		14-Sep	0.96
35	3.2	3.3	3.5			19-Sep	0.95

Special Tests

An interesting test intended to know how the sample is being sheared was carried out using thin vertical bands of red sand, as depicted in figure IV-8.
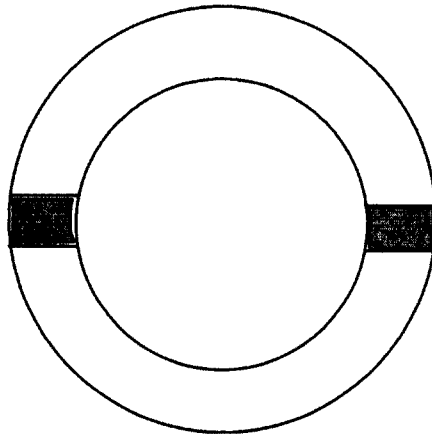
Figure IV-8. Special test with colored sand.

Pictures IV-9a and IV-9b were taken after excavating the colored zones in the chamber:

Sheared zone

Intact material after shearing

Figure IV-9a. Colored sample after excavation

Sheared zone

Intact material
after shearing
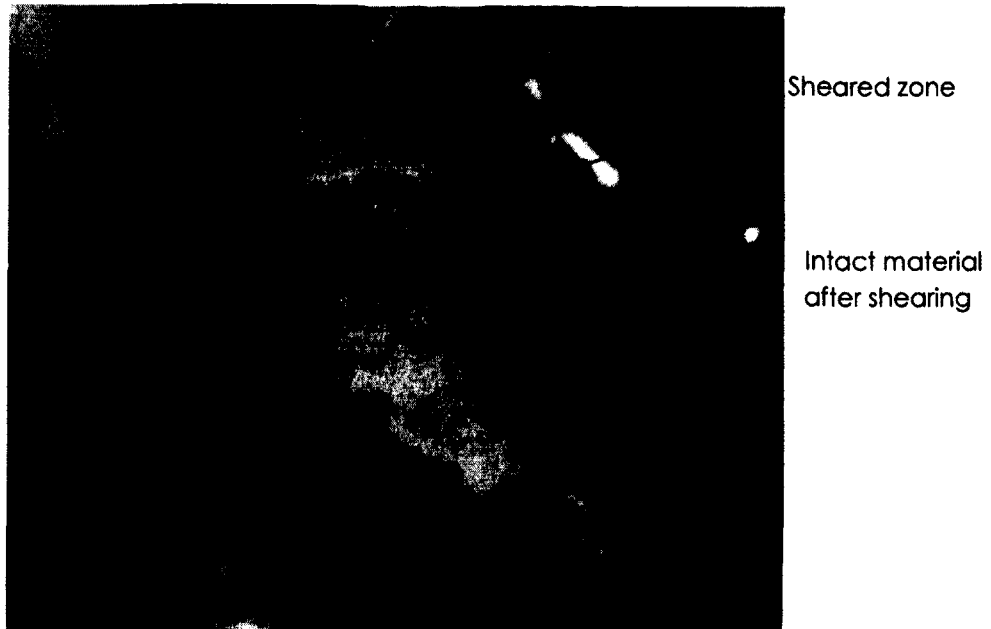
Figure IV-9b. Colored sample after excavation

As it can be seen, the sample was failing through a thin band, which was 6mm thick, in average (20 times D_{50}). This brings as a consequence a change in the strain rates that were originally calculated, based on the entire thickness of the sample:

Thickness of sheared zone: 0.2362 in

Table IV-3. Calculated velocities and shear strain rates

Rotation velocity (rpm)	5	10	15	20
Angular velocity (deg/sec)	30	60	90	120
Angular velocity (rad/sec)	0.5236	1.0472	1.5708	2.0944
Shear strain rate ($\dot{\gamma}$)	11.0838	22.1676	33.2514	44.3352

Note a maximum strain rate of 44 1/sec is obtained, which is representative of real flow slides (Bryant et al, 1983).

Testing with Standard Material

In order to calibrate the ring shear device and to improve the accuracy of the results that are obtained, it was decided to use a material for which the rheological properties have been well identified. A standard material N62000 (Cannon Instrument Company) with a viscosity of 200000 mPa· sec (centipoises) (0.029 lb-sec/in²) was used. This material behaves as a Newtonian fluid, which means that the viscosity is constant and that it does not experience any shear resistance when it is in repose. The following plot shows the behavior of this standard.
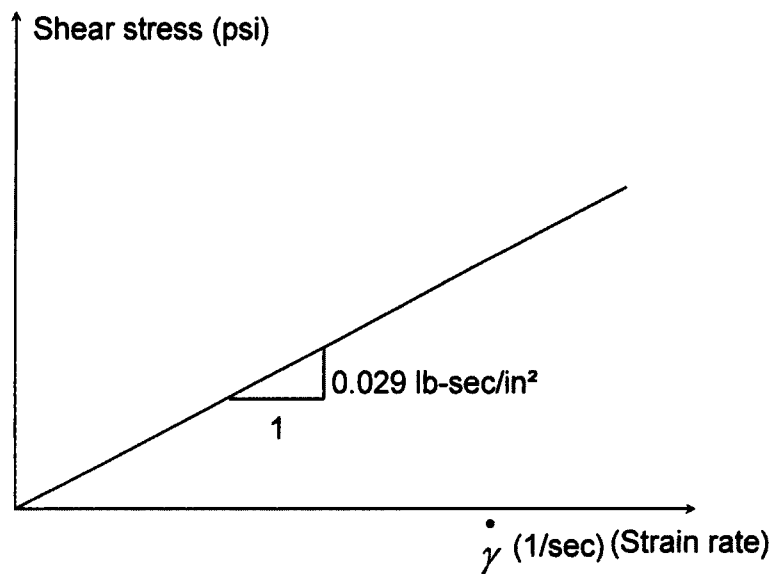
Figure IV-10. Theoretical behavior of Standard Material.

The procedure followed to test the standard material is similar to that used during testing with sand, with a few changes, including the inclusion of the use of red sand to monitor the way the sample is being sheared:

- Saturation lines were removed so they wouldn't get damaged.

- Drainage holes were plugged with corks.

- O-rings were cleaned, lubricated and placed on the groves. Note the friction is to be measured at the very end of the test, since it was controlled by the standard material.

- Two aluminum tubes (3/4" diameter, 4" long) were placed inside the chamber, opposite to the drainage holes. The standard material was also placed in the chamber in the same way described in Chapter III.

- The tubes were filled with the red sand and carefully removed along with the screen. It was observed that the sand did not mix with the standard material, due to its high viscosity.

- Top ring was brought down and an external pressure of 15 psi was applied checking that some standard material was observed to come out through the drainage hole of the top ring, after which it was closed.

- Green jacks were placed below the table and the machine was lifted using the red jacks to remove any air inside the chamber.

- The test was run using the same speeds that were used during conventional testing (5rpm, 10rpm, 15 rpm and 20 rpm).

- Once the test was complete, the friction in the o-rings was measured, by removing the external pressure and lifting the top ring so it was not in contact with the sample anymore.

- The raw data was retrieved from LabView and reduced in Excel:
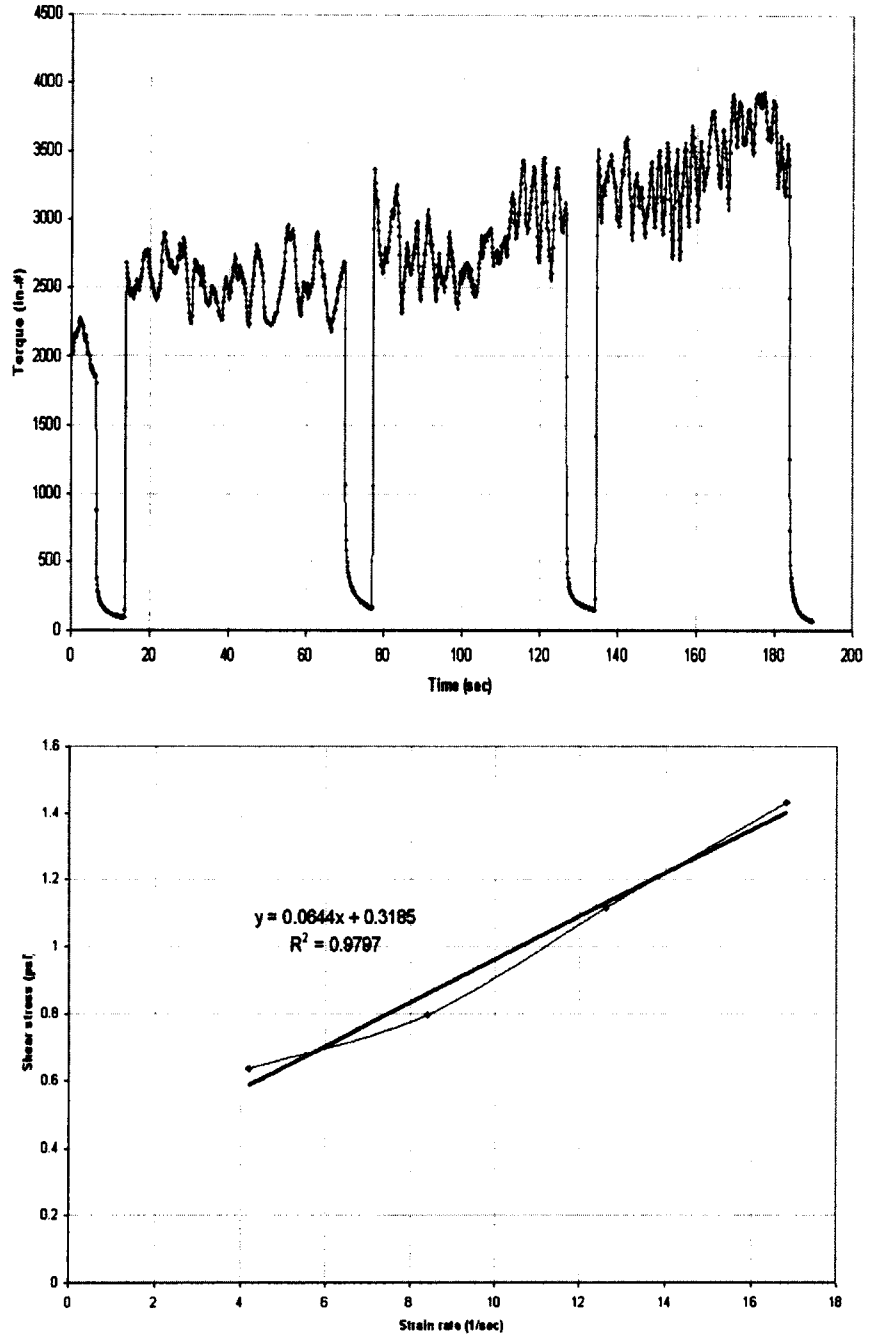
Figure IV-11. Raw and reduced data from test with Standard Material.

Figure IV-11 shows that the machine obtains a different value for the viscosity: instead of 0.029 lb-sec/in^2, a value of 0.06 lb-sec/in^2 is obtained; also, results show that the line has an initial intercept (zero offset) of about 0.31 psi with the shear stress axis. This zero intercept is attributed to the machine and is considered as a correction that needs to be applied to the reduced values of shear stress. It was observed that the red sand moved in its entire section, which means that all the mass was being sheared, as a difference with the sand; this is due to the nature itself of the standard material (a viscous fluid).

Corrected Tests Data

The following plot shows the reduced data of the successful tests, including the zero offset correction from the testing with the standard material.
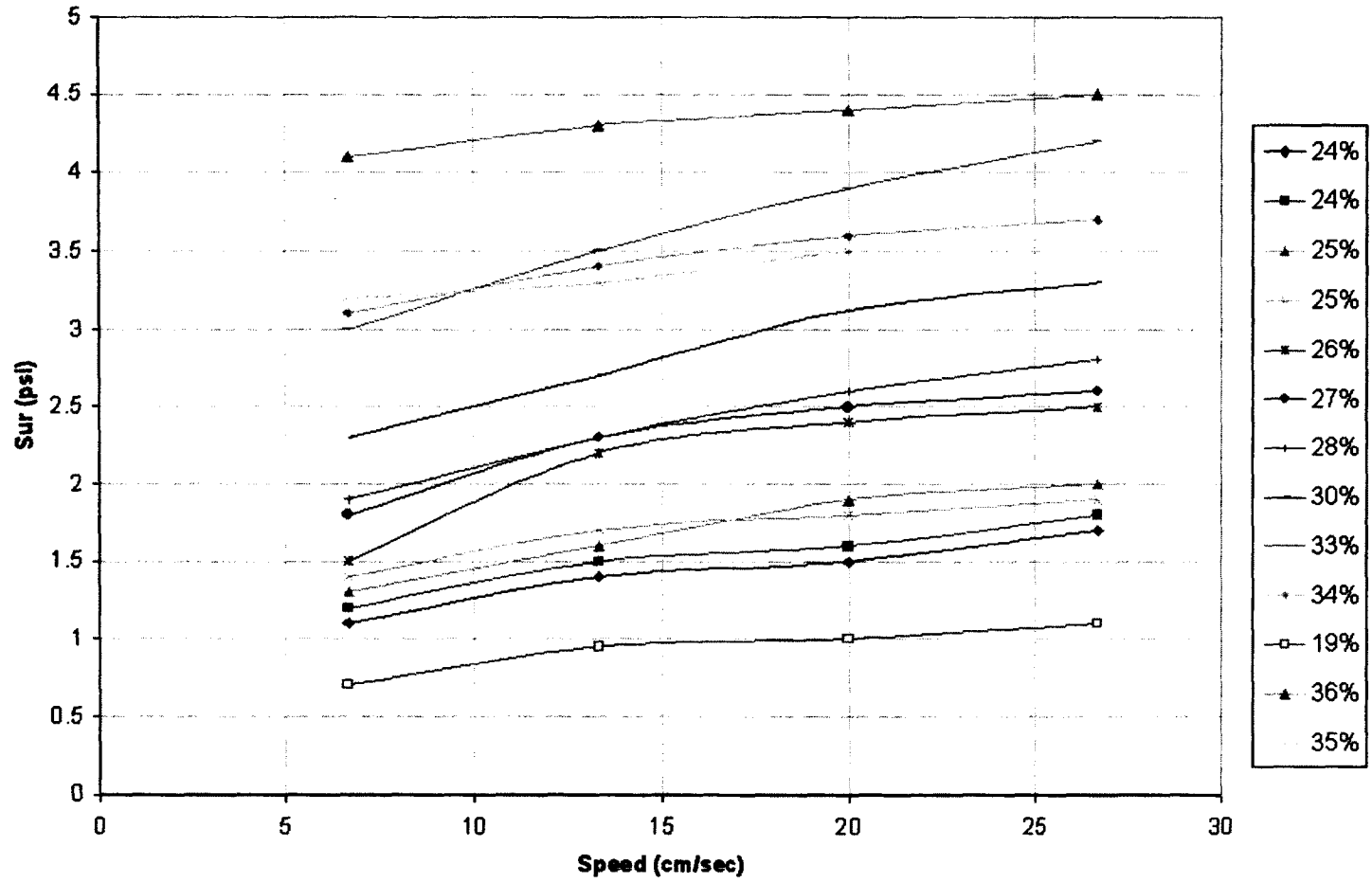
Figure IV-12. Reduced data of successful tests.

CHAPTER V

ANALYSIS OF THE RESULTS

This chapter is intended to discuss and analyze the results that were obtained during testing with the ring shear device (RSD) and to propose a simple mathematical model that fits the experimental data, which can be used to predict the residual strength of the tested material at strain rates larger than those used in the lab.

Several rheological models can be implemented to fit the experimental data; for instance, Chen and Lee (2002) mention the Bingham model to identify flowing materials such as slurry flows, liquefied mine tailing materials, coal slurries, fine graded flows and snow avalanches; others have used the Herschel-Bulkley model with mudflows, whose behavior is also influenced by the concentration of particles in the mixture and for landslides with shear strain rates in the order of 50 to 100 sec^{-1} (Govier and Aziz, 1982 and O'Brien

and Julien, 1988). The latter model (Herschel-Bulkley) can be implemented in this dissertation using the following equation:

$$\tau = \tau_y + K \dot{\gamma}^m$$

Where:

τ: Shear stress

τ_y :yield stress

$\dot{\gamma}$: Shear strain rate

K, m: empirical parameters

The experimental data that was reported in chapter IV is used in this section to implement the Herschel-Bulkley model for each test. Regressions shown in figures V-1 and V-2 were carried with the simple regression tool in Excel (type of regression: power).
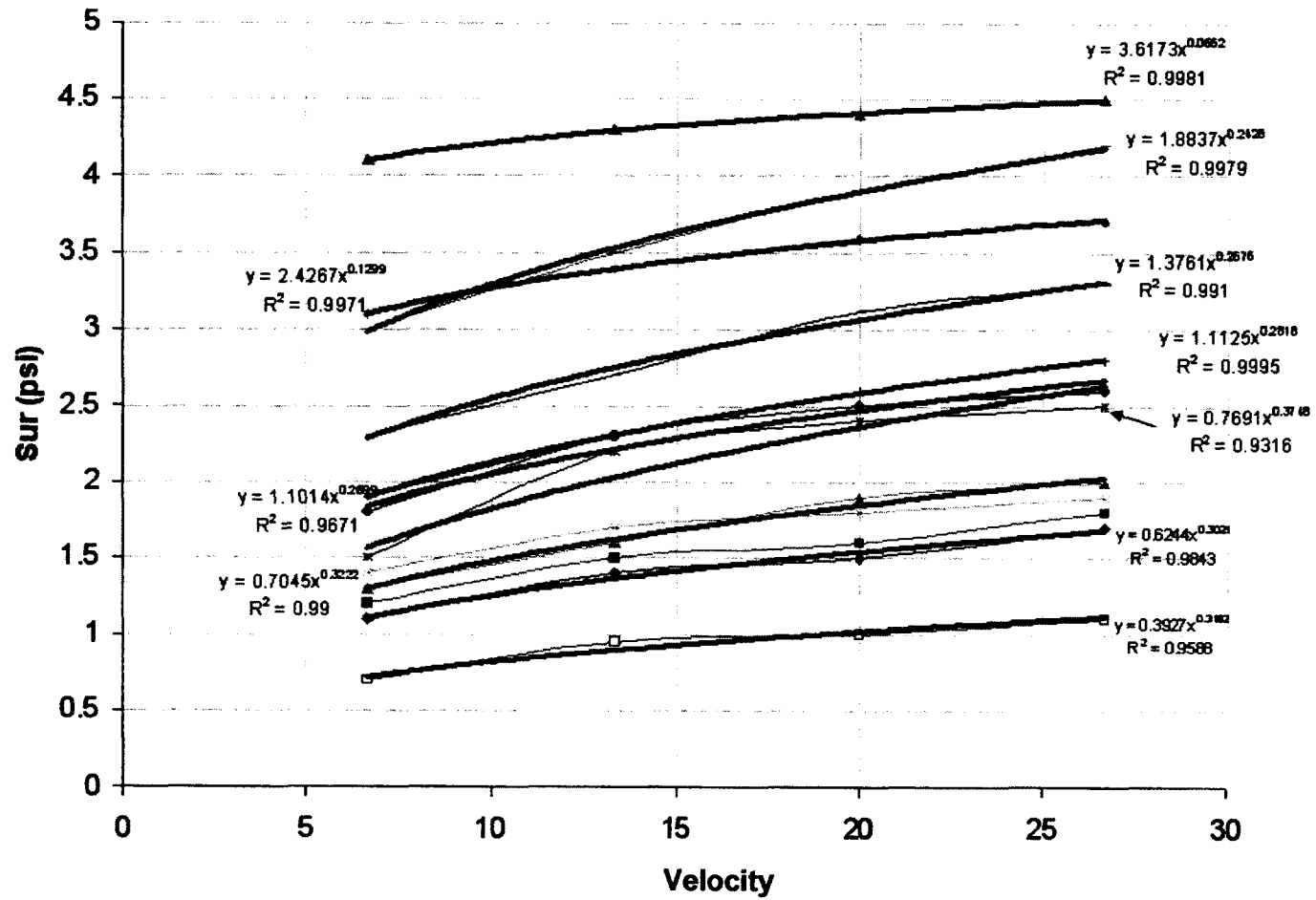
Figure V-1. Trend lines for Power regression (Sur vs. Velocity)
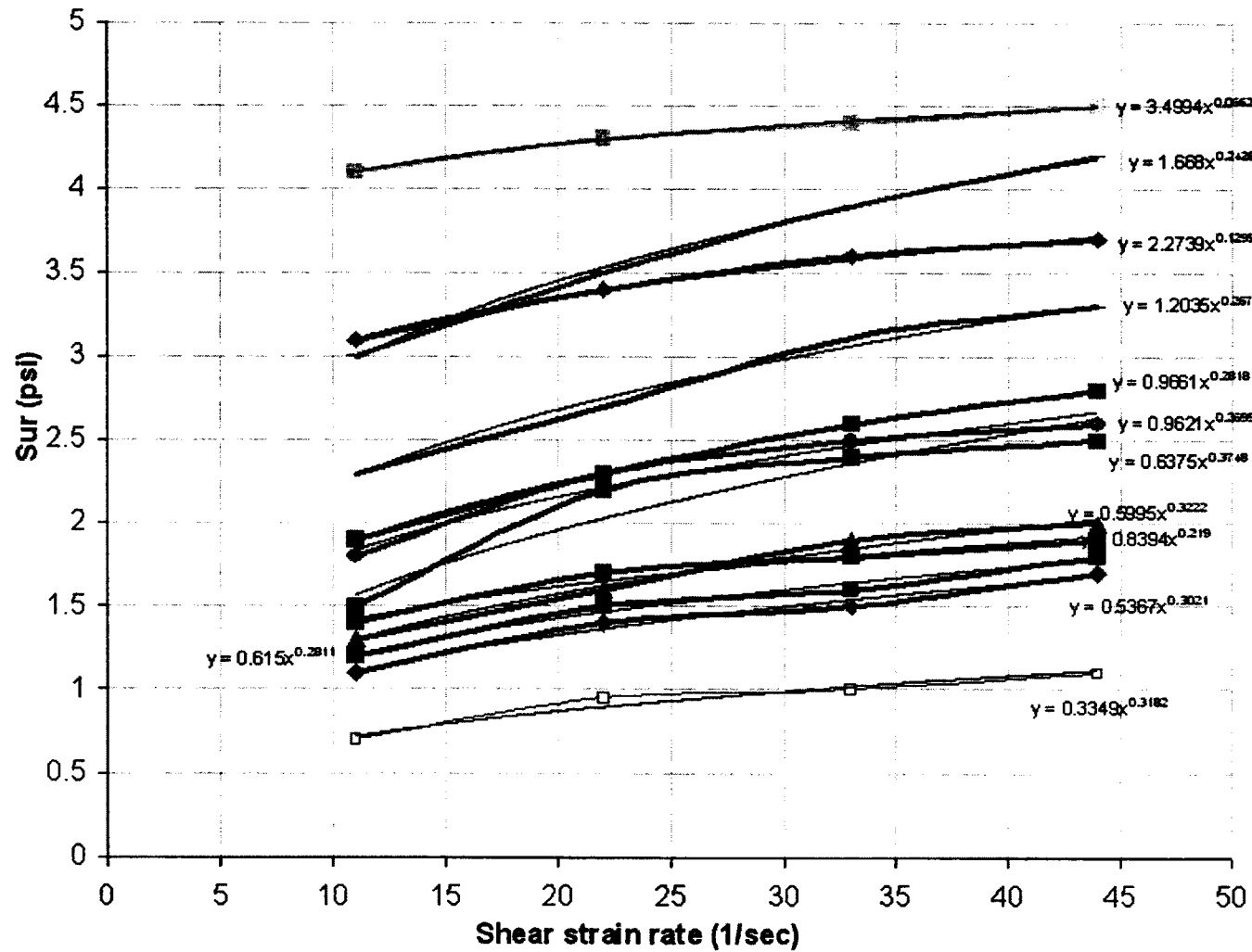
Figure V-2. Trend lines for Power regression (Sur vs. Shear strain rate).

The following table summarizes the results from the regression analysis for the figure V-2 (Sur vs. shear strain rate), including the empirical coefficients and exponents obtained for each relative density:

Table V-1. Herschel-Bulkley coefficients

Dr	K	m
19	0.3349	0.3182
24	0.5367	0.3021
24	0.615	0.2811
25	0.839	0.219
25	0.5995	0.3222
26	0.6375	0.3748
27	0.9621	0.2699
28	0.9661	0.2818
30	1.2035	0.2676
33	2.2739	0.1299
34	1.668	0.2428
36	3.499	0.0662
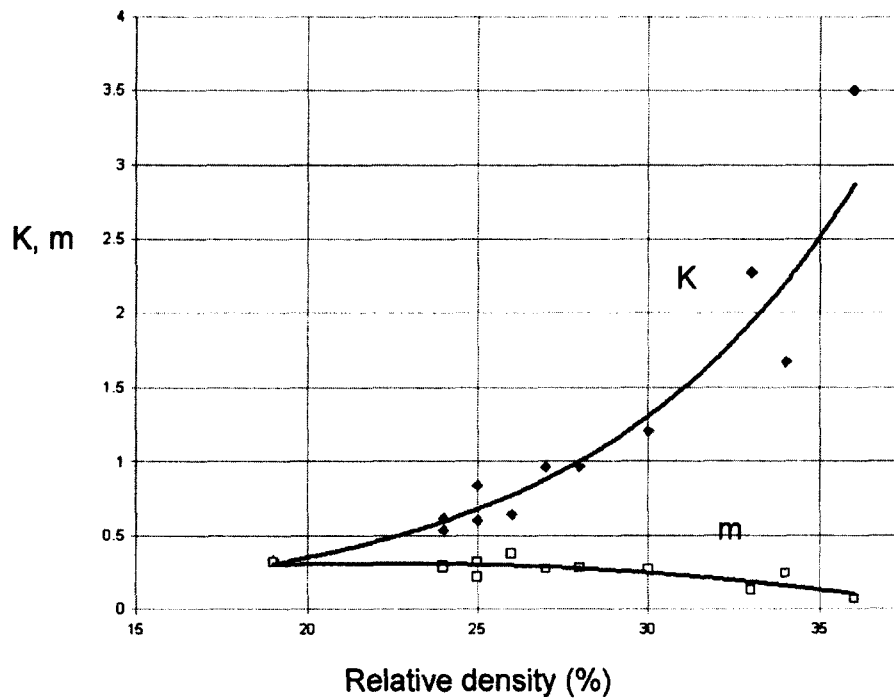
Figure V-3. Variation of empirical parameters (K and m) with relative density.

Experimental data suggests that as the relative density increases, the parameter m decreases and its limit would be a small number; this means that eventually, for high relative densities, the term γ^m would be one and the residual strength would be constant; however, because no experimental data is available for relative densities of more than 40%, the analysis carried in this dissertation is to be limited to the range 19% to 36%.

Even though the Mohr-Coulomb equation is not being used in this dissertation to model the liquefied soil, it can be thought as an upper bound for the values obtained with the ring shear device.

Comparison with other Residual Strength Data

In this section, the experimental results the writer obtained with the RSD are compared with those obtained by means of back-calculation of the residual strength from collected data of case histories of liquefaction failures. As it was mentioned in Chapter I, two approaches have been proposed: the first was initially stated by Seed and Harder (1990) (recall figure I-10), which correlates Sur with the Equivalent Clean Sand SPT Corrected Blowcount $(N_1)_{60CS}$. Figure V-4 shows the comparison with the RSD residual strength.

Since the residual strength is correlated with the Equivalent Clean Sand SPT Corrected Blowcount $(N_1)_{60CS}$, a similar correction needs to be used in order to bring the Dr to $(N_1)_{60CS}$. A crude (and experimental) correlation proposed by Mayne, et. al (2001) is used:

$$(N_1)_{60\text{-}CS} = 60 \cdot (Dr/100)^2$$
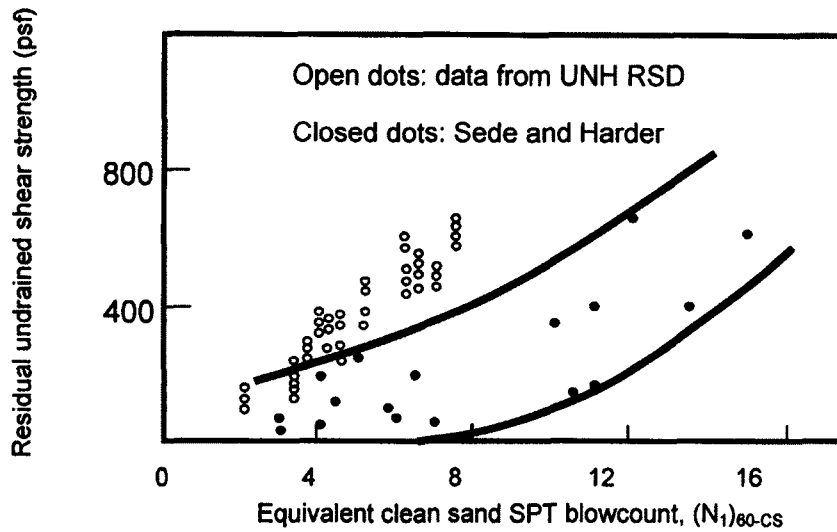
Figure V-4. Comparison of RSD with Seed and Harder's.
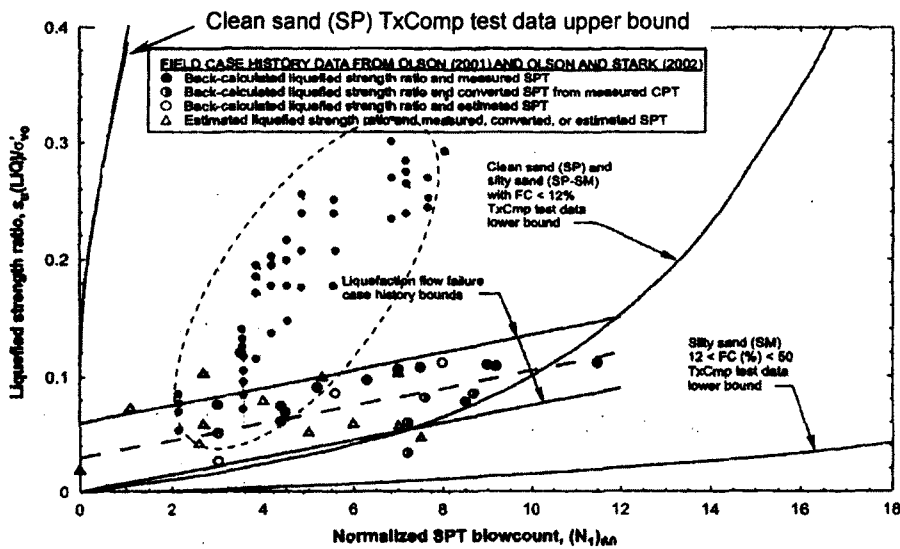
Figure V-5. Comparison of RSD with Olson and Stark's.

Previous figures suggest that the data obtained with the RSD is consistent with the field data reported by Seed and Harder. However, such agreement is not shown when the residual strength is normalized using the initial vertical effective stress, as proposed by Olson and Stark, even though the RSD data falls between the conventional triaxial tests bounds. Actually, it has been pointed out that the normalization of the residual strength by the vertical effective stress might not be appropriate, except for compressible soils, such as silty sands and tailing sands (NSF Workshop "Post-liquefaction shear strength of granular soils", 1998); there are also other factors that are involved in field failures such as void ratio distribution which produces trapped water films under less permeable layers, thus resulting in a lower equivalent residual shear strength.

Strain Rate Applied by the RSD

As it was mentioned in Chapter IV, a special test with colored sand suggested that the sheared zone is 0.6mm thick (0.2362 in), which changes the strain rates that were initially estimated with the entire thickness of the sample. Figure V-6 shows how the residual strength changes with the strain rate. According to Bryant et al (1983) shear strain rates in the field are between 10 and 100 1/sec are observed in flow slides, which are in accordance with the 44 1/sec measured with the RSD.
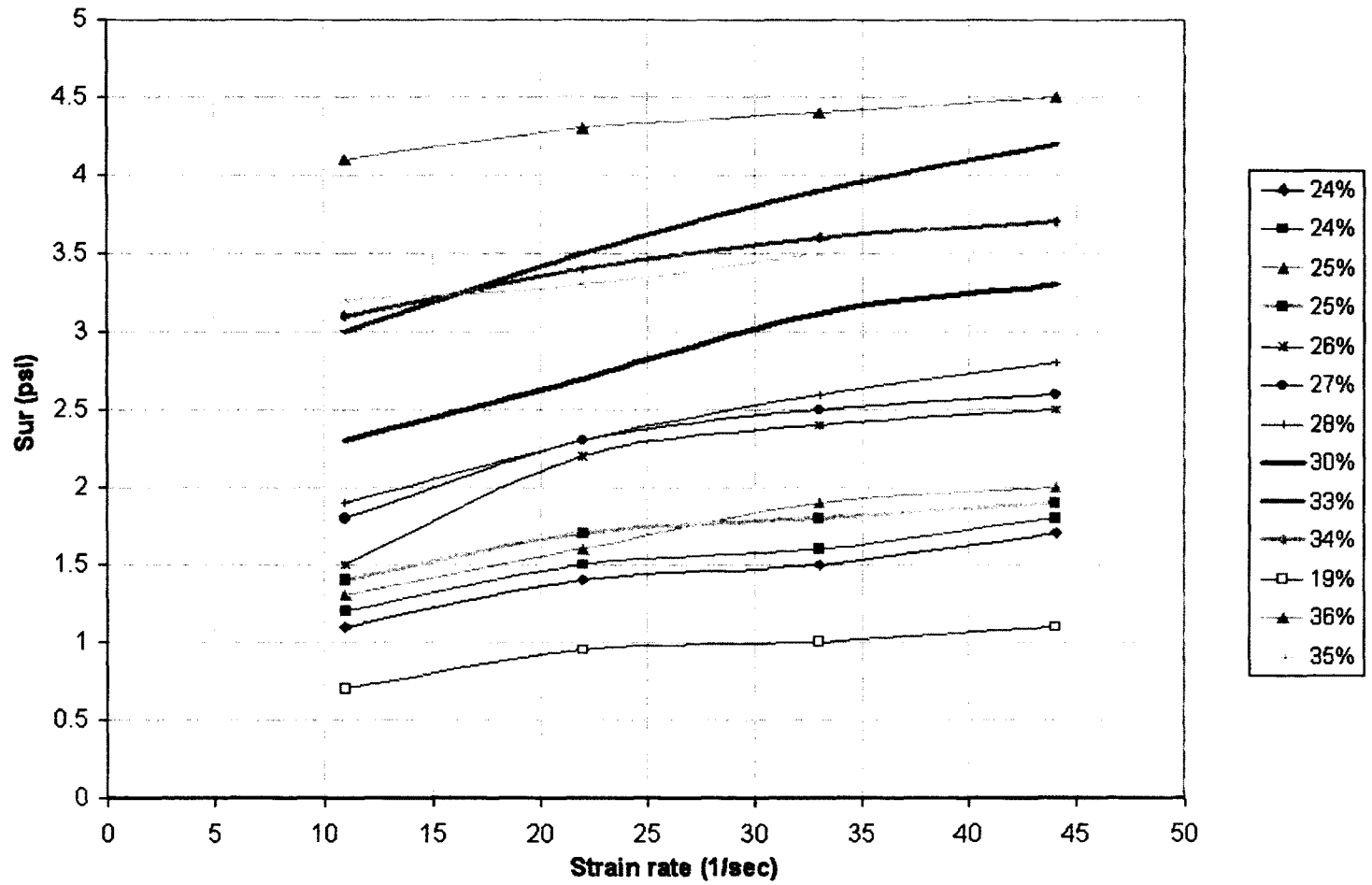
Figure V-6 Residual strength vs. strain rate

CHAPTER VI

CONCLUSIONS

The basic objective of this research has been to develop a new design for a ring shear testing system, intended to study strain-rate dependency in the residual shearing strength of liquefied sand. The ultimate goal of this work is to better model the behavior of destructive flow slides. A basic test series for a soil highly susceptible to liquefaction and flow, a fine uniform sand in the 20% to 40% relative density range, has led to several basic conclusions:

1. Experimental results using the UNH ring shear device suggest that the behavior of liquefied sands under undrained conditions is rate dependent; therefore it can be modeled as viscous non-Newtonian fluid in terms of shearing resistance versus shear strain rate. The best fit to the experimental data was found to be the Herschel-Bulkley model:

$$\tau = \tau_y + K \, \dot{\gamma}^m$$

99

Where:

τ: Shear stress $\dot{\gamma}$: Shear strain rate

τ_y :yield stress   K, m: empirical parameters

K and m were found to be dependent on the relative density, as follows (recall figure V-3):
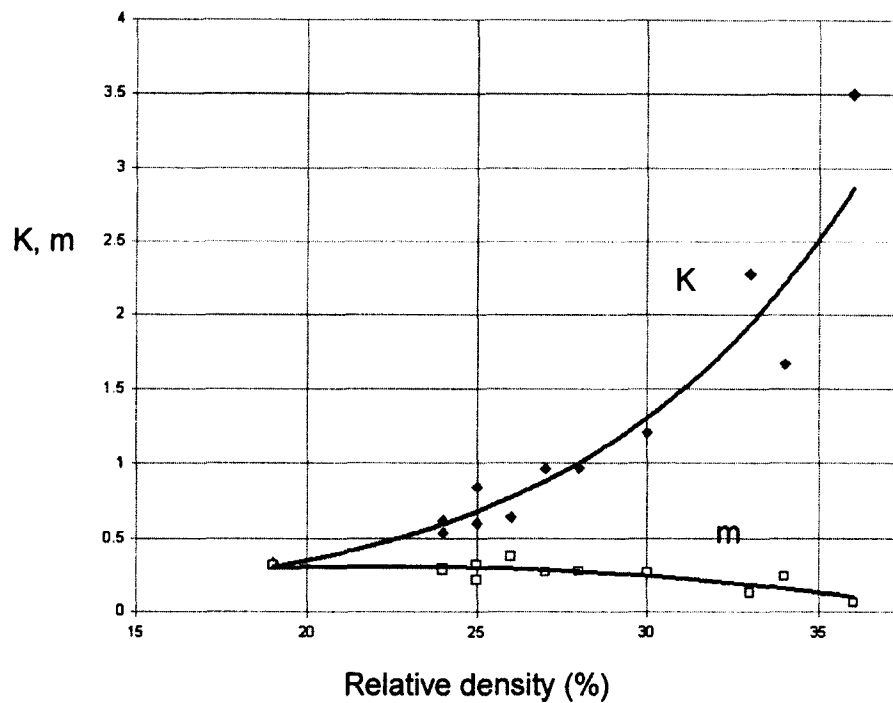
Relative density (%)

2. As previously noted, measurements were made with relative densities between 20% and 40%, and data suggest that the exponent (m) decreases to a small value at higher densities and consequently the model seems to tend towards a density-dependent constant at higher densities. In terms of absolute values of shearing resistance, the UNH RSD data

compare well with the latest data reported by Sassa and co-workers (Igwe, Sassa and Wang, 2007).

3. Due to the limitations of the conventional triaxial test, and given the experimental results obtained in this thesis, it may be concluded that the behavior of fully liquefied materials cannot be investigated using the triaxial device; the main disadvantages of it are: shear strains that can be imposed are not large enough to compare them with shear strains observed in real flow slides, and velocities (i.e., shear strain rates) that can be applied are lower than those observed in the field.

4. In terms of shear strength values obtained, the laboratory data compare well with field data back-calculated from field failures, as reported by Seed and Harder (1990). On the other hand, when the field shear strength data were normalized by a vertical (pre-slide) effective stress value (Olson and Stark, 2002) the ring shear data plotted above the back-calculated field values, although in the center of the scatter band obtained from triaxial tests; it should be noted in this regard that Riemer (1997) and others do not consider normalization to be accurate nor appropriate for characterizing liquefied soils, especially because it is very difficult to find a representative pre-slide vertical effective stress for the sliding mass.

5. Several aspects are still to be investigated with the RSD; among others, these are the most important:

- Partial drainage. This would bring as a consequence a decrease in the pore water pressure, which would bring an increase in the effective stress, thus an increase in the shear strength, point at which the material can reach a limit, perhaps controlled by the Mohr-Coulomb criteria.

- Fines content. It has been recognized (Kramer, 1996) that fines tend to prevent liquefaction, but there is little research on their effect on the steady state behavior.

- Effect of higher relative densities. As it was mentioned, the experimental data presented in this dissertation was calculated for a range of relative densities between 20% and 40%; beyond this maximum limit it is very difficult to extrapolate, specially because it is uncertain what the upper bound of Sur can be, and at what point dilation starts to control.

BIBLIOGRAPHY

1. Anderson, F. W. and Hammoud, F., "Effect of Testing Procedure in Ring Shear Tests," Technical note, Geotechnical Testing Journal, GTJODJ, Vol. 11, No. 3, September 1988, pp. 204-207.

2. Andrianopoulos, K. I., Bouckovalas, G. D. and Papadimitriou, A. G., "A Critical State Evaluation of Fines Effect on Liquefaction Potential," Proceedings: Fourth International Conference on Recent Advances in Geotechnical Earthquake Engineering and Soils Dynamics and Symposium in Honor of Professor W.D. Liam Finn, San Diego, California, March 26-31, 2001, Paper No. 4.06.

3. Been, K. and Jefferies, M., "A State Parameter for Sands", Geotechnique, Vol. 35, No. 1, 1985, pp. 99-112

4. Been, K., Jefferies, M. and Hachey, J., "The Critical State of Sands", Geotechnique, Vol. 41, No. 3, 1991, pp. 365-381

5. Bolton, M. D., 'The Strength and Dilatancy of Sands," Geotechnique,.

6. Boulanger, R. W., "Relating $K\alpha$ to Relative State Parameter Index," Journal of Geotechnical and Geoenvironmental Engineering, Vol. 129, No. 8, August 1, 2003, pp. 770-773.

7. Bryant, S., Duncan, J. M. and Seed, H. B., "Application of Tailing Flows Analyses to Field Conditions", Report UCB/GT/83-03 to US Bureau of Mines, Department of Civil Engineering, University of California, Berkeley, 312 pp., 1983

8. Byrne, P. and Beaty, M., "Assesment of Residual Strength for Embankments", Earthquake Geotechnical Engineering, Sêco e Pinto (Ed.), Balkema, Rotterdam, ISBN 9058091163, pp. 1069-1075, 1998.

9. Carter, J. P., Brooker, J. R. and Wroth, C. P., "A Critical State Soil Model for Cyclic Loading," Research Report No. CE 6, Department of Civil Engineering, University of Queensland, October 1979.

10. Castro, G. and Poulos, S. J., "Factors Affecting Liquefaction and Cyclic Mobility," Journal of the Geotechnical Engineering Division, Proceedings of the American Society of Civil Engineers, Vol. 103, No. GT6, June 1977, pp. 501-516.

11. Castro, G., "Liquefaction and Cyclic Mobility of Saturated Sands", Journal of the Geotechnical Engineering Division, ASCE, Vol. 101, No. GT6, pp. 551-569, 1975

12. Chapuis, R. P., et al., "A user's Approach to Assess Numerical Codes for Saturated and Unsaturated Seepage Conditions," Canadian Geotechnical Journal, Vol. 38, 2001, pp. 1113-1126.

13. Chen, H., and Lee, C. F., "Runout Analysis of Slurry Flows with Bingham Model," Journal of Geotechnical and Geoenvironmental Engineering, Vol. 128, No. 12, December 1, 2002, pp. 1032-1042.

14. Crudden, D. M., et al., "Thirty-Five Years of Activity at the Lesueur Landslide, Edmonton, Alberta," Canadian Geotechnical Journal, Vol. 39, 2002, pp. 266-278.

15. De Alba, P. and Ballestero, T, "Residual Strength after Liquefaction: A Rheological Approach", 11th International Conference on Soil Dynamics and Earthquake Engineering, Berkeley CA, January 7-9, 2004

16. De Alba, P., Seed, H. B., Retamal, E. and Seed, R., "Analyses of Dam Failures in 1985 Chilean Earthquake", Journal of Earthquake Engineering, Vol. 114, No. 12, pp. 1414-1434, 1988

17. Desrosiers, R. and Silva, A. J., "Strength Behavior of Marine Sands at Elevated Confining Stresses," Marine Georesources and Geotechnology, Vol. 20, 2002, pp. 1-19.

18. Eckersley, J., "Instrumented Laboratory Flowslides", Geotechnique, Vol. 40, No. 3, pp. 489-502, September 1990.

19. Elgamal, A., et al., "Numerical Analysis of Embankment Foundation Liquefaction Countermeasures," Journal of Earthquake Engineering, Vol. 6, No. 4, 2002, pp. 447-471.

20. Emery, J. J., Liam Finn, W. D., "Uniformity of Saturated Sand Specimens," Evaluation of Relative Density and its Role in Geotechnical Projects Involving Cohesionless Soils, ASTM STP 523, American Society for Testing and Materials, 1973, pp. 182-194.

21. Finn, L., "Post-Liquefaction Flow Deformations," Soils Dynamics and Liquefaction, ASCE STP 107, 2000, pp. 108-122.

22. Finno, R. J., et al., "Strain Localization and Undrained Steady State of Sand," Journal of Geotechnical Engineering, Vol. 122, No. 6, June, 1996, pp. 462-473.

23. Fletcher, L., Hungr, O. and Evans, S. G., "Contrasting Failure Behaviour of two Large Landslides in Clay Silt," Canadian Geotechnical Journal, Vol. 39, 2002, pp. 2002.

24. Fourie, A. B. and Papageorgiou, G., "Defining an Appropriate Steady State Line for Merriespruit Gold Tailings," Canadian Geotechnical Journal, Vol. 38, 2001, pp. 695-706.

25. Gabet, E. J. and Mudd, S. M., "The Mobilization of Debris Flows from Shallow Landslides," Geomorphology, Vol. 74, 2006, pp. 207-218.

26. Garga, V. K. and Infante S., J. A., "Steady State Strength of Sands in a Constant Volume Ring Shear Apparatus," Geotechnical Testing Journal, Vol. 25, No. 4, December 2002, pp. 1-8.

27. Garga, V. K. and Zhang, H., "Volume Changes in Undrained Triaxial Tests on Sands," Canadian Geotechnical Journal, Vol. 34, 1997, pp. 762-772.

28. Hwang, J. L. et al., "Viscous Fluid Characteristics of Liquefied Soils and Behavior of Piles Subjected to Flow of Liquefied Soils," Soils Dynamics and Earthquake Engineering, Vol. 26, 2006, pp. 313-323.

29. Igwe, O., Sassa, K. and Wang, F., "The Influence of Grading on the Shear Strength of loose Sands in Stress-controlled Ring Shear Tests," Landslides, Vol. 4, 2207, pp. 43-51.

30. Ishihara, K., "The Rankine Lecture: Liquefaction and Flow Failure During Earthquakes", Geotechnique, 43(3), 351-415

31. Iverson, R. M. and Vallance, J. W., "New Views of Granular Mass Flows," Geology, Vol. 29, No. 2, February 2001, pp. 115-118.

32. Iverson, R., "Shear Behavior of Liquefied Soils: Interdisciplinary Perspectives", Proc. NSF Workshop on Post-liquefaction Strength of Granular Soils, April 17-19, 1997, University of Illinois, Urbana IL

33. Iverson, R., "The Physics of Debris Flows", Reviews of Geophysics, Vol. 35, No. 3, pp. 245-296, August 1997

34. Jefferies, M. G., "A Critical State View of Liquefaction," Proceedings of the international Workshop on the Physics and Mechanics of Soil Liquefaction, Baltimore-Maryland (USA), September 10-11, 1998.

35. Kakou, B. G., Shimizu, H. and Nishimura, S., "Residual Strength of Colluvium and Stability Analysis of Farmland Slope," Agriculture Engineering International: The CIGR Journal of Scientific Research and Development Department, Vol. III, March 2001, pp. 1-12.

36. Khazai, B. and Sitar, N., "Evaluation of Factors Controlling Earthquake-Induced Landslides Caused by Chi-Chi Earthquake and Comparison with

the Northridge and Loma Prieta Events," Engineering Geology, Vol. 71, 2003, pp. 79-95.

37. Kokeguchi, K., et al., "Post-Liquefaction Torsion Shear Tests on Sand with Various Strain Rates," Proceedings: Fourth International Conference on Recent Advances in Geotechnical Earthquake Engineering and Soils Dynamics and Symposium in Honor of Professor W.D. Liam Finn, San Diego, California, March 26-31, 2001, Paper No. 1.56.

38. Konrad, J., "Minimum Undrained Strength Versus Steady State Strength of Sands", Journal of Geotechnical Engineering, Vol. 116, No. 2, 1990, pp. 948-963

39. Konrad, J. and Watts, B., "Undrained Shear Strength for Liquefaction Flow Failure Analysis", Canadian Geotechnical Journal, Vol. 32, 1995, pp. 783-794

40. Konrad, J. M. and Pouliot, N., "Ultimate State of Reconstituted and Intact Samples of Deltaic Sand," Canadian Geotechnical Journal, Vol. 34, 1997, pp. 737-748.

41. Kramer, S., "Triggering of Liquefaction Flowslides in Coastal Soil Deposits", Engineering Geology, Vol. 26, 1988, pp. 17-31

42. Kramer, S., "Geotechnical Earthquake Engineering", Prentice Hall, Inc., Upper Saddle River, NJ, 1996

43. Ladd, R. S., "Preparing Test Specimens Using Undercompaction," Geotechnical Testing Journal, GTJODJ, Vol. 1, No. 1, March 1978, pp. 16-23.

44. Ladd, R. S., "Specimen Preparation and Cyclic Stability of Sands," Journal of the Geotechnical Engineering Division, Vol. 103, No. GT6, June 1977, pp. 535-547.

45. Lade, P. V. and Yamamuro, J. A., "Effects of Nonplastic Fines on Static Liquefaction of Sands," Canadian Geotechnical Journal, Vol. 34, 1997, pp. 918-928.

46. Lee, C., "Static Shear and Liquefaction Potential of Sand", Proc. 3rd International Conference on Recent Advances in Geotechnical Earthquake Engineering and Soil Dynamics, St. Louis, Missouri, April 2-7, 115-118

47. Li, J., "Soil Viscous Behavior in Response to Torsional Cyclic Loading," Proceedings: Fourth International Conference on Recent Advances in Geotechnical Earthquake Engineering and Soils Dynamics and Symposium in Honor of Professor W.D. Liam Finn, San Diego, California, March 26-31, 2001, Paper No. 1.01.

48. Marin, S., et al., "A Probabilistic Approach to Seismic Hazard in Metropolitan France," Bulletin of Seismological Society of America, Vol. 94, No. 6, December 2004, pp. 2137-2163.

49. Martin, G. R., Finn, L. and Seed, B. H., "Fundamentals of Liquefaction Under Cyclic Loadings," Journal of the Geotechnical Division,

Proceedings of the American Society of Civil Engineers, Vol. 101, No. GT5, May 1975, pp. 423-438.

50. Martin, S., et al. "A probabilistic Approach to Seismic Hazard in Metropolitan France", Bulletin of the Seismological Society of America, Vol. 94, No. 6, pp. 2137-2163, December 2004.

51. Matternicht, G., Hurni, L. and Gogu, R., "Remote Sensing of Landslides: An Analysis of the Potential Contribution to Geo-spatial Systems for Hazard Assessment in Mountainous Environments," Remote Sensing of Environment, Vol. 98, 2005, pp. 284-303.

52. Mesri, G., "Yield Strength and Critical Strength of Liquefiable Sands in Sloping Ground," Technical note, Geotechnique, Vol. 57, No. 3, 2007, pp. 309-311.

53. Mita, K. A., Dasari, G. R. and Lo, K. W., "Performance of a Three-Dimensional Hvorslev-Modified Cam Clay Model for Overconsolidated Clay," International Journal of Geomechanics, Vol. 4, No. 4, December 1, 2004, pp. 296-309.

54. Mizuhashi, M., et al., "Examination of Slope Hazard Assessment by Using Case Studies of Earthquake- and Rainfall- Induced Landslides," Soils and Foundations, Vol. 26, No. 6, December 2006, pp. 846-853. Japanese Geotechnical Society.

55. Mulilis, J. P., et al., "Effects of Sample Preparation on Sand Liquefaction," Journal of the Geotechnical Engineering Division," Vol. 103, No. GT2, February 1977, pp. 91-108.

56. Nemat-Nasser, S. and Takahashi, K., "Liquefaction and Fabric of Sand", Journal of the Geotechnical Engineering Division," Vol. 110, No. GT9, September 1984, pp. 1291-1306

57. Ng, T., "Behavior of Gravity Deposited Granular Material Under Different Stress Paths," Canadian Geotechnical Journal, Vol. 42, 2005, pp. 1644-1655.

58. Nishimura, S., Towhata, I. and Honda, T., "Laboratory Shear Test on Viscous Nature of Liquefied Sand", Soils and Foundations, Vol. 42, No. 4, pp. 89-98, August 2002

59. Norris, G., et al., "Liquefaction and Residual Strength of Sands from Drained Triaxial Tests," Journal of Geotechnical and Geoenvironmental Engineering, Vol. 123, No. 3, March 1997, pp. 220-228.

60. Olson, S. M. and Stark, T. D., "Liquefied Strength Ratio From Liquefaction Flow Failure Case Histories," Canadian Geotechnical Journal, Vol. 39, 2002, pp. 629-647

61. Olson, S. M. and Stark, T. D., "Use of Laboratory Data to Confirm Yield and Liquefied Strength Ratio Concepts," Canadian Geotechnical Journal, Vol. 40, 2003, pp. 1164-1184.

62. Olson, S. M. and Stark, T. D., "Yield Strength Ratio and Liquefaction Analysis of Slopes and Embankments," Journal of Geotechnical and Environmental Engineering, Vol. 129, No. 8, August 1, 2003, pp. 727-737.

63. Pitman, E. B., et al., "Computer Granular Avalanches and Landslides," Physics of Fluids, Vol. 15, No. 12, December 2003, pp. 3638-3646.

64. Poulos, S. J., Castro, G. and France, J. W., "Liquefaction Evaluation Procedure," Journal of Geotechnical Engineering, Vol. 111, No. 6, June 1985, pp. 772-792.

65. Pritchard, D. "The Rheology of Muddy Fluids," Thesis, Appendix B, pp. 283-289. http://www.bpi.cam.ac.uk/david/papers.htm

66. Riemer, M., Seed, R., Nicholson, P. and Jong, H., "Steady State Testing of Loose Sands" Limiting Minimum Density", Journal of Geotechnical Engineering, Vol. 116, No. 2, 1990, pp. 332-337

67. Riemer, M. and Seed, R., "Factors Affecting Apparent Position of Steady State Line", Journal of Geotechnical and Geoenvironmental Engineering, Vol. 123, No. 3, 1997, pp. 281-288

68. Rivera, L., Verbal communication (2005)

69. Sasaki, Y., Ohbayashi, J. and Ogata, Y., " Compressibility of Liquefied Sand," Proceedings: Fourth International Conference on Recent Advances in Geotechnical Earthquake Engineering and Soils Dynamics and Symposium in Honor of Professor W.D. Liam Finn, San Diego, California, March 26-31, 2001, Paper No. 1.62.

70. Sassa, K., "Geotechnical Model for the Motion of Landslides," Proceedings: Fifth International Symposium on Landslides, 1988, pp. 37-55.

71. Sassa, K., "Mechanism of Flows in Granular Soils," Proc. GeoEng 2000, Melbourne, Australia, V.1, pp. 1671-1702, 2000

72. Sassa, K., Wang, G. and Fukuoka, H., "Performing Undrained Shear Tests on Saturated Sands in a New Intelligent Type of Ring Shear Apparatus", Geotechnical Testing Journal, ASTM, Vol. 26, No. 3, pp. 257-265, September 2003

73. Schanz, T. and Vermeer, P. A., "Angles of Friction and Dilatancy of Sand," Geotechnique, Vol. 46, No. 1, 1996, pp. 145-151.

74. Schmitt, R. and Feise, H., "Influence of Tester Geometry, Speed and Procedure on the Results from a Ring Shear Tester," Particle & Particle Systems Characterization, Vol. 21, No. 5, December 2004, pp. 403-410.

75. Schofield, A. and Wroth, C., "Critical State Soil Mechanics", McGraw-Hill Book Company, 1968

76. Seed, H. B., "Design Problems in Soil Liquefaction", Journal of Geotechnical Engineering, ASCE, Vol. 113, No. 8, pp. 827-845, 1986

77. Seed, R. and Harder, L., "SPT-Based Analysis of Cyclic Pore Pressure Generation and Undrained Residual Strength", Proc. H. Bolton Seed Memorial Symposium, Vol. 2, pp 351-376, BiTech Publishers Ltd., 1990

78. Sladen, J., D'Hollander, R. and Krahn, J., "The Liquefaction of Sands, a Collapse Approach", Canadian Geotechnical Journal, Vol. 22, 1985, pp. 564-578

79. Sladen, J. and Handford, G., "A Potential Systematic Error in Laboratory Testing of Very Loose Sand", Canadian Geotechnical Journal, Vol. 24, 1987, pp. 462-466

80. Stark, T. D. and Contreras, I. A., "Constant Volume Ring Shear Apparatus," Geotechnical Testing Journal, GTJODJ, Vol. 19, No. 1, March 1996, pp. 3-11.

81. Stark, T. and Mesri, G., "Undrained Strength of Liquefied Sand for Stability Abalysis", Journal of Geotechnical Engineering, ASCE, Vol. 118, No. 11, pp. 1727-1747, 1992

82. Tabesh, A. and Poulos H. G., "Design Charts for Seismic Analysis of Single Piles in Clay," Proceedings of the Institution of Civil Engineers, Geotechnical Engineering 160, April 2007, Issue GE2, p.p. 85-96.

83. Talaganov, K. V., "Stress-Strain Transformations and Liquefaction of Sands," Soils Dynamics and Earthquakes Engineering, Vol. 15, 1996, pp. 411-418.

84. Vaid, Y. P. and Negussey, D., "Preparation of Reconstituted Sand Specimens," Advanced Triaxial Testing of Soil and Rock," ASTM STP 977, 1988, pp. 405-417.

85. Vaid, Y. P., "Laboratory Characterization of Stress-Strain Behavior of Soils by Stress and/or Strain Path Loading," Geotechnical Testing Journal, GTJODJ, Vol. 24, No2, June 2001, pp. 200-208.

86. Vaid, Y. P., Chung, E. K. F., Kuerbis, R. H., "Stress Path and Steady Steate," Canadian Geotechnical Journal, Vol 27, 1990, pp. 1-7.

87. Vaid, Y. P., Sivathayalan, S. and Stedman, J. D., "Influence of Specimen-Reconstituting Method on the Undrained Response of Sand," Geotechnical Testing Journal, GTJODJ, Vol. 22, No. 3, September 1999, pp. 187-195.

88. Vaid, Y. P., Stedman and J. D, Sivathayalan, S., "Confining Stress and Static Shear Effects in Cyclic Liquefaction," Canadian Geotechnical Journal, Vol. 38, 2001, pp. 580-591.

89. Vaid, Y. P. and Sivathayalan, S., "Fundamental Factors Affecting Liquefaction Susceptibility of Sands", Canadian Geotechnical Journal, V. 37, pp. 592-606, 2000

90. Wan, R. G. and Guo, P. J., "Drained Cyclic Behavior of Sand with Fabric Dependence," Journal of Engineering Mechanics, Vol. 127, No. 11, November 2001, pp. 1106-1116.

91. Wang G. and Sassa, K., "Post-failure Mobility of Saturated Sands in Undrained Load-Controlled Ring Shear Tests", Canadian Geotechnical Journal, Vol. 39, pp. 821-837, July 2002

92. Wood, D. M., "Soil Behavior and Critical State Soil Mechanics", Cambridge University Press, Cambridge, UK, 1990

93. Wang, G. and Sassa, K., "Post-failure Mobility of Saturated Sands in Undrained Load-Controlled Ring Shear Tests," Canadian Geotechnical Journal, Vol. 39, 2002, pp. 821-837.

94. Wu, G., "Earthquake-Induced Deformation Deformation Analysis of the Upper San Fernando Dam Under the 1971 San Fernando Earthquake," Canadian Geotechnical Journal, Vol. 38, 2001, pp. 1-15.

95. Xue, Q., "Assessing the Accuracy of the Damping Models Used in Displacement-Based Seismic Demand Evaluation and Design of Inelastic Structures," Earthquake Engineering and Engineering Seismology, Vol. 3, No. 2, September 2001, pp. 37-45.

96. Yamagami T. and Ueta, Y., "Back Analysis of Average Strength Parameters for Critical Slip Surfaces," Computer and Physics Modeling in Geotechnical Engineering, Balasubramaniam et al. (eds), 1989, Balkema, Rotterdam, ISBN 90 6191 864 2.

97. Yao, Y. P., Sun, D. A. and Luo, T., "A Critical State Model for Sands Dependent on Stress and Density," International Journal for Numerical and Analytical Methods in Geomechanics, Vol. 28, 2004, pp. 323-337.

98. Yoshimine, M. and Ishihara, K., "Flow Potential of Sand During Liquefaction", Soils and Foundations, Vol. 38, No. 3, 1993, pp. 189-198

99. Yu, H., et al., "Seismic Response Calculation of Saturated Soft Soil," Proceedings: Fourth International Conference on Recent Advances in Geotechnical Earthquake Engineering and Soils Dynamics and

Symposium in Honor of Professor W.D. Liam Finn, San Diego, California, March 26-31, 2001, Paper No. 1.05.

100.   Zhang, H. and Garga, V., "Quasi-Steady State: a Real Behavior?" Canadian Geotechnical Journal, Vol. 34, 1997, pp. 749-761